



Università degli Studi di Palermo



Unione Europea



Ministero dell'Università e della Ricerca
Scientifica e Tecnologica

Facoltà di Farmacia

PhD in Pharmaceutical Sciences

**Design and Synthesis of new
Inhibitors of Carcinogenic Processes**

PhD Student

Dr. Ilenia Abbate

Supervisor

Prof. Anna Maria Almerico

PhD Coordinator

Prof. Girolamo Cirrincione

Dipartimento Farmacochimico, Tossicologico e Biologico
A.A. 2006-2007 (CICLO XXII) SSD:CHIM/08

INDEX

1. INTRODUCTION	Pag. 1
1.1. HALLMARK OF CANCER CELLS	“ 2
<i>1.1.1. Self-Sufficiency in Growth Signals</i>	“ 2
<i>1.1.2. Insensitivity to Antigrowth Signals</i>	“ 3
<i>1.1.3. Evading Apoptosis</i>	“ 4
<i>1.1.4. Limitless Replicative Potential</i>	“ 5
<i>1.1.5. Sustained Angiogenesis</i>	“ 6
<i>1.1.6. Tissue Invasion and Metastasis</i>	“ 7
1.2. Genome Instability	“ 7
2. HEAT SHOCK PROTEINS	“ 10
2.1. HSP90: more than a folding tool	“ 14
2.2. HSP90: the cancer chaperone	“ 16
<i>2.2.1. Process of Carcinogenesis</i>	“ 17
<i>2.2.2. HIF: pathways and binding partners</i>	“ 18
<i>2.2.3. HSP90 inhibitors: targeting signal transduction in cancer</i>	“ 20
2.3. EXTRACELLULAR HSP90: CHAPERONING IMMUNE RESPONSE AND CELL INVASION	“ 22
3. AIM OF THE WORK	“ 25
4. RESULTS AND DISCUSSION	“ 26
4.1. Leads Identification	“ 26
4.1.1. Structure of Hsp90	“ 26
<i>4.1.1a N-Terminal Domain—Nucleotide and Drug Binding</i>	“ 27
<i>4.1.1b Middle Segment—Client Protein Binding and Catalytic Loop</i>	“ 28
<i>4.1.1c C-Terminal Domain—Dimerization</i>	“ 29
4.1.2. Multivariate protocol	“ 29
4.1.3. Pharmacophore Based Virtual Screening	“ 35
4.2. Synthetic methodologies for the selected leads	“ 39
<i>4.2.1. Annelated triazolopyrimidines</i>	“ 39
<i>4.2.2. Dihydropyrazoles and amino-cyanopyridines</i>	“ 46
4.3. Biological Activity	“ 52
5. CONCLUSION	“ 70
6. EXPERIMENTAL SECTION	“ 71
6.1. Chemistry	“ 71
6.2. Biology	“ 93
REFERENCES	“ 97

1. INTRODUCTION

In recent years cancer has become less of an enigma. After decades of rapid advances in cancer research, several lines of evidence indicate that during the course of tumor progression, cancer cells gradually acquire a number of dynamic genetic alterations, that drive the progressive transformation of normal human cells into highly malignant derivatives [1].

Most tumors are formed by a stepwise progression of cells from a transformed but minimally altered state, that can grow and form nodules or polyps (in solid tumors) to a multiply deviated state that is capable of unlimited growth, manipulation of local environment, invasion of surrounding tissues and escape into the circulation to found new colonies of secondary tumors and metastases. Such a progression involves diverse molecular and morphological changes. In fact the foundation has set in the discovery of mutations that produce oncogenes with dominant gain of function and tumor suppressor genes with recessive loss of function.

Over the past decades, the research has revealed a small number of molecular, biochemical, and cellular traits—acquired capabilities—shared by most and perhaps all types of human cancer. Our faith in such simplification derives directly from the teachings of cell biology that virtually all mammalian cells carry a similar molecular machinery regulating their proliferation, differentiation, and death.

These observations have been rendered more concrete by a large body of work indicating that the genomes of tumor cells are invariably altered at multiple sites, having suffered disruption through lesions as both subtle point mutations and obvious changes in chromosome complement. Transformation of cultured cells is itself a multistep process: rodent cells require at least two introduced genetic changes before they acquire tumorigenic competence, while their human counterparts are more difficult to transform.

The barriers to development of cancer are embodied in a teleology: cancer cells have defects in regulatory circuits that govern normal cell proliferation and homeostasis. The vast catalog of cancer cell genotypes is a manifestation of six essential alterations in cell physiology [2], that collectively dictate malignant growth:

1. self-sufficiency in growth signals,
2. insensitivity to growth-inhibitory (antigrowth) signals,
3. evasion of programmed cell death (apoptosis),

4. limitless replicative potential,
5. self-sustained supply of nutrients and oxygen (angiogenesis),
6. capacity to tissue invasion and metastasis.

Each of these physiologic changes—novel capabilities acquired during tumor development—represents the successful breaching of an anticancer defense mechanism hardwired into cells and tissues. These six capabilities are shared by several types of human tumors (Fig. 1).



Figure 1. *Acquired capability of cancer cells*

1.1. Hallmark of Cancer Cells

1.1.1. Self-sufficiency in Growth Signals

Normal cells require mitogenic growth signals (GS) before they can move from a quiescent state into an active proliferative state. These signals are transmitted into cell by transmembrane receptors that bind distinctive classes of signaling molecules: diffusible growth factors, extracellular matrix components, and cell-to-cell adhesion/interaction molecules. No type of normal cell can proliferate in the absence of such stimulatory signals.

Dependence on growth signaling is apparent when propagating normal cells in culture, which typically proliferate only when supplied with appropriate diffusible mitogenic factors and a proper substratum for their integrins. Such a behaviour

contrasts strongly with that of tumor cells, which invariably show a greatly reduced dependence on exogenous growth stimulation. The conclusion is that tumor cells generate many of their own growth signals, thereby reducing their dependence on stimulation from their normal tissue microenvironment. This liberation from dependence on exogenously derived signals disrupts a critically important homeostatic mechanism that normally operates to ensure a proper behaviour of the various cell types within a tissue.

Three common molecular strategies for achieving autonomy are evident, involving alteration of extracellular growth signals, of transcellular transducers of those signals, or of intracellular circuits that translate those signals into action.

While most soluble mitogenic growth factors (GFs) are made by one cell type in order to stimulate proliferation of another—the process of heterotypic signaling—many cancer cells acquire the ability to synthesize GFs, to which they are responsive, creating a positive feedback signaling loop often termed autocrine stimulation. Clearly, the manufacture of a GF by a cancer cell obviates dependence on factors from other cells within the tissue. The cell surface receptors, that transduce growth stimulatory signals into the cell interior, are themselves targets of deregulation during tumor pathogenesis. GF receptors, often carrying tyrosine kinase activities in their cytoplasmic domains, are overexpressed in many cancers.

1.1.2. Insensitivity to Antigrowth Signals

Within a normal tissue, multiple antiproliferative signals operate to maintain cellular quiescence and tissue homeostasis. These signals include both soluble growth inhibitors and immobilized inhibitors embedded in extracellular matrix and on the surfaces of nearby cells. These growth-inhibitory signals, like their positively acting counterparts, are received by transmembrane cell surface receptors coupled to intracellular signaling circuits. Antigrowth signals can block proliferation by two distinct mechanisms. Cells may be forced out of the active proliferative cycle into the quiescent (G_0) state from which they may reemerge on some future occasion when extracellular signals permit. Alternatively, cells may be induced to permanently relinquish their proliferative potential by being induced to enter into postmitotic states, usually associated with acquisition of specific differentiation-associated traits. Incipient cancer cells must evade these antiproliferative signals if they are to prosper. Much of the circuitry that enables normal cells to respond to antigrowth signals is

associated with the cell cycle clock, specifically the components governing the transit of the cell through the G₁ phase of its growth cycle. Cells monitor their external environment during this period and, on the basis of sensed signals, decide whether to proliferate, to be quiescent, or to enter into a postmitotic state. Cell proliferation depends on more than an avoidance of cytostatic antigrowth signals, involved in signaling pathways. These converge on retinoblastoma-related proteins, which govern cell transit through the G₁ phase of the cell division cycle. Hypophosphorylated retinoblastoma blocks proliferation by sequestering and altering the function of E2F transcription factors, which control the expression of a wide variety of genes essential for progression from G₁ to S phase.

1.1.3. Evading Apoptosis

The ability of tumor cell populations to expand in number is determined not only by the rate of cell proliferation but also by the rate of cell attrition. Programmed cell death—apoptosis—represents a major source of this attrition. The apoptotic program is present in latent form in virtually all cell types throughout the body. Once triggered by a variety of physiologic signals, this program unfolds in a series of steps. Cellular membranes are disrupted, the cytoplasmic and nuclear skeletons are broken down, the cytosol is extruded, the chromosomes are degraded and the nucleus is fragmented. The apoptotic machinery can be broadly divided into two classes of components—sensors and effectors. The sensors are responsible for monitoring the extracellular and intracellular environment for conditions of normality or abnormality that influence whether a cell should live or die. These signals regulate the second class of components, which function as effectors of apoptotic death. The sentinels include cell surface receptors that bind survival or death factors.

Intracellular sensors monitor the cell's well-being and activate the death pathway in response to detecting abnormalities, including DNA damage, signaling imbalance provoked by oncogene action, survival factor insufficiency, or hypoxia. Further, the life of most cells is in part maintained by cell–matrix and cell–cell adherence-based survival signals whose abrogation elicits apoptosis. Both soluble and immobilized apoptotic regulatory signals likely reflect the needs of tissues to maintain their constituent cells in appropriate architectural configurations.

Altering components of the apoptotic machinery can dramatically affect the dynamics of tumor progression, providing a rationale for the inactivation of this

machinery during tumor development [3]. Resistance to apoptosis can be acquired by cancer cells through a variety of strategies. Apoptosis can be inhibited by the activation of prosurvival signaling pathways, while, at same time, the decreased expression of proapoptotic factors. Signals evoked by other abnormalities, including hypoxia and oncogene hyperexpression, are also centralized in part *via* p53 to the apoptotic machinery.

1.1.4. Limitless Replicative Potential

Three acquired capabilities—growth signal autonomy, insensitivity to antigrowth signals, and resistance to apoptosis—all lead to an uncoupling of a cell's growth program from signals in its environment. In principle, the resulting deregulated proliferation program should suffice to enable the generation of the vast cell populations that constitute macroscopic tumors. This acquired disruption of cell-to-cell signaling does not ensure expansive tumor growth. Many and perhaps all types of mammalian cells carry an intrinsic, cell-autonomous program that limits their multiplication. This program appears to operate independently of the cell-to-cell signaling pathways described above. It too must be disrupted in order for a clone of cells to expand to a size that constitutes a macroscopic, life threatening tumor. Cells in culture have a finite replicative potential. Once such cell populations have progressed through a certain number of doublings, they stop growing—a process termed senescence. The senescence of cultured human fibroblasts can be circumvented by disabling their pRb and p53 tumor suppressor proteins, enabling these cells to continue multiplying for additional generations until they enter into a second state termed crisis. The crisis state is characterized by massive cell death, karyotypic disarray associated with end-to-end fusion of chromosomes, and the occasional emergence of a variant cell that has acquired the ability to multiply without limit, the trait termed immortalization. Most types of tumor cells that are propagated in culture appear to be immortalized, suggesting that limitless replicative potential is a phenotype that was acquired *in vivo* during tumor progression and was essential for the development of their malignant growth state. This result suggests that at some point during the course of multistep tumor progression, evolving premalignant cell populations, exhaust their endowment of allowed doublings and can only complete their tumorigenic agenda by breaching the mortality barrier and acquiring unlimited replicative potential. The evolving premalignant and malignant

cell populations evidence chronic, widespread apoptosis and consequently suffer considerable cell attrition concomitant with cell accumulation. Thus, the number of cells in a tumor greatly under-represents the cell generations required to produce it, the generational limit of normal somatic cells as a barrier to cancer. Replicative generations are counted by the 50–100 bp loss telomeric DNA from the ends of every chromosome during each cell cycle. This progressive shortening has been attributed to the inability of DNA polymerases to completely replicate the 3' ends of chromosomal DNA during each S phase. The progressive erosion of telomeres through successive cycles of replication eventually causes them to lose their ability to protect the ends of chromosomal DNA. The unprotected chromosomal ends participate in end-to-end chromosomal fusions, yielding the karyotypic disarray associated with crisis and resulting, almost inevitably, in the death of the affected cell. Telomere maintenance is evident in virtually all types of malignant cells; 85%–90% of them succeed in doing so by upregulating expression of the telomerase enzyme, which adds hexanucleotide repeats onto the ends of telomeric DNA, while the remainder have invented a way of activating a mechanism, termed ALT, which appears to maintain telomeres through recombination-based interchromosomal exchanges of sequence information transitory.

1.1.5. Sustained Angiogenesis

The oxygen and nutrients supplied by the vasculature are crucial for cell function and survival, obligating virtually all cells in a tissue to reside within 100 μ m of a capillary blood vessel. During organogenesis, this closeness is ensured by coordinated growth of vessels and parenchyma. Once a tissue is formed, the growth of new blood vessels—the process of angiogenesis—is transitory and carefully regulated. Because of this dependence on nearby capillaries, it would seem plausible that proliferating cells within a tissue would have an intrinsic ability to encourage blood vessel growth. Angiogenic ability is acquired during tumor development *via* an angiogenic exchange from vascular quiescence.

One common strategy for shifting the balance involves altered gene transcription. The coordinated expression of other pro- and anti-angiogenic signaling molecules, such as thrombospondin, growth factors, integrin or plasmin, and their modulation by proteolysis, appear to reflect the complex homeostatic regulation of normal tissue angiogenesis and of vascular integrity.

1.1.6. Tissue Invasion and Metastasis

During the development of most types of human cancer, primary tumor masses spawn pioneer cells that move out, invade adjacent tissues, and thence travel to distant sites where they may succeed in founding new colonies [4]. These distant settlements of tumor cells—metastases—are the cause of 90% of human cancer deaths. The capability for invasion and metastasis enables cancer cells to escape the primary tumor mass and colonize new terrain in the body where, at least initially, nutrients and space are not limiting. The newly formed metastases arise as amalgams of cancer cells and normal supporting cells conscripted from the host tissue. Several classes of proteins, involved in the cellular functions towards their surroundings in a tissue, are altered and possessed invasive or metastatic capabilities. The affected proteins include cell–cell adhesion molecules (CAMs)—notably members of the immunoglobulin and calcium-dependent cadherin families, both of which mediate cell-to-cell interactions—and integrins, which link cells to extracellular matrix substrates.

The second general parameter of the invasive and metastatic capability involves extracellular proteases. Protease genes are upregulated, protease inhibitor genes are downregulated, and inactive zymogen forms of proteases are converted into active enzymes. Matrix-degrading proteases, such as metalloproteinase-2, are characteristically associated with the cell surface, by synthesis with a transmembrane domain, binding to specific protease receptors, or association with integrins. The matrix metalloproteinase-2 (MMP2) can degrade the matrix, providing cancer cells with access to the vasculature and lymphatic system, allowing tumor dissemination.

1.2. Genome Instability

The available evidence suggests that most of those physiologic changes are acquired, directly or indirectly, through changes in the genomes of cancer cells. But mutation of specific genes is an inefficient process, reflecting the unceasing, fastidious maintenance of genomic integrity by a complex array of DNA monitoring and repair enzymes. Malfunction of specific components of these genomic “caretaker” systems has been invoked to explain this increased mutability. A growing number of genes involved in sensing and repairing DNA damage, or in assuring correct chromosomal

segregation during mitosis, is found to be lost in different cancers, labeling these caretakers as tumor suppressors. Their loss of function is envisioned to allow genome instability and variability and the generation of consequently mutant cells with selective advantages.

These cancer-associated hallmark characteristics actually reflect genetic alterations in multiple ‘safeguard’ genes of the cell, namely oncogenes and tumor suppressor genes. These genes are responsible for the regulation of signal transduction molecules, including among others receptor tyrosine kinases (RTKs), products of the Ras and Raf genes, and protein kinases, as mitogen-activated protein kinase (MAPK), phosphoinositide 3-kinase (PI3K) and Akt. These molecules in normal cells control the tight coordination of diverse processes such as cell survival, proliferation, growth, differentiation and motility.

All of these proteins belong to various ‘signal transduction’ pathways, which refer to the flow of biological information from the cell’s micro-environment (extracellular matrix, neighbouring cells) *via* detection systems, such as surface receptors and through intermediate molecules, inside the cell (Fig. 2). The latter include a wide array of intracellular elements interacting through cascades of chemical signals and ultimately controlling the activities of specific intracellular effectors, resulting in the tight coordination of fundamental processes of cellular life.

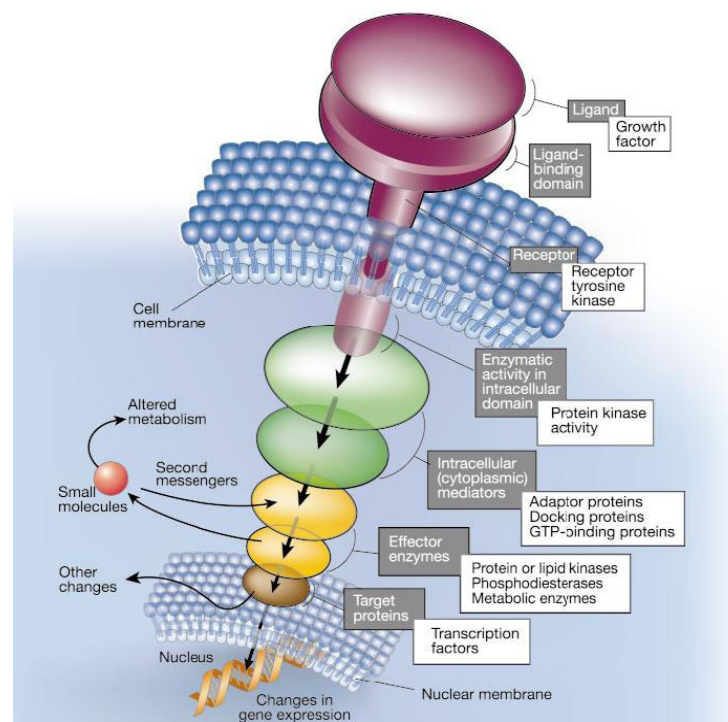


Figure 2. Signal transduction pathways

Signaling pathways are not isolated from each other, but instead they are interconnected, forming a labyrinth of intersecting and overlapping networks, enhancing thus the robustness and diversity of signaling and permitting fine-tuning and amplification or attenuation of the output [5].

Advances in the understanding of aberrant signaling pathways in various types of cancers have directly promoted the development of targeted therapies, that is the development of drugs that influence the action and/or activity of a specific signaling molecule. Elucidation of the roles of many kinase signaling pathways in cancer, including growth factor receptors and their downstream effectors, along with the identification of kinases as an attractive drug-target class, has led to the expectation of innovating cancer-treatment strategies with more specific mechanisms of action than conventional chemotherapeutic agents. However, the crucial challenge to select appropriate targets/approaches in cancer therapeutics still remains.

The genetic instability of many tumor diseases represents one of the most difficult obstacles to overcome. In the last decades, promising efforts have been made in the improvement of chemotherapy regimens through the development of novel and more selective therapeutic agents. However the massive exposure to a previous successful chemotherapy scheme activates multiple overlapping signal pathways, with the global effect to protect the cancer cells from further harm. Therefore, it is clear why the understanding of molecular mechanisms underlying the multi-factorial stress response is of great importance in the drug design phase of cancer therapy. From early 1990s, several groups [6-9] reported that the cells respond to stresses by increasing the synthesis of a number of molecular chaperones known as heat shock proteins (because they first were observed in cells exposed to high temperatures).

2. HEAT SHOCK PROTEINS

Heat shock proteins (HSPs) were first discovered in 1962 as a small set of highly evolutionary conserved family of proteins whose expression increased in response to a variety of different metabolic insults. Despite their designation, most of the HSPs are constitutively expressed and perform essential functions. Most important is their role as molecular chaperones, facilitating the synthesis and folding of proteins throughout the cell. In addition, HSPs have been showed to participate in proteins assembly, secretion, trafficking, protein degradation, and in the regulation of transcription factors and protein kinases [10-13]. Increased levels of HSPs after several types of stress plays a central role in cellular homeostasis [14] (Table 1).

Table 1. Type of stresses in cellular homeostasis

STRESS OR STRESSOR TYPE	NAME OR DESCRIPTION
Physical	Heat (including fever, cold, several types of irradiation, including ultraviolet light, and magnetic fields)
Oxygen	Oxygen derived free radicals (reactive oxygen species), hydrogen peroxide, a shift from anaerobiosis to aerobiosis (e.g. reperfusion), hypoxia-anoxia (ischemia)
pH	Alkalosis, acidosis, pH shift
Biologic	Infection, inflammation, fever
Psychological	Emotion, emotional conflicts, hormonal imbalance (hypothalamic-pituitary, adrenal axis, and autonomic nervous system)
Osmotic	Changes in the concentrations of salt, sugar, and other osmolytes (hyperosmotic or hypoosmotic shock)
Nutritional	Starvation involving multiple nutritional components (carbon, glucose, nitrogen, phosphate, and nitrate) or anyone of these
Antibiotics	Puromycin, tetracycline, nalidixic acid, doxorubicin
Alcohols	Ethanol, methanol, butanol, propanol, octanol
Metals	Cadmium, copper, chromium, zinc, tin, aluminum, mercury, lead, nickel
Mechanical	Compression, shearing, stretching
Other	Desiccation, benzene and derivatives, phenol and derivatives, teratogens, carcinogens, mutagens, arsenite, arsenate, amino acid analogs, nicotine, anesthetics, insecticides, pesticides

All organisms exhibit homeostatic-like responses when subjected to rapid changes in their environment. The ability of the organism to successfully adapt or acclimate to its new environment is critical to its survival, and likely represents an integral driving force in evolution. One well studied response to sudden adverse environmental changes is the so-called heat shock or stress response. When

confronted with physiologically relevant increases in temperature, cells from all organisms respond similarly by rapidly increasing the synthesis of a select group of proteins, the HSPs. Changes in the expression of the HSPs are controlled by a set of transcription factors referred to as heat shock factors (HSFs). The resultant increase and accumulation of the HSPs now gives the stressed cell added protection, thereby allowing for continued cell survival. In addition to increased temperatures, other insults also result in increased HSP expression. These include exposure of cells to various metals, amino acid analogues, hypoxia, and a large number of agents/treatments which result in reduced ATP levels. Therefore many adverse conditions lead to increased HSP expression, the heat shock response now is commonly referred to as the “stress response.” Despite their designation as HSPs or stress proteins, almost all of these proteins are in fact synthesized in cells grown under normal conditions (i.e. constitutive) and that their expression increases (i.e. induced) after metabolic stress. The realization that many of the HSPs function as “molecular chaperones” helps explain why these proteins are so critical for normal growth, as well as the ability of the cell to survive different metabolic insults [15]. Specifically, in their role as molecular chaperones, the different HSPs facilitate the early stages of folding and assembly of other cellular proteins. Although they do not convey any information for the folding or assembly process, molecular chaperones act by stabilizing maturing polypeptides and thereby reduce the probability of incorrect folding or aggregation. Thus, under normal growth conditions where they are expressed at modest levels, members of the HSP family participate in the early stages of protein synthesis, protein folding, and the transport of newly synthesized proteins from the cytoplasm into different intracellular compartments (Fig. 3).

Under conditions of stress, where protein folding/assembly events may be compromised, the increased expression and accumulation of the stress proteins facilitates the ability of cells to both repair and synthesize new proteins to replace those that were damaged after the particular metabolic insult. In addition to their critical role in cellular homeostasis, the stress response proteins are implicated in human disease. Various medical conditions, including fever, ischemia, hemodynamic overload or neurological injuries are well known activators of the stress response *in vivo*. The ability of the affected tissue or organ to mount a robust stress response is thought to be important for its survival and recovery. In infectious diseases, stress

proteins present within different pathogens are known to be major targets of our immune system.

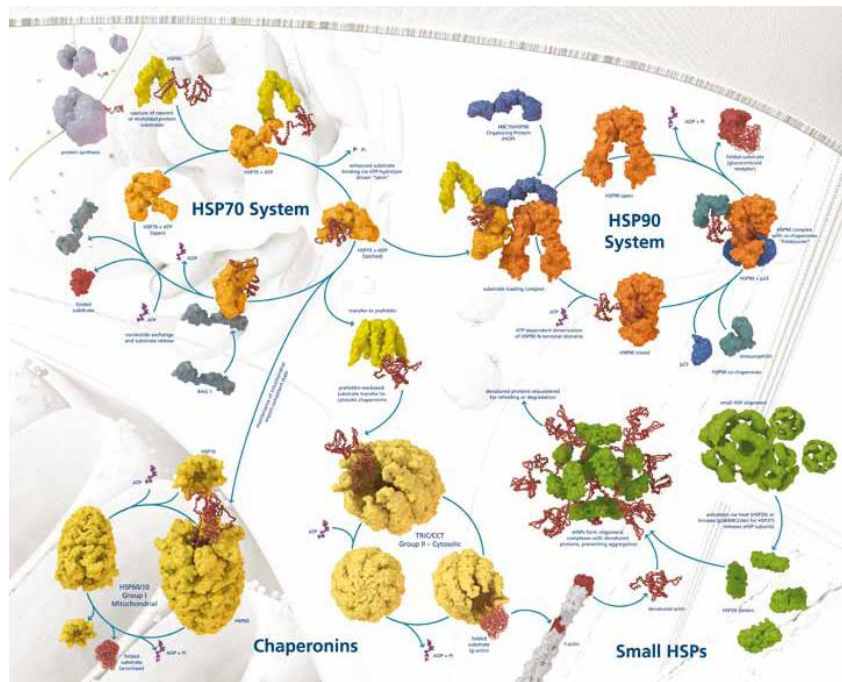


Figure 3. The HSP system

Among the members of the family, the 90-kDa heat shock protein (Hsp90) is the most abundant, representing almost 1% of total cellular protein in unstressed cells [16], where it performs housekeeping functions, controlling the stability, maturation, activation, intracellular disposition and proteolytic turn-over of “client proteins” [17].

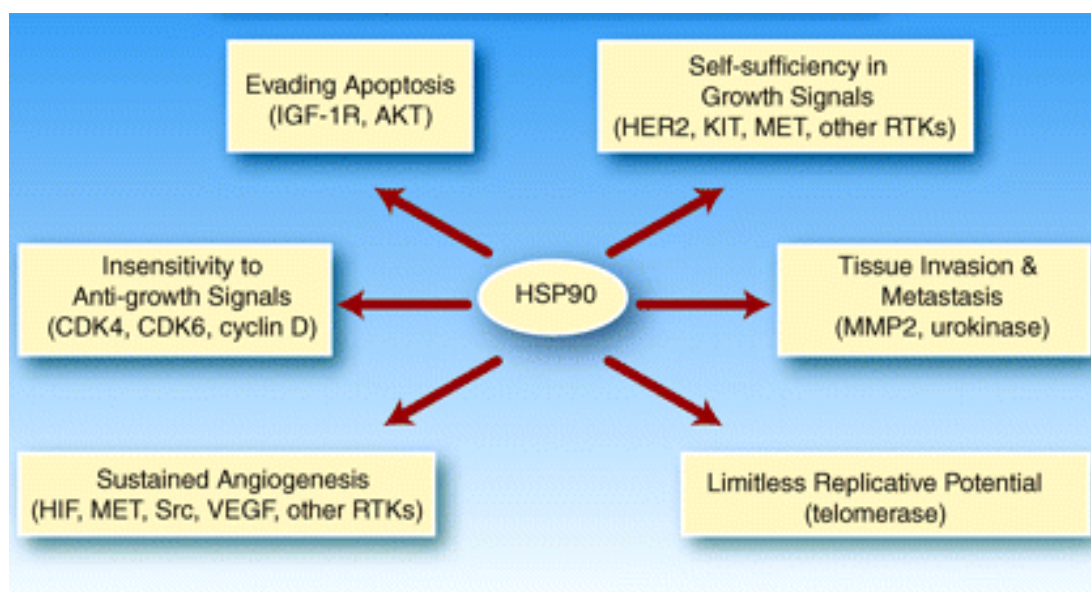


Figure 4. Hsp90 and the six hallmarks of cancer cell

Unlike some of the other well characterized HSPs whose chaperone role involves their interaction with many cellular proteins, Hsp90 exhibits some selectivity for a distinct set of “client proteins”, including mutant p53, HER-2, HIF-1, Akt/PKB c-Raf -1, hTERT and CDK4 [18]. These are members of the “most-wanted” list of proteins considered responsible for the multiple hallmark traits of malignancy (Fig. 4, Table 2).

Table 2. Hsp90 clients and the multiple hallmarks of cancer

Cancer-associated Cellular Traits	Hsp90 Client Proteins
Self-sufficiency in growth signals	MEK SRC tyrosine kinases Steroid hormone receptors
Insensitivity to antigrowth signals	Akt CDK2, CDK4 HIF-1 α RTKs SRC tyrosine kinases Steroid hormone receptors
Evading apoptosis	Akt RTKs Survivin
Tissue invasion and metastasis	MMP2
Limitless replicative potential	CDK2, CDK4 Telomerase
Sustained angiogenesis	VEGFR2 HIF-1 α

Thus, for example, when GF receptors, overexpressed in many cancers, often carry tyrosine kinase activities in their cytoplasmic domains, many of these are client proteins of the molecular chaperone, Hsp90, involved in their assembly, stability and degradation [11, 19]. Increased activity of these kinases, because of overexpression or activating mutations, is strongly correlated with cancer progression. In particular, the cell surface tyrosine kinase ErbB2 has confirmed role in tumorigenesis. In animal mode, overexpression of this protein (~30% in breast and prostate cancer) was observed in specific tissues. The stability of the ErbB2 protein is inherently dependent on Hsp90, and inhibition of Hsp90 causes a dramatic decrease in ErbB2 protein level, both in cultured cells and in animal tumor model.

Moreover, in the acquired insensitivity in growth signals, when the function of E2F transcription factors is altered by phosphorylation by activated cyclin-dependent kinase 4 (CDK4), retinoblastoma protein is inactivated and its inhibition of E2F is relaxed, enabling the cell to traverse the cell cycle. CDK4 is a client protein of Hsp90, and Hsp90 inhibitors induce degradation of CDK4 [20]. Hence, inhibition of

Hsp90 function is expected not only to block cancer cells from entering the cell cycle, but also to block their progress through that cycle.

In the case of tumor dissemination, as well, although Hsp90 is an intracellular chaperone, it has recently been found at cell membrane of highly metastatic cancer cells. A more recent study has shown the Hsp90 involvement in maturation of the cell surface enzyme matrix metalloproteinase, in fact it was found to form a complex with cell surface Hsp90, therefore the chaperone is required for cancer invasion and metastasis [21].

When the limitless replicative potential is concerned, both the assembly of telomerase and the enzymatic activity to permit unlimited chromosomal replication, require the function of Hsp90 [22]. Thus, its inhibition significantly decreases telomerase activity, reverses the inhibition of telomerase shortening, and limits the replication potential of cancer cells.

2.1. Hsp90: more than a Folding Tool

Hsp90 is a highly conserved and essential stress protein, expressed throughout the eukaryotic lineage. Higher eukaryotes possess multiple Hsp90 homologues, including the highly conserved Hsp90- α and Hsp90- β isoforms (86% amino acid conservation) which are mainly cytoplasmic, GRP94 in the endoplasmic reticulum, and TRAP1 in the mitochondrial matrix. Although the Hsp90 bacterial homolog HtpG is typically nonessential, eukaryotes require a functional cytoplasmic Hsp90 for survival under all conditions tested. Indeed whereas the term ‘heat shock protein’ is perfectly appropriate for other HSPs, it is really somewhat of a misnomer for Hsp90. Hsp90, like many of HSPs, exerts its molecular chaperone activity by conformational cycles of binding and release which are dependent upon its ATPase activity [23,24] (Fig. 5).

This ATP-driven conformational cycle is regulated by specific co-chaperones, such as Hsp70, Hop, immunophilins, cdc37 and p23, that complex with Hsp90 and assemble into the Hsp90 chaperone machinery, in order to assist the loading and release of client proteins (Fig. 6).

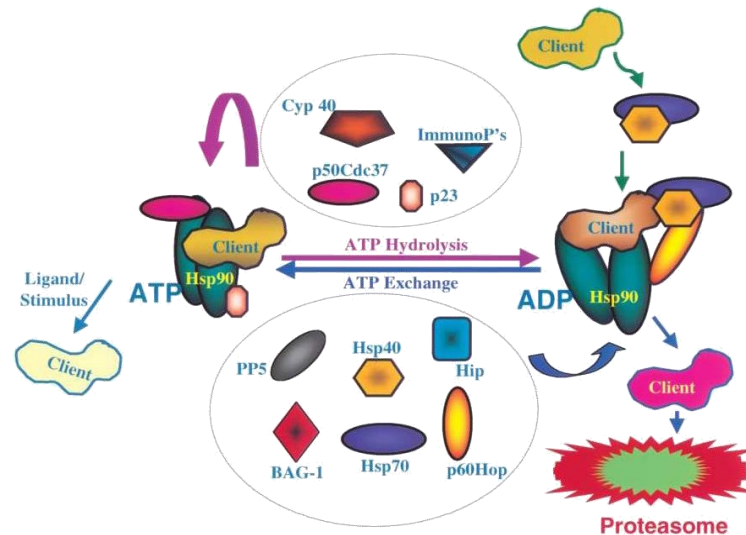


Figure 5. Nucleotide-dependent cycling of the Hsp90-based super-chaperone machine. Hsp90 forms the basis of a super-chaperone machine that promotes the proper folding of client proteins so that they can respond to a stimulus or bind ligand. However, the machine is in constant flux and cycles between two Hsp90 conformations, determined by nucleotide binding, which in turn specify which set of cochaperones associate with the chaperone complex. Cochaperones that can associate with one conformation or the other include p23, p50Cdc37, p60Hop, immunophilins, cyclophilins, Hsp70, Hip, phosphatase PP5, Hsp40, and BAG-1. Cycling of this machine is driven by ATP hydrolysis. Although Hsp90 is a weak ATPase, its activity is regulated by cochaperones and dramatically enhanced by client protein binding. A client protein's half-life may be stochastically determined by the length of time it resides in association with the Hsp90-Hsp70 form of the chaperone machine, because at this time, the client protein is susceptible to ubiquitination and delivery to the proteasome.

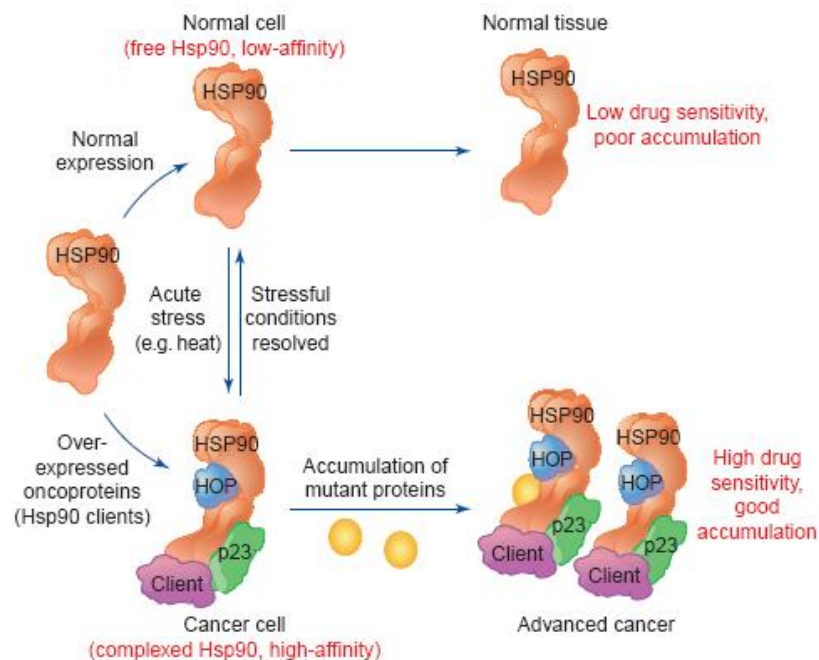


Figure 6. Model for tumor selectivity of Hsp90 inhibitors and Hsp90-dependent malignant progression. Hsp90 in normal cells exists in an uncomplexed form that has low affinity for Hsp90 inhibitor drugs, which accumulate poorly in normal tissues, and normal cells exhibit poor drug sensitivity. By contrast, the Hsp90 in cancer cells is involved in the active chaperoning of overexpressed oncoproteins and exists in a complexed form with co-chaperone proteins (p23 and Hop are not in the same complex). Complexed Hsp90 in cancer cells exhibits high-affinity binding to Hsp90 inhibitor drugs, which accumulate in tumor tissues, and tumor cells exhibit good drug sensitivity. This model predicts that the accumulation of mutant proteins in advanced cancer would further increase Hsp90 usage and make tumor cells more Hsp90 dependent. Furthermore, this model suggests that the high-affinity change of Hsp90 can be driven by the overexpression of oncoproteins, as well as by stressful conditions in normal cells (e.g. heat).

These key-components of the cell's signaling machinery are often activated, mutated and/or over-expressed in cancer cells and are considered responsible for the acquisition of the malignant phenotype. Subsequently, Hsp90 is viewed as a key player in the subversion of normal cells towards transformation and therefore an exciting new target for the development of innovating molecular cancer therapeutics.

2.2. Hsp90: the Cancer Chaperone

Hsp90, playing a pivotal role in the acquisition and maintenance of the malignant phenotype, is expressed in malignant cells from 2- to 10- fold higher than in normal cells [25]. These higher expression levels are coupled to multiple fundamental oncogenic pathways and indicate a crucial role associated with the development and maintenance of the malignant phenotype as well as the acquisition of drug resistant phenotypes. The abundance of Hsp90 in tumors in part reflects an appropriate cytoprotective stress response to the hostile hypoxic, acidotic and nutrient-deprived tumor microenvironment. Consequently, the increased activities of this molecular chaperone allow tumor cells to cope and adapt to environmental changes as well as to the imbalanced signaling, associated with neoplastic transformation, and thereby to escape apoptosis [26]. Malignant transformation involves the over-expression and/or mutation of multiple Hsp90-dependent key-regulators of cellular growth. Almost 50 proteins known to play important roles in the control of cell cycle and growth, including receptor protein kinases and transcription factors have been identified as oncogenic clients of Hsp90. It is indispensable for maintaining these proteins in an active conformation, and thereby it is considered to drive the cell to self-sufficiency in growth signals. Moreover, Hsp90 confers survival advantages to cancer cells through its association with important elements of apoptosis such as the Akt-survival pathway and the Raf/MAPK growth regulatory pathway. Finally, Hsp90 plays important anti-apoptotic roles by interfering with the intrinsic caspase apoptotic pathway. In addition to permitting autonomous growth and facilitating cell survival with respect to stressful environmental challenges, Hsp90 also allows tumor cells to tolerate genetic alterations, including mutations of critical signaling molecules that would otherwise be lethal. It not only moderates the impact of potentially lethal mutations in cancer cells, but also stabilizes and permits the accumulation of mutant proteins, therefore functioning as a capacitor of evolution.

Thus, Hsp90 might also serve as a biochemical buffer for the genetic instability frequently found in cancers. As a result of this capacity, phenotypic diversity within the tumor cell population increases and the evolution of invasive, metastatic and drug resistant phenotypes accelerates. To summarize, one can say that Hsp90 participates in almost all the key processes of oncogenesis, such as self-sufficiency in growth signals and stabilization of mutant proteins. The involvement of this molecular chaperone in the acquisition and maintenance of the transformed phenotype is particularly interesting and suggests that inhibiting Hsp90 may have a coordinated effect on all of the key alterations on which cancer cells depend for their growth and survival. Consequently it is no wonder that Hsp90 has emerged as a promising and exciting target for the development of cancer therapeutics.

2.2.1. Process of Carcinogenesis

The ability of a tumor to induce the formation of a tumor vasculature has been termed the “angiogenic switch” and can occur at different stages of the tumor progression pathway depending on the type of tumor and the environment [27]. Acquisition of the angiogenic phenotype can result from genetic changes or local environmental changes that lead to the activation endothelial cells (ECs). One way for a tumor to activate ECs is through the secretion of proangiogenic growth factors, which then bind to receptors on nearby latent ECs that line the interior of vessels, leading to vasodilatation and increase in vessel permeability. The ECs migrate and proliferate to form new branches from the pre-existing vasculature by detaching from the extracellular matrix and basement membrane (Fig. 7).

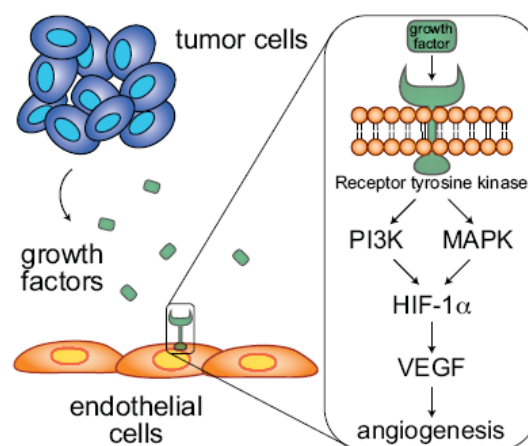


Figure 7. Tumor cells secrete proangiogenic growth factors. PI3K indicates phosphoinositide 3-kinase; MAPK, mitogen-activated protein kinase; HIF-1, hypoxia inducible factor-1; VEGF, vascular endothelial growth factor.

The proangiogenic growth factors may be overexpressed because of genetic alterations of oncogenes and tumor suppressors, or in response to the reduced availability of oxygen. Tumor cell expression of many of the angiogenic factors, including vascular endothelial growth factor (VEGF), is regulated by hypoxia through the transcription factor hypoxia inducible factor (HIF) [28]. As the tumor cells proliferate, oxygen becomes depleted and a hypoxic microenvironment occurs within the tumor. HIF is degraded in the presence of oxygen, and therefore formation of hypoxic conditions leads to HIF activation and transcription of target genes (Fig. 8). The strongest activation of HIF results from hypoxia, but several other factors can contribute to the increased expression and activity of HIF, including growth factors and cytokines such as tumor necrosis factor- α (TNF- α), interleukin-1 β (IL-1 β), epidermal growth factor (EGF), and insulin-like growth factor-1 (IGF-1), which lead to increased cell signaling. Along similar lines, oncogenes that trigger increased expression of growth factors and overactive signaling pathways can increase HIF expression and activity. For example, mutant Ras can contribute to tumor angiogenesis by enhancing the expression of VEGF through increased HIF activity. The oncogenes v-Src and HER2, PI3K and MAPK signaling pathways have also been shown to up-regulate HIF expression and HIF transcriptional activity.

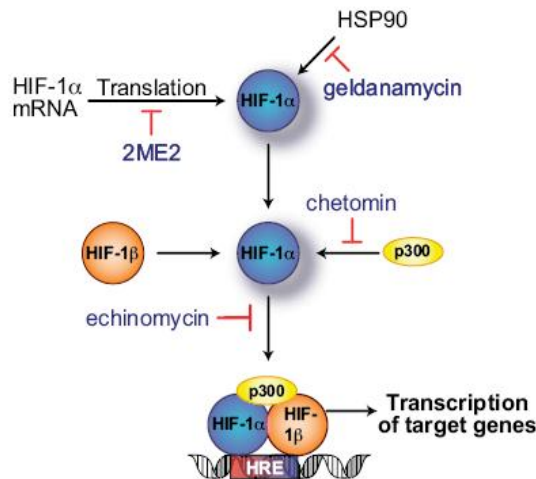


Figure 8. Examples of inhibitors known to act on hypoxia inducible factor and/or HIF regulatory pathways. 2ME2, 2-methoxyestradiol; HRE, hypoxia response element.

2.2.2. HIF: Pathways and Binding Partners

HIF is a transcription factor involved in cellular adaptation to hypoxia. HIF transcriptional activity is regulated by the presence of oxygen and becomes active in low oxygen conditions (hypoxia). It controls a large number of genes involved in

angiogenesis. The active HIF complex is comprised of an α and β subunit, in addition to coactivators including p300 and CREB binding protein (CBP). The HIF- β subunit (also known as ARNT) is a constitutive nuclear protein with additional roles in transcription not associated with HIF- α . In contrast to HIF- β , the levels of the HIF- α subunits and their transcriptional activity are regulated by oxygen availability. There are three related forms of human HIF- α (HIF-1 α , HIF-2 α , and HIF-3 α), each of which is encoded by a distinct genetic locus. HIF-1 α and HIF-2 α have been the best characterized, possessing similar domain structures that are regulated in a related manner by oxygen, although each isoform has distinct and separate roles. The role of HIF-3 α is not fully understood, although a truncated form of murine HIF-3 α , known as inhibitory Per/Arnt/Sim (PAS) domain protein (IPAS), has been found to act as an inhibitor of HIF *via* dimerization with HIF- β . Both the HIF- α and HIF- β subunits are produced constitutively, but in normoxia HIF-1 α and HIF-2 α are degraded by the proteasome in an oxygen-dependent manner. Hydroxylation of two prolines in HIF- α enables the protein to bind to the von Hippel-Lindau tumor suppressor protein (pVHL), which links HIF- α to a ubiquitin ligase complex. This ligase catalyzes polyubiquitinylation of HIF- α , targeting it for degradation by the proteasome. In addition, hydroxylation of an asparagine residue in HIF- α disrupts the interaction between HIF- α and the coactivator p300, through a process independent of proteasomal degradation, which leads to reduced HIF transcriptional activity. In this manner, asparaginyl hydroxylation acts as a regulatory switch controlling the activity and specificity of HIF gene expression, as opposed to the prolyl hydroxylations, which control HIF- α stability. In hypoxia, minimal to no hydroxylation occurs, enabling HIF- α to avoid proteasomal degradation and to dimerize with HIF- β and coactivators, forming the active transcription complex on the hypoxia response element (HRE) associated with HIF target genes (Fig. 9).

Because HIF regulates genes that enable cell survival in a hypoxic environment, including those involved in glycolysis, angiogenesis, and expression of growth factors, it has significance in the biology and regulation of tumor growth.

The central role of HIF in the activation of angiogenic-related genes makes it a promising target for the treatment of solid tumors, particularly because HIF-1 α and/or HIF-2 α are reported to be overexpressed in the majority of solid tumors. HIF-1 α (and occasionally HIF-2 α) overexpression in tumors has been found to be positively correlated with angiogenesis, aggressiveness, metastasis, and resistance to

radiation/chemotherapy and negatively correlated with disease progression, survival, and outcome.

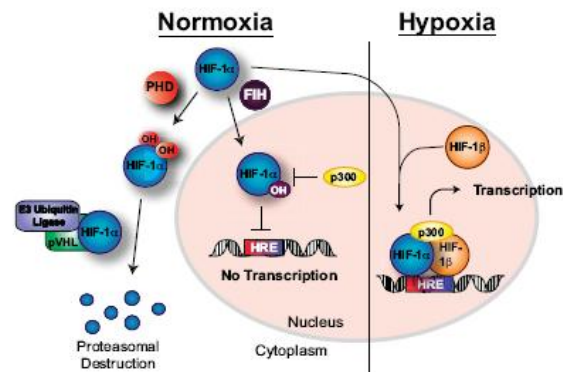


Figure 9. *HIF- α and HIF- β subunits are both produced constitutively in normoxia and in hypoxia*

Downstream from HIF-1 α , several factors regulate the proliferation and mobility of target vascular endothelial cells and at least two of these, VEGF and nitric oxide synthase, require Hsp90 or their induction and stability in vascular endothelial cells. Also HIF is regulated at the level of protein stability, and increased amount of Hsp90 is needed to mediate its stabilization and accumulation. HIF interacts with Hsp90 [29] and both geldanamycin (GA) and radicicol (the first discovered inhibitors, see below) reduce HIF-dependent transcriptional activity [9,30,31]. Hur et al. demonstrated that HIF from radicicol treated cells was unable to bind DNA [30], suggesting that Hsp90 is necessary for mediating the proper conformation of HIF and/or recruiting additional cofactors [32]. Additionally, GA downregulates HIF expression by stimulating the protein's VHL-independent proteasomal degradation [31].

2.2.3. Hsp90 Inhibitors: Targeting Signal Transduction in Cancer

The earliest inhibitor of Hsp90 was the natural product geldanamycin which is a member of the family of ansamycin antibiotics. This agent has featured in the literature for several years as an antitumor agent, and was originally isolated based on its ability to promote a significant decrease in the activity of oncogenic tyrosine kinases such as v-Src and ErbB-2. In 1994, Whitesell et al. [33] reported that ansamycins, and GA in particular, exerts its function by acting as a nucleotide mimetic and by binding specifically to the ATPase domain of Hsp90. This action

results in inhibition of its chaperone function, and consequently in the ubiquitination and degradation of client proteins by the proteasome pathway. Despite their promising activity as anticancer agents, these antibiotics proved to have limited clinical potential, because of their high liver toxicity and/or cellular instability. However, subsequent derivatization of GA yielded analogues with reduced liver toxicity, that however retained the potent antitumor activity of the parent compound. One such example is the analogue 17-allylamino-17-demethoxygeldanamycin (17AAG) which has already entered clinical trials [34-36].

Table 3. Hsp90 inhibitors

Name	Chemical Class	Binding Site
GA	Benzoquinone ansamycin	N-terminal ATP-binding pocket
17-AAG	GA-derivative	N-terminal ATP-binding pocket
17-DMAG	GA-derivative	N-terminal ATP-binding pocket
Radicol	Macrolide	N-terminal ATP-binding pocket
PU24FC1	Purine scaffold	N-terminal ATP-binding pocket
CCT018159	Pyrazole	N-terminal ATP-binding pocket
Radamycin	Hybrid	N-terminal ATP-binding pocket
Novobiocin	Noviosylcoumarin crosslinker	C-terminus

At present, several derivatives of natural products or fully synthetic small-molecule drugs that target Hsp90 have been discovered as potential anticancer agents (Table 3, Fig. 10). These drugs are considered as unique in that, although they are directed against a specific molecular target, they simultaneously inhibit multiple signaling pathways by inactivating, destabilizing, and eventually leading to degradation of numerous chaperone dependent client proteins. As a consequence they are competent to mount a multi-pronged assault on cancer cells. Moreover, although initially there were concerns that Hsp90 targeted drugs would attack proteins expressed both in normal and malignant cells, and thus would lack specificity and cause damage to normal tissues, these fears were proved unfounded. Interestingly, exclusively tumor cells were shown to exhibit sensitivity to Hsp90 inhibition, thus lending credence to the feasibility of selectively targeting cancer

tissues *via* the pharmacological modulation of Hsp90 function [37,38]. Even more remarkably, Hsp90 inhibitors sensitize tumor cells to the cytotoxic effects of a variety of standard therapeutic agents.

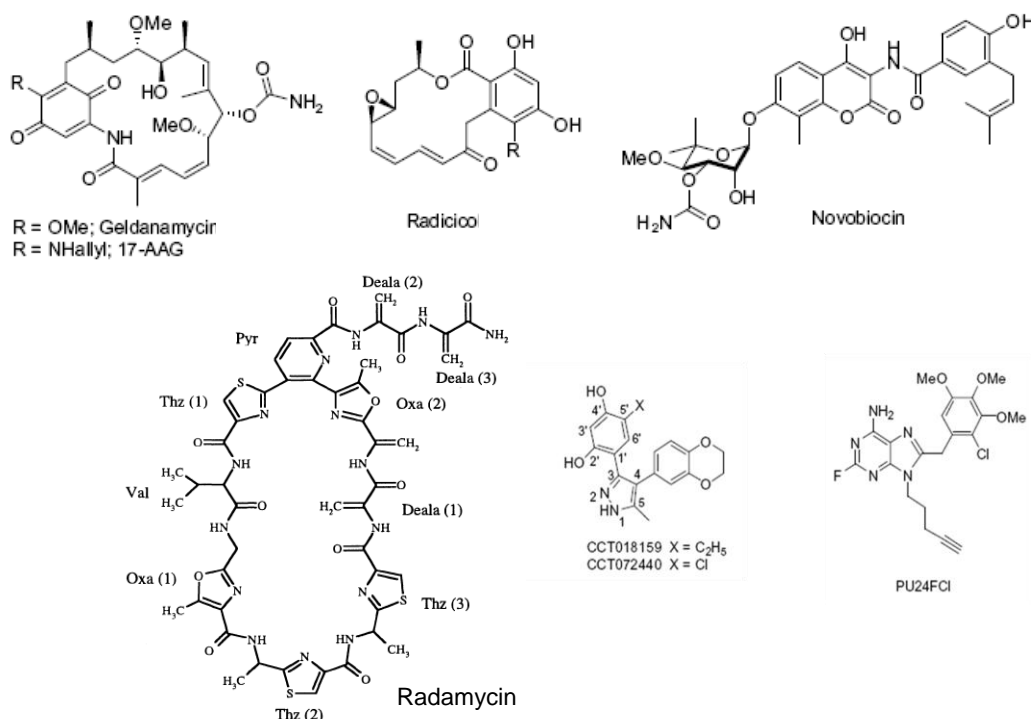


Figure 10. Structure of Hsp90 inhibitors

Consequently they are likely to have broad utility in combination therapy. At present, structurally unique Hsp90 inhibitors are undergoing preclinical and clinical evaluation. These anti-Hsp90 drugs show great promise through their potential to block a wide spectrum of the main pathways of autonomous tumor growth.

2.3. Extracellular Hsp90: Chaperoning Immune Response and Cell Invasion

While Hsp90 was originally discovered and perceived as an intracellular molecular chaperone, more than two decades later, a number of studies challenged this view. In 1986, Ullrich et al. identified Hsp90 as a tumor-specific antigen localized on the surface of mouse cells [39]. Since then, several researchers have reported the presence of this molecular chaperone on the cell surface. However these studies did not attribute precise functions to this pool of the molecule and the best studied cases of extracellular Hsp90 concerned innate and adaptive immunity. More specifically,

Hsp90 has been documented as a key player in antigen processing and presentation during immune responses, where it was reported to play crucial roles in antitumor and antiviral responses through interaction with various HSP receptors on APCs, such as CD40, CD91 and TLR4 [40,41].

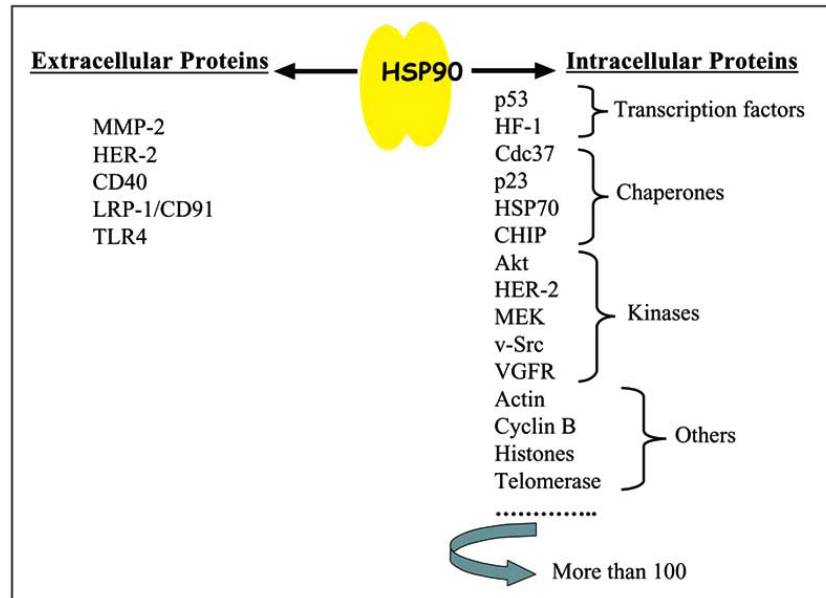


Figure 11. Summarised list of the extracellular and intracellular Hsp90-interacting molecules

Different independent studies are in agreement and strongly indicate that extracellular Hsp90 is involved in the molecular pathways leading to cell motility, invasion and cancer cell metastasis. As shown in Fig.11, while more than 100 intracellular Hsp90 interacting proteins have been reported, a relatively small number of surface molecules have been identified so far to interact with the extracellular pool of Hsp90. However, the above mentioned studies demonstrate that the presence of Hsp90 on the cell surface is a wide-ranging phenomenon suggesting that this extracellular pool of the molecule performs “extra-ordinary” chaperoning activities to a number of surface molecules similarly to its intracellular counterpart. This scenario is confirmed by accumulating data reporting that several components of the Hsp90 chaperone machinery, such as Hsp70, Hop, p23 and cdc37 are also present on the cell surface. On the other hand, it was suggested that surface Hsp90 participates in cancer cell invasion through the signaling processes involved in the regulation of focal adhesion formation and cell migration, a complex and multistep process, based on a multitude of cellular and molecular mechanisms (Fig. 12).

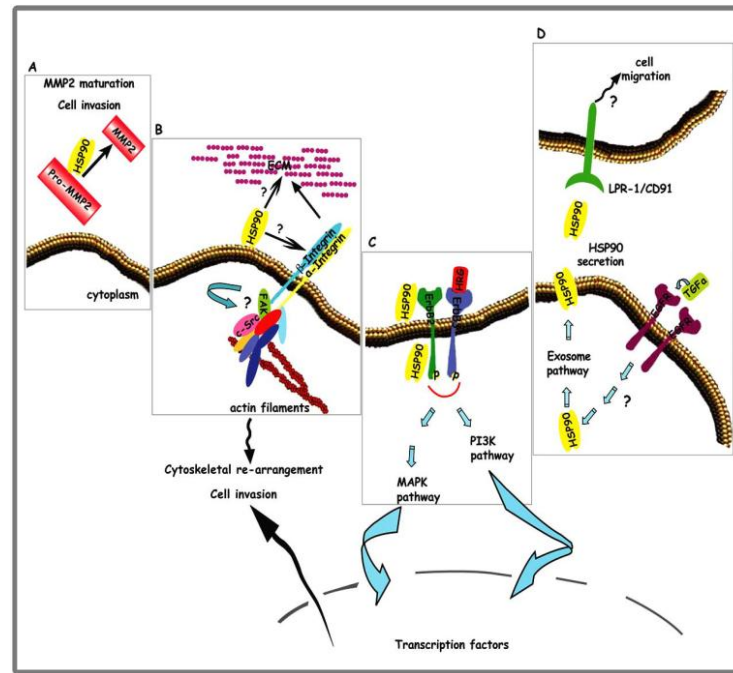


Figure 12. Schematic representation of 4 proposed models concerning the involvement of extracellular Hsp90 in cell migration and invasion.

A. Hsp90 is identified extracellularly, in association with MMP2 and this interaction is suggested to be necessary for the maturation of the enzyme, which in turn is crucial for fibrosarcoma cell invasion.

B. Surface Hsp90 is shown to participate in melanoma and prostate cancer cell invasion through regulation of focal adhesion formation, including ECM-induced c-src/integrin association and re-organization of the actin cytoskeleton.

C. Surface Hsp90 is shown to be involved in breast cancer cell invasion, stimulated by the presence of HRG. The model suggests that Hsp90 exerts its function through an interaction with the extracellular domain of ErbB2, essential for the activation of the downstream signal transduction pathways leading to actin cytoskeletal re-arrangement and cell invasion.

D. TGF α is shown to trigger keratinocytes to secrete Hsp90 in the culture medium through the exosome pathway.

The basic steps include the coordinated assembly and dis-assembly of adhesions and the reorganization of the actin cytoskeleton in order to generate productive movement. Molecules from the environment, including chemoattractants, growth factors and extracellular matrix proteins, regulate cell polarization through the spatially controlled recruitment of signaling complexes that modulate the actin cytoskeleton and mediate the extension of membrane protrusions at the leading edge. Finally several molecules have been described as being tightly involved in the re-organization of the actin cytoskeleton of a cell. These include among others adhesion molecules, like integrins and selectins, transmembrane receptor tyrosine kinases (EGF-R, ErbB-2), phospholipids, focal adhesion kinases (FAKs) and GTPases.

3. AIM OF THE WORK

The discovery of Hsp90 on the surface of cancer cells, in combination with accumulating evidence reporting its involvement in invasion and metastasis commences a new and exciting era in the field of cancer therapeutics [42]. Cell surface and intracellular Hsp90 provides a novel and promising molecular target for the development of effective antimetastatic drugs. Although compounds targeting Hsp90 already exist, the need for further development of Hsp90 inhibitors is emerging.

Therefore, due to the interest on Hsp90 as biological target in the search of anticancer drugs, the first part of my PhD research work was devoted to the design of new polyheterocycle derivatives as potential Hsp90 inhibitors.

These were identified by molecular modeling studies and then optimized through the introduction of appropriate substituents. The new potential inhibitors were prepared by using the suitable synthetic methodologies. The selected compounds were tested in biological screening to investigate their activity as antiproliferative compounds, but also in particular for their specific effect towards protein targets such as Hsp90 and transcriptional factor HIF-1.

4. RESULTS AND DISCUSSION

4.1. Leads Identification

In the last decade the application of computational methodologies in all the medicinal chemistry fields has found an amazing development. All these efforts were focused on the searching of new leads possessing a specific bio-molecular target affinity. Thus, different molecular modeling approaches were used in simulation of molecular behaviour for a specific biological target.

During my PhD experimental work the *in silico* approach, in the search of new Hsp90 inhibitors, was performed by using two different points of views. The first, called the multivariate protocol, consists in the application of a chemiometric methodology [43] on an “*in house*” ligands-descriptors matrix database. The second deals with the well known pharmacophore based virtual screening on a large database. However, both approaches require preliminary a deep knowledge and analysis of the structure of the biological target. By crystallographic studies it was possible to characterize the individual domains and the structure for ATP-bound conformation of the intact dimeric chaperone.

4.1.1. Structure of Hsp90

Crystallization of a full-length Hsp90 was first reported nearly 10 years ago. However, well-ordered diffraction-quality crystals capable of yielding an atomic resolution structure remain elusive, although some progress is being made [10]. An enormous amount has been learned from structural studies of domains and large subconstructs, so that atomic structures for almost all segments of the Hsp90 structure are now known (Fig. 13).

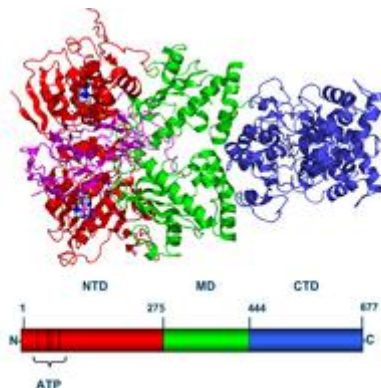


Figure 13. Schematic of the domain structure of yeast Hsp90

4.1.1a N-Terminal Domain—Nucleotide and Drug Binding

The first breakthrough into Hsp90 structure came from the identification of an N-terminal ~25kDa domain, which was readily released from the protein by limited proteolysis. Crystal structures of this domain, from human and yeast Hsp90s revealed a two-layer α/β sandwich structure in which the helices delimit a pocket extending from the surface to the buried face of the highly twisted antiparallel β -sheet [10, 44]. In the human structure, this pocket was found to be the binding site for the macrocyclic antitumor agent geldanamycin [45], whose binding to Hsp90 had been shown to disrupt productive complexes with protein kinase and steroid hormone receptor clients. In the absence of any mechanistic model for Hsp90 function at the time, inhibition by geldanamycin was erroneously attributed to competitive blockade by the macrocycle of a putative binding site for an unfolded client protein [46]. A cocrystal structure of the yeast Hsp90 N terminus and ATP/ADP revealed the N-terminal pocket as the binding site for adenine nucleotides, identifying key conserved functional residues and explaining the action of geldanamycin and related compounds as competitive inhibitors of ATP binding (Fig. 14).

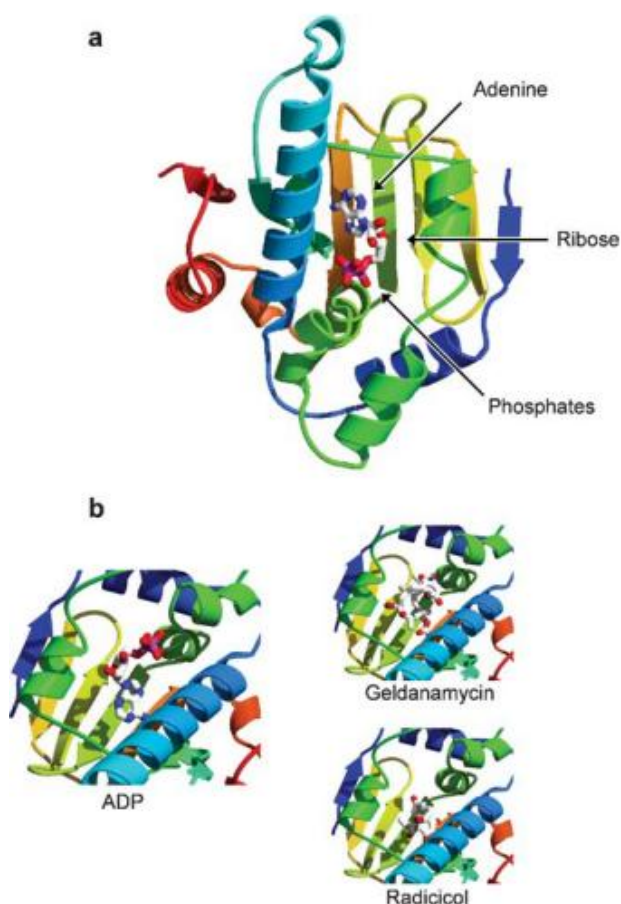


Figure 14.

(a) Crystal structure of the N-domain of yeast Hsp90, showing the binding site for ATP/ADP. The protein is shown as a secondary structure cartoon rainbow (blue-red) from the N to the C terminus of the construct.

(b) Comparison of co-crystal structures of yeast Hsp90 N-domain and bound ADP, with complexes of the antibiotics GA and radicicol.

Involvement of ATP in Hsp90 function had been suggested several years earlier, but it was associated with apparent autophosphorylation, suggesting contamination with protein kinases, although subsequent biochemical analysis seemed to show conclusively that Hsp90 lacked significant ADP/ATP affinity. With the realization that geldanamycin was a highly specific competitive inhibitor of ATP binding to Hsp90 [47], it became possible to measure the low inherent ATPase of Hsp90s accurately, without interference by contamination kinases or other more active ATPases. The identification of key residues in the N-terminal structure made it possible to demonstrate unequivocally, by mutagenesis in engineered yeast strains, that the biological function of Hsp90 was absolutely dependent on its ability to both bind and hydrolyze ATP.

4.1.1b Middle Segment—Client Protein Binding and Catalytic Loop

Following from structural analysis of the yeast and human N-terminal domains, the crystal structure of a proteolytically resistant middle segment from yeast Hsp90 was determined (Fig. 15a). This structure consists of a large α - β - α domain at the N-terminus of the construct connecting to a small α - β - α domain at the C-terminus *via* a series of short α -helices in a tight coil [48]. The middle segment is a major site for client protein interactions, with a conserved hydrophobic patch centered on Trp 300 and an unusual amphipathic protrusion formed by residues 327–340, with one exposed hydrophobic side and one positively charged side, being particularly important (Fig. 15b).

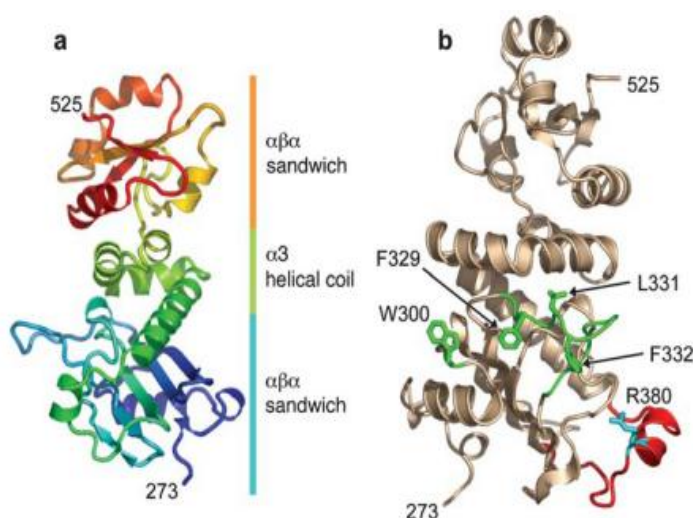


Figure 15.

(a) Crystal structure of the middle segment of yeast Hsp90, showing the three subdomains.

(b) As in (a) but rotated $\sim 90^\circ$ around the vertical, with the hydrophobic residue implicated in client protein binding (green) and the catalytic loop bearing the essential residue Arg 380 (red).

Again by analogy with other GHKL proteins, it was anticipated that the middle segment also contributed a key catalytic lysine residue that would interact with the γ -phosphate of an ATP molecule bound in the N-terminal domain. Instead, a conserved arginine, Arg 380, was found by mutagenesis to be essential for ATPase activity *in vitro* and for the essential functions of Hsp90 in yeast *in vivo*, suggesting that it plays the same role of polarizing the β - γ phosphodiester bond. However, at least in the isolated Hsp90 middle segment, this connecting loop is highly structured with Arg 380 involved in a short α -helix, so that substantial remodeling of this segment would be required for Arg 380 to fulfill its catalytic role.

4.1.1c. C-Terminal Domain—Dimerization

More recently the structure of the C-terminal domain from the *E. coli* Hsp90 homologue HtpG has been determined (Fig. 16). Consistent with previous biochemical observations that the C-terminal domain is essential for Hsp90 dimerization, the HtpG C-terminal structure is a dimer of a small mixed α/β domain [49]. The dimer interface is formed by a pair of helices at the C-terminal end of the domain packing together to create a four-helix bundle. Nonetheless, the C-terminal domains in eukaryotic and bacterial Hsp90 is important for the recruitment of other cochaperones, which form the superchaperone complex with Hsp90.

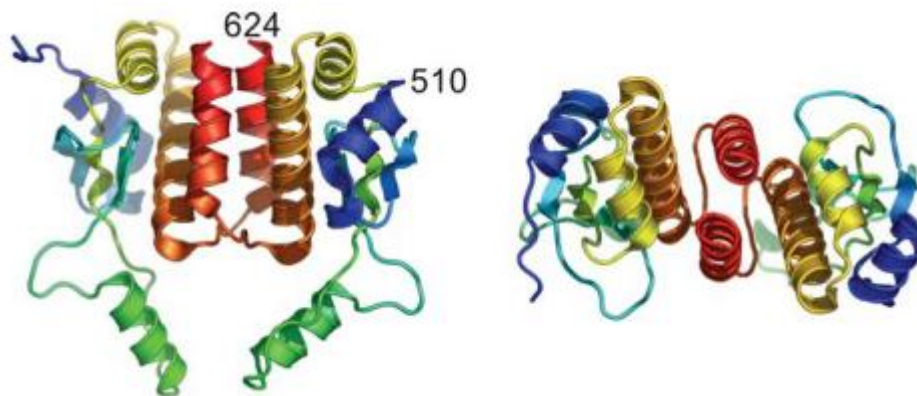


Figure 16. Crystal structure of the dimeric C-terminal domain of the *E. coli* Hsp90 homologue, HtpG (left) and viewed down the local pseudotwofold symmetry axis (right). This region corresponds to residues 549–674 of the yeast protein and lacks the extreme C-terminus of ~30 residues that provides the binding site for TPR domain cochaperones in eukaryotic Hsp90s.

4.1.2. Multivariate Protocol

In this *in silico* approach, the selection of suitable compounds was performed on the “*in house*” database of structures incorporating pyrimidine core structure of

type **1-15** (Fig. 17). The designed derivatives are all synthesizable through well known and optimized experimental procedures, developed by the research group I worked with. [50-53].

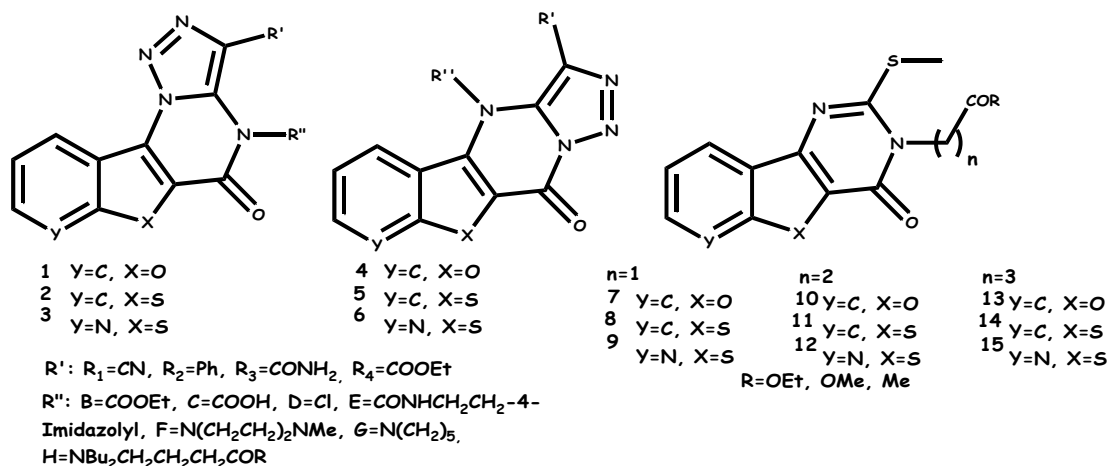


Figure 17. Structures included in the “in house” database

Initially we started by choosing 48 heterogeneous biological targets (Table 4), including Hsp90, for which it is known a consistent set of inhibitors with activity or binding affinity available data, resulting a total of 7490 molecular structures, 138 of which are known inhibitors of Hsp90.

The molecular structures were downloaded from binding DataBase [54], a public available database of measured binding affinities, focused on the interaction between proteins considered to be drug targets with small drug-like molecules. These structures were used as input data for CODESSA PRO program [55], where calculation of molecular descriptors was carried out. CODESSA PRO (Comprehensive DEscriptors for Structural and Statistical Analysis) is a multi-purpose program providing various methods for statistical analysis of experimental data such as Partial Least Squares, (Multiple) Linear and Non-Linear Regressions, and Principal Components Regression. A set of 615 molecular descriptors derived from geometrical and quantum-chemical structures was computed in our study, as available in the program. All descriptors were divided into five groups: constitutional, topological, geometric, electrostatic, and quantum-chemical. Constitutional descriptors reflect only the molecular composition of the compounds as the number of atoms, the number of bonds and the molecular weight, and so on. Topological descriptors describe the atomic connectivity in a molecule. Geometric descriptors are calculated from the three-dimension atomic coordinates of the

molecule, and comprise moments of inertia, shadow indices, molecular volume, and molecular surface area-like descriptors.

Table 4. Biological targets and number of inhibitors

Target names (bindingDB ID)	
11-beta-Hydroxysteroid Dehydrogenase (11betaHSD1)	40
ABL Kinase (ABL)	70
Adenosine receptor A1 (ARA1)	110
Aldose Reductase (ALR2)	126
Aldosterone Synthase (CYP11B2)	129
Androgen Receptor (AR)	244
Angiotensin Converting Enzyme (ACE)	51
Angiotensin Converting Enzyme 2 (ACE2)	73
Anthrax lethal factor (ALF)	130
Aromatase (AROM)	440
Asparaginyl Endopeptidase (AE)	27
Aurora Kinase A (Aurora-A)	179
BCL-2 (BCL-2)	31
BCL-x1 (BCL-x1)	50
Ca-Moduline kinase 2 (CaMK2)	20
Cannabinoid Receptor 2 (CannRec2)	104
Carbonic Anhydrase 1 (CA-1)	305
Carbonic Anhydrase 2 (CA-2)	402
Carbonic Anhydrase 4 (CA-4)	203
Caspase-1 (CSP1)	83
Caspase-3 (CSP3)	226
Checkpoint kinase (ChK1)	57
Chymotrypsin (CT)	33
Collagenase (CLG)	309
Corticotropin Releasing Factor Rec 1 (CRFR1)	62
Cyclin-Dependent kinase (CDK4)	631
Delta Opioid Receptor (DOR)	25
DiacylglycerolAcylTransferase (DGAT-1)	14
Dihydrofolate Reductase (DHFR)	144
Dopamine Transporter (DAT)	58
EGF-R Tyrosin Kinase (EGF-R TK)	979
ERK-2 Kinase (ERK-2)	66
Estrogen Receptor (ER-alpha)	199
Factor Xa (Fxa)	109
Ghrelin Receptor (GHR)	90
Glucocorticoid Receptor (GR)	109
Glutaminy Cyclase (GC)	183
Glycogen Synthase Kinase 3 α (GSK3 α)	229
Heat Shock Protein 90 (HSP90)	138
Histone Deacetylase 1 (HD1)	143
Matrix MetalloProteinase 13 (MMP-13)	142
Matrix MetalloProteinase 3 (MMP-3)	80
Neutrophil EndoPeptidase (NEP)	26
PDK1 Kinase (PDK1)	97
PhosphoDiEsterase Type 10A (PDE10A)	41
Plasmepsin 1 (PSP1)	51
Protein Tyrosin Phosphatase (PTP1B)	336
Tyrosin Kinase C-kit (TKC-kit)	96
	7490

Electrostatic descriptors reflect characteristics of the charge distribution in the molecule, calculated by the Zefirov method. Quantum-chemical descriptors add important information to the conventional descriptors. They are divided into three subgroups: charge distribution-related, valence-related and quantum mechanical energy-related descriptors.

Among the whole set of calculated properties a total of 173 descriptors (not correlated) were selected. Therefore the resulting matrix, 7490 rows (structures) versus 173 columns (descriptors), was submitted to Principal Component Analysis (PCA). PCA is one of the most-widely used multivariate exploratory techniques [56]. Principal Components are able to detect internal relations between characteristics of a set of objects, thus enabling a drastic reduction of the dimensionality of the original raw data. This reduction is achieved by transforming the original matrix to a new one, whose set of variables, termed as Principal Components (PCs), appear to be orthogonal to each other (uncorrelated) and ordered so that the first few, with descending importance, retains most of the variance content from the total set of original variables.

In PCA, the initial data matrix D is represented as the inner product of two matrices (eq. 1):

$$D = RC \quad (\text{eq. 1})$$

The row matrix R , named the score matrix, has the dimensionality $r \times n$, where r is the number of observations (compounds in our case) in the initial data set, and n is the number of PCs. The column matrix C , named the loadings matrix, has the dimensionality $n \times c$, where c is the number of observable properties (molecular descriptors in our case) in the initial data.

PCA can be highly useful for data classification and pattern recognition. In the two-dimensional plotting of a score vector against another score vector, objects with similar properties are clustered. Moreover, in the two-dimensional plotting of a loading vector against another loading vector, the initial statistical properties reflected in those two score loadings are clustered together. The number of PCs (scores, loadings) existing in a characteristic vector space can be equal to, or less than, the number of variables in the data set. The first Principal Component is defined as that giving the largest contribution to the respective PCA of linear relationships exhibited in the data. The second component may be considered as the second best linear combination of variables that accounts for the maximum possible

of the residual variance after the effect of the first component is removed from the data; next components are defined until practically all the variance in the data is exhausted. For this study PCA was performed with STATISTICA 6.0 package. From the analysis of the significant components emerges that 68% of the variance is comprised in the first five components (Table 5).

Table 5. Statistics of PCs 1-5

PCs	Eigenvalue	Cumulative Eigenvalue	% Total	% Cumulative
1	61.30897	61.3090	35.43871	35.4387
2	29.63579	90.9448	17.13052	52.5692
3	11.02439	101.9692	6.37248	58.9417
4	9.08724	111.0564	5.25274	64.1944
5	6.10995	117.1664	3.53177	67.7262

In Fig. 18, the 2D representation (PC1 versus PC2) for all matrix compounds is reported.

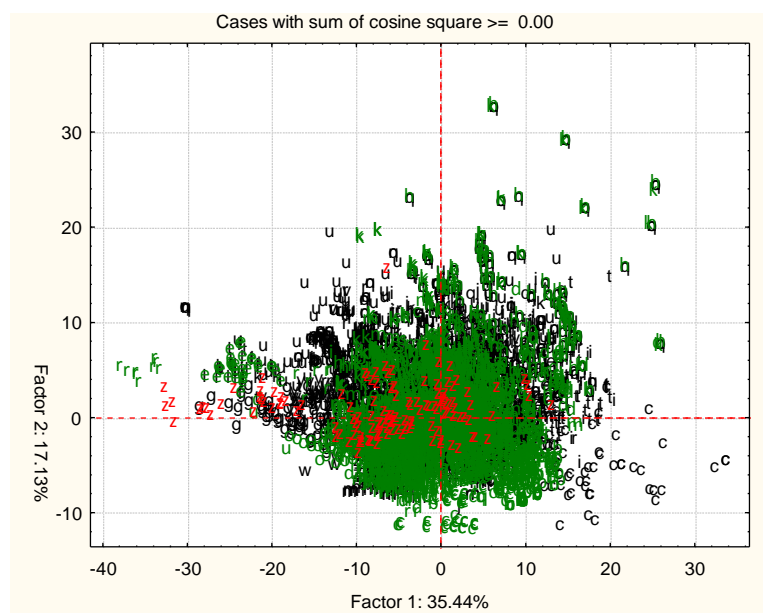


Figure 18. Projection of the cases on the factor-plane

For each of 48 biological targets, the 5-dimensional barycentric coordinates were computed (in Fig. 19 the two-dimensional coordinates are reported).

4.1.3. Pharmacophore Based Virtual Screening

According to this approach the entire ZINC Database, a collection of over 5 million purchasable and non-purchasable compounds, was used as starting point in a virtual screening on ATP site of the Hsp90. The molecular docking protocol, showed in figure 21, was build up.

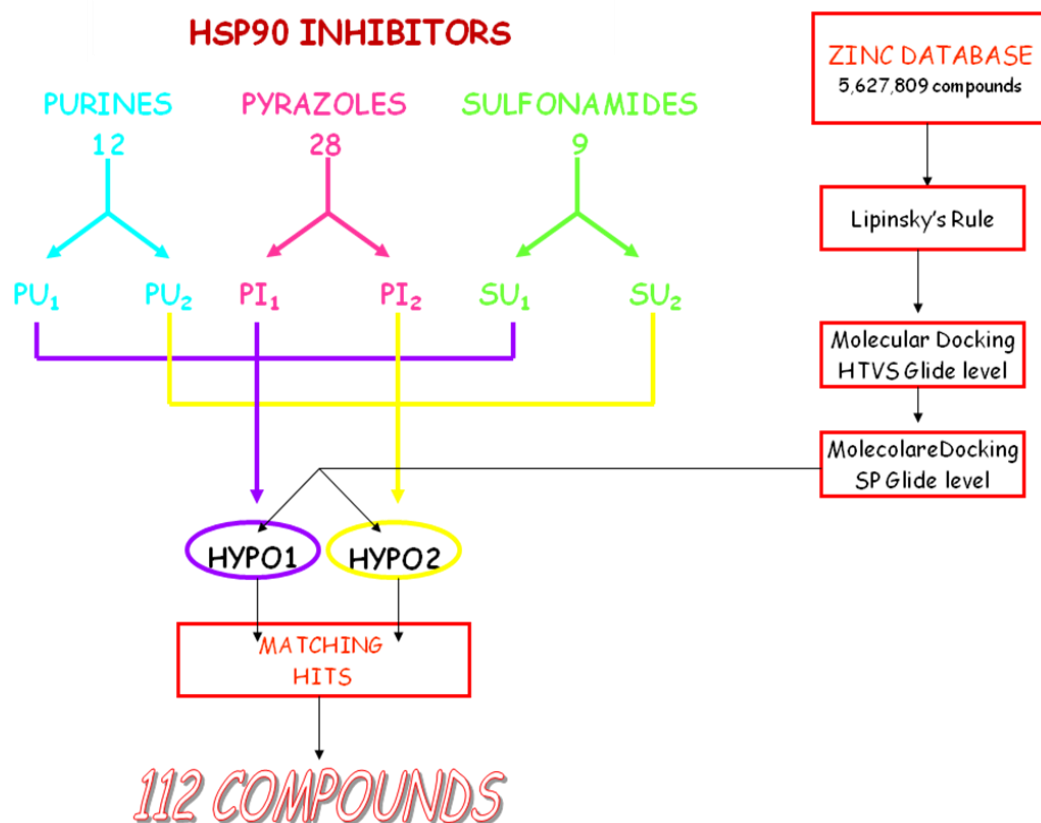


Figure 21. Virtual screening flowchart

Preliminarily a first discrimination by means Lipinski's Rule of Five was applied. In the second step, the survival compounds were submitted to a two accuracy levels Molecular Docking Screening, using the software Glide [57]. The first level, termed High Throughput Virtual Screening (HTVS) allowed a rapid evaluation of the whole data set; the most highly ranked compounds (providing a GlideScore < -7) were further submitted to the Standard Precision (SP) molecular docking, which involved a more accurate algorithm for the evaluation of interactions.

The top scored compounds (GlideScore < -7.5) were further discriminated using two set of pharmacophoric hypotheses, both built using as training set the Hsp90 inhibitors included in the binding DataBase. When our work started this database contained a total of 49 derivatives classified as Hsp90 inhibitors, belonging

to different structural classes including purines (12), pyrazoles (28), and sulfonamides (9) (Fig. 22).

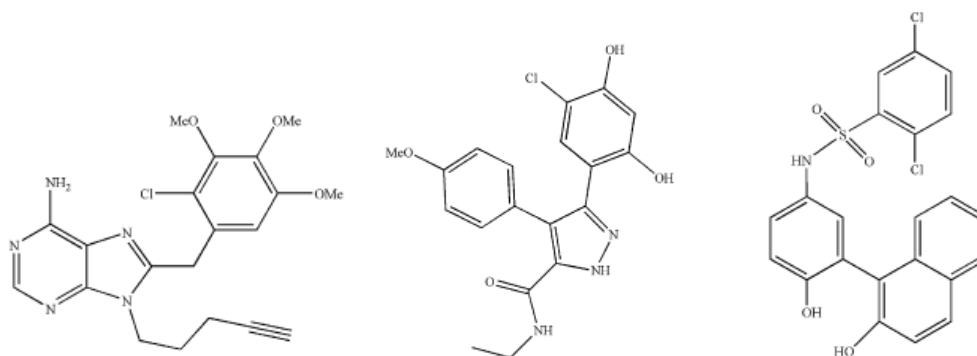


Figure 22. Structure of representative *Hsp90* inhibitor of each class

First, as described in the case of ZINC database, Molecular Docking experiments were carried out using Glide software, in order to obtain information on the conformations adopted by ligands at the active site of their molecular target. Analysis of the results allowed to appreciate that each class of inhibitors shares a common binding mode (Fig. 23).

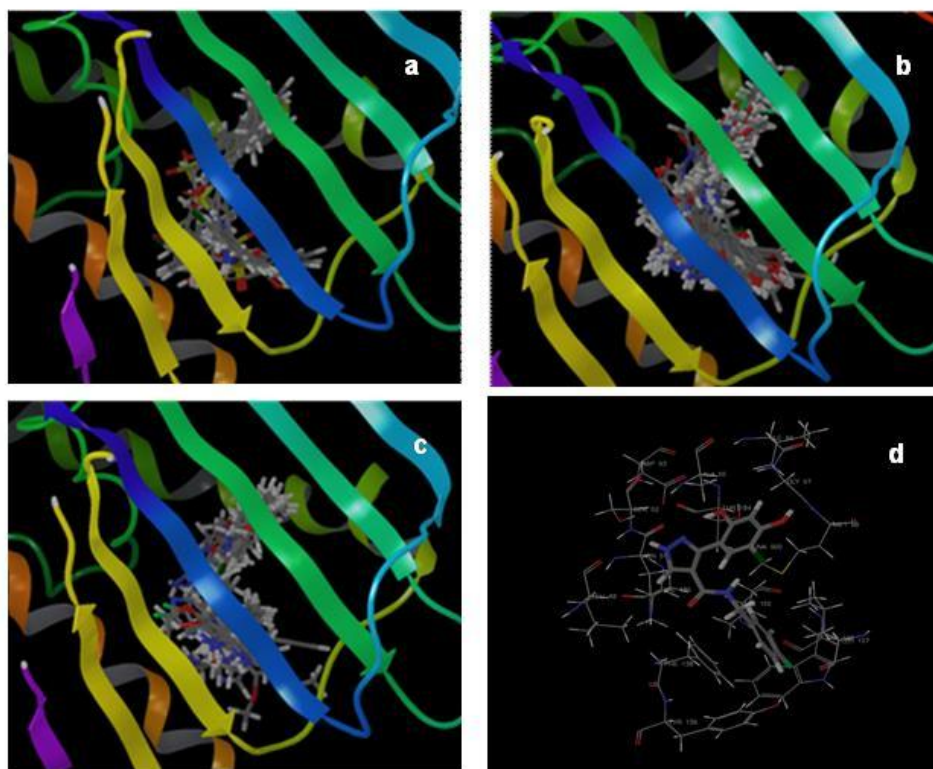


Figure 23. Inhibitors binding modes: *a*: sulfonamides, *b*: pyrazoles, *c*: purines, *d*: interactions at the binding site.

Despite the differences occurring in the orientation of the substituents, the core structures (purine, pyrazole, or sulfonamide ring) are well superimposed for each class of derivatives. Moreover, the results evidenced the occurrence of several recurrent interactions with the active site, confirming the role of some key residues such as Asp51, Asp54, Lys58, Asp93, Gly97, Lys112, Phe138, Thr184, Thr 162, Val 150 and Val 186, which provide direct hydrogen interactions, as also suggested by recent docking studies [58].

The first hypothesis (Hypo1), called Docking derived pharmacophore, performed by Phase software [59], was built using the frozen conformations obtained by the docking of all 49 compounds, in the N-terminal domain of Hsp90 (PDB id: 2BZ5). Therefore this is a receptor-based hypothesis, since the active site architecture influenced the training set conformations. Hypo1 consists of two H-bond acceptors regions located at 7.98 Å distance each other, and two ring-containing regions, located at 4.03 Å each other and at 3.46-2.78 Å from the two H-acceptors centers (Fig. 24).

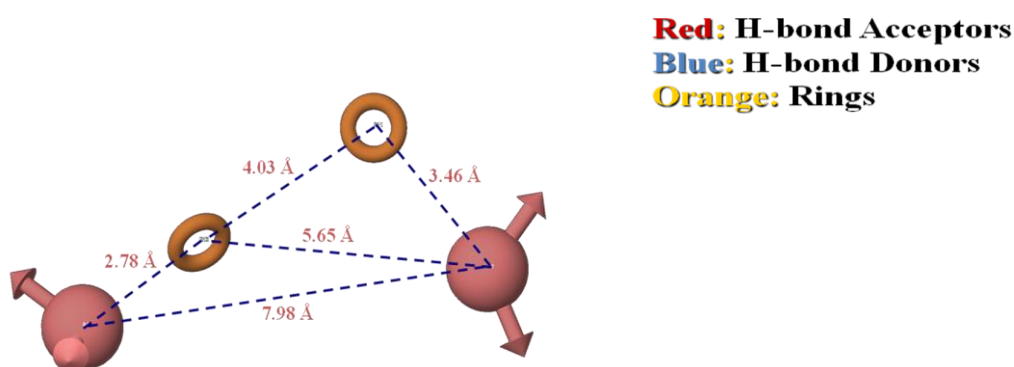


Figure 24. Docking derived pharmacophore

The second hypothesis (Hypo2), called *in vacuo* derived pharmacophore, was built using the conformations obtained through an *in vacuo* conformational search involving the generation of a maximum of 10^3 conformers for each compound of the training set. Thus, this is a structure-based hypothesis, since it only takes into account the structural diversity of the inhibitors, without considering the active site shape. Hypo2 consists of two H-acceptors regions placed at 7.89 Å each other, with two ring-containing regions placed at 4.65 Å each other and 2.80-2.56 Å from the

H-acceptors. An additional H-donors region is situated at 6.63-3.58 Å from the rings and at 4.79 Å from the H-acceptor region (Fig. 25).

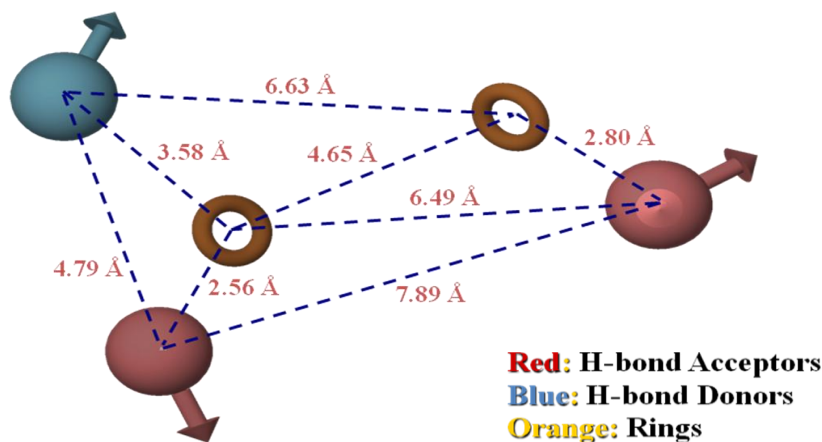


Figure 25. “In vacuo” derived pharmacophore

By means this virtual screening approach it was possible to select 112 derivatives included in the ZINC Database which resulted common to both pharmacophore hypotheses and provided a good docking score using both HTVS and SP accuracy levels. These compounds can constitute suitable leads for new Hsp90 inhibitors. The selected structures can be classified into four main classes, quinazoline of type **16**, pyrrolo-phthalazines of type **17**, pyrazoles of type **18** and aminocyanopyrimidines of type **19** (Fig. 26).

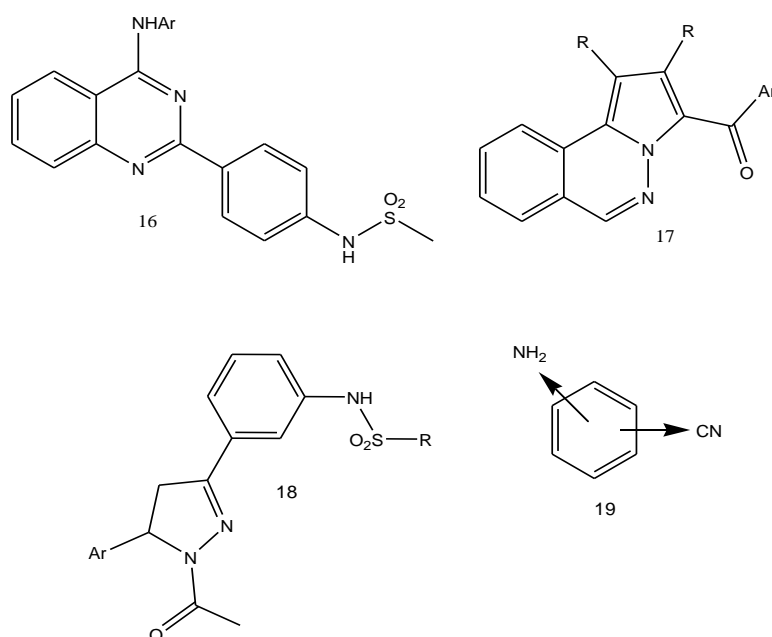


Figure 26. Identified lead scaffolds

4.2. Synthetic Methodologies for the Selected Leads

4.2.1. Annelated triazolopyrimidines

According to the results of computational studies, compounds of type **3** (cfr Fig. 17) presenting the pyrido[3',2':4,5]thieno[2,3-e][1,2,3]triazolo[1,5-a]pyrimidine core structure, a tetracyclic system identified as potential Hsp90 inhibitor, were prepared. The synthetic access to this heterocyclic ring system could be provided by suitable domino reactions. The methodology was exhaustively investigated by our research group [50,53,60]. In fact pyrido-thieno-triazolo-pyrimidine can be related to other class of flat heterocyclic structures of type **20** that, in turn, are similar to anticancer compounds known in literature, such as acridines, anthracyclines, and actinomycins (Fig. 27).

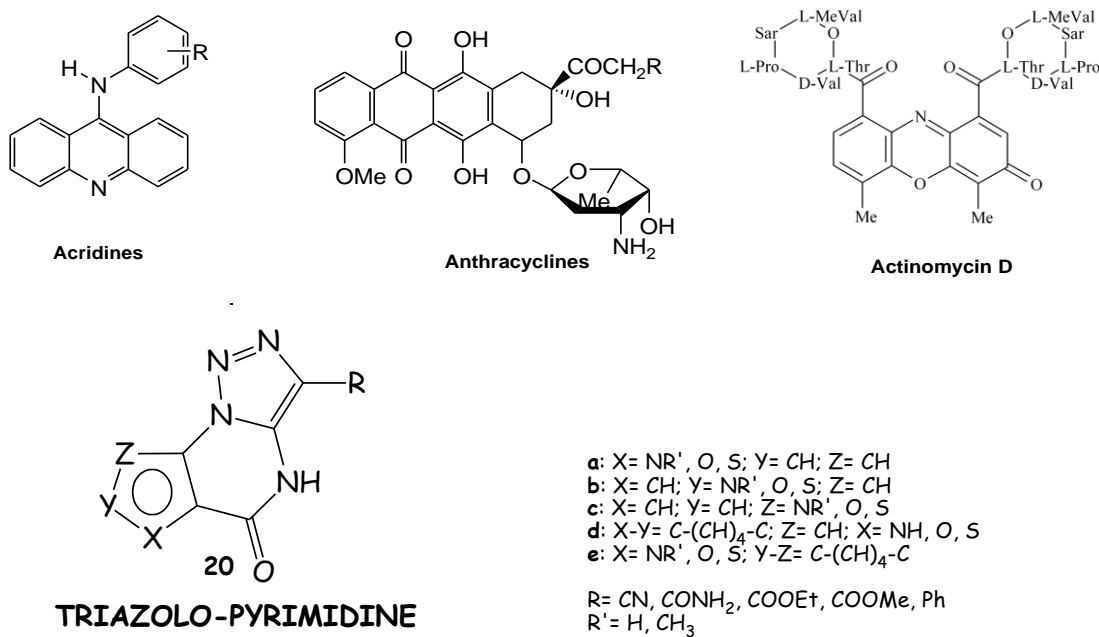
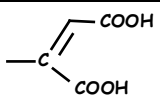
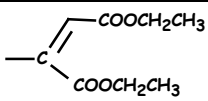
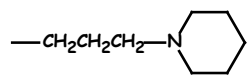
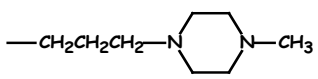

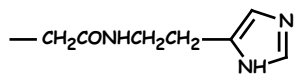
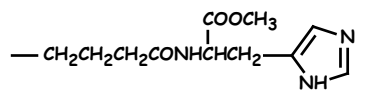
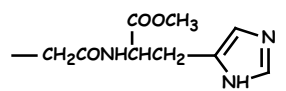



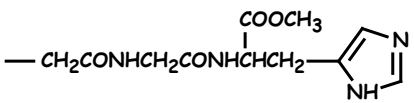


Figure 27

In fact they present moieties suitable for the intercalation into DNA, being capable of interactions such as charge-transfer, as well as hydrogen bonding and electrostatic interactions. Moreover if they bear suitable side chain, further interactions of these ligands with the other important architectural feature of DNA, its minor groove, can be envisaged. In fact the core polycyclic nucleus can be functionalized at NH in 4 position by insertion of appropriate chain shape moieties of

variable length and with different physicochemical character, which can enhance the antitumor activity (Table 6).

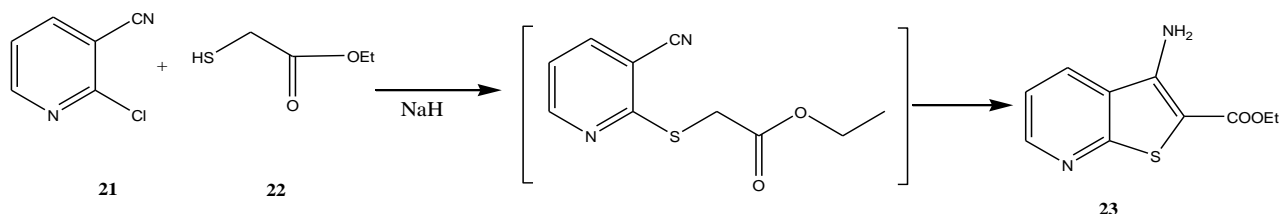
Table 6

SIDE CHAINS	
$\text{—CH}_2\text{CH}_2\text{CH}_2\text{COOH}$	$\text{—CH}_2\text{CH}_2\text{CH}_2\text{COOCH}_2\text{CH}_3$
$\text{—CH}_2\text{COOH}$	$\text{—CH}_2\text{COOCH}_2\text{CH}_3$
	
$\text{—CH}_2\text{CH}_2\text{CH}_2\text{Cl}$	$\text{—CH}_2\text{CH}_2\text{CH}_2\text{N}(\text{CH}_2\text{CH}_2\text{CH}_2\text{CH}_3)_2$
	
$\text{—CH}_2\text{CH}_2\text{CH}_2\text{CONHCH}_2\text{COOCH}_2\text{CH}_3$	$\text{—CH}_2\text{CONHCH}_2\text{COOCH}_2\text{CH}_3$
$\text{—CH}_2\text{CH}_2\text{CH}_2\text{CONHCH}_2\text{COOH}$	$\text{—CH}_2\text{CONHCH}_2\text{COOH}$
	
	
	
	

The synthetic methodology always involved a domino reaction between an azidothienopyridine and substituted acetonitriles. In fact a domino reaction is a process involving two or more bond-forming transformations (usually C-C or C-N bonds), which takes place under the same reaction conditions without additional reagents and catalysts, and in which the subsequent reaction results as a consequence of the functionality formed in the previous step. The azido moiety acts as a 1,3-dipolar reagent in cycloaddition reactions with dipolarophiles such as anions from methylene active derivatives. The intermediate resulting from the 1,3-cycloaddition reaction is a 1-(2-carboxyethyl-heteroaryl)-2-aminotriazole, which presents an amino group able to give rise to the pyrimidine ring, being within reacting distance to the carboxylate function.

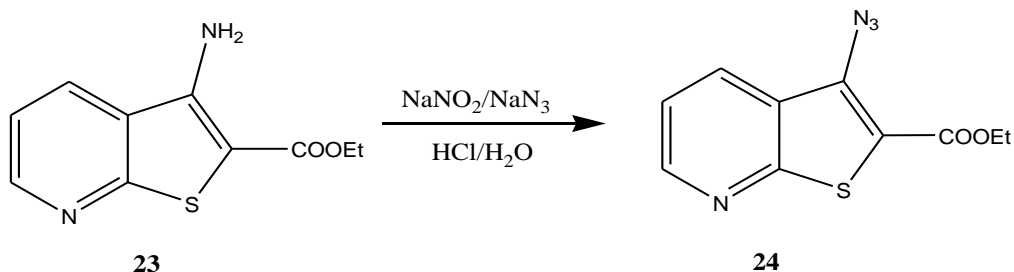
The starting 3-aminothienopyridine **23** was obtained from commercially available 2-chloro-3-cyanopyridine and ethyl thioglycolate as described in literature [61] (Scheme 1).

SCHEME 1



It was diazotized with sodium nitrite and *in situ* addition of sodium azide, in acetic acid at 0°C or in concentrated sulfuric acid according to the classical method used for the preparation of azides. But, in our case it was impossible to isolate the desired compound. However azide **24** was suitably isolated, in good yields, using 6N hydrochloric acid and cooling to -10°C (Scheme 2).

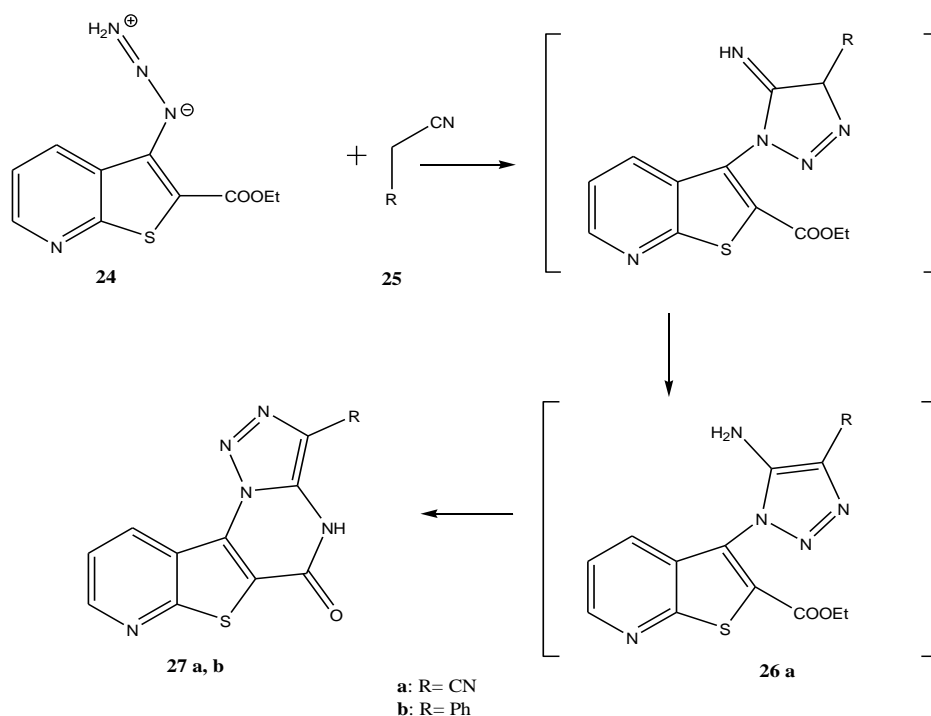
SCHEME 2



The azide **24** was added at room temperature to the sodium salt of acetonitriles **25** in absolute ethanol. After 24 hours, the TLC analysis showed mainly a new compound, that was purified by column chromatography using dichloromethane/methanol 9:1 as eluant (Scheme 3).

The structures of **27a,b** were confirmed by spectroscopic data, in particular by the presence in the IR spectra of the typical absorption bands (at 3405-3368 and 1685-1630 cm⁻¹) due to the presence of a cyclic-amide structure. Moreover, in the ¹³C NMR the diagnostic signal of the amide carbonyl moiety was found in the range 162.3-160.7 ppm.

SCHEME 3

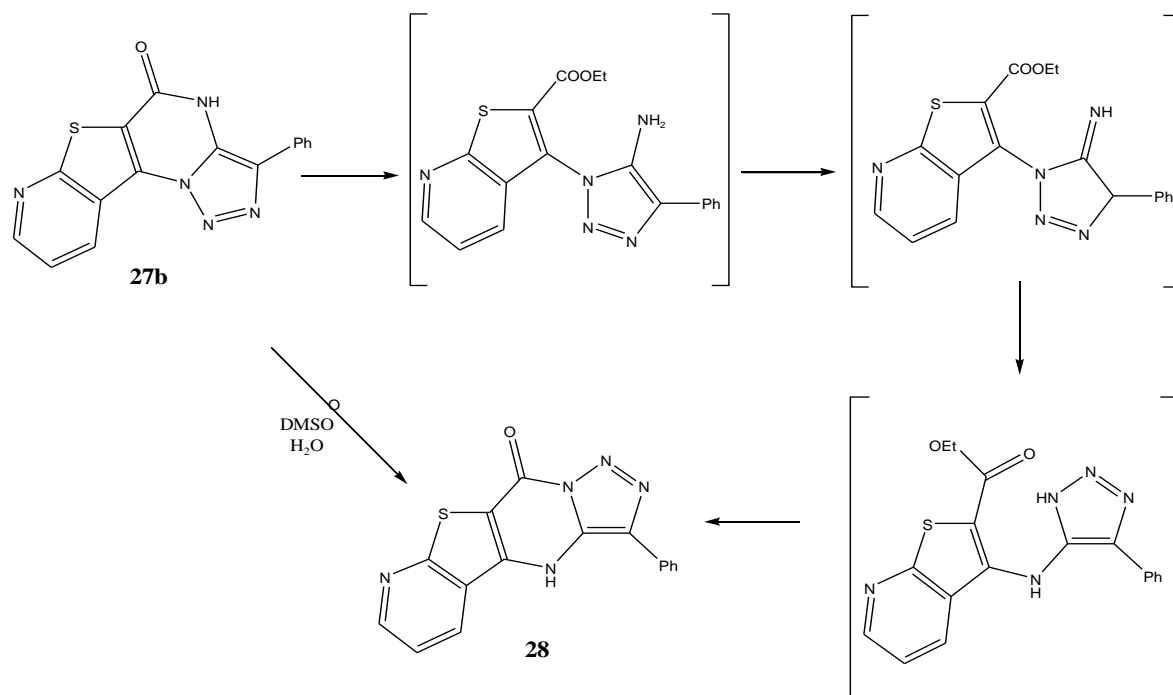


A particular behaviour was observed in the reaction of azidothienopyridine with malonitrile. In this case, it was possible to isolate the intermediate 3-(triazol-1-yl) compound **26a** with the amino group and carboxylate function unreacted. The cyclization originating the pyrimidine ring and the yield of the reaction are influenced by the amount of the solvent, in fact a smaller volume of the solvent allows to isolate the compound of type **26**. Moreover, the isolation of the intermediate confirmed the mechanism of these reactions.

As already found in the case of pyrrolo[3,4-*e*][1,2,3]triazolo[1,5-*a*]pyrimidine derivatives which rearranged to pyrrolo[3,4-*d*][1,2,3]triazolo[1,5-*a*]pyrimidines [50], and of pyrazolo[3,4-*e*][1,2,3]triazolo[1,5-*a*]pyrimidine converted into pyrazolo[3,4-*d*][1,2,3]triazolo[1,5-*a*]pyrimidine [51], compound **27b** heated under reflux in basic condition and aqueous DMSO can give rise to the linear isomer **28** (Scheme 4).

Molecular Modeling studies and biological screening on series of isosters evidenced that derivatives of polycyclic systems, such as pyrido[3',2':4,5]thieno[2,3-*e*][1,2,3]triazolo[1,5-*a*]pyrimidin-6(5H)-one, can modify their electronic and steric feature, physicochemical character and permeability through the cell membrane, by the introduction of side chain moieties in the 4 position of the ring. Therefore the synthesis of such compounds was performed.

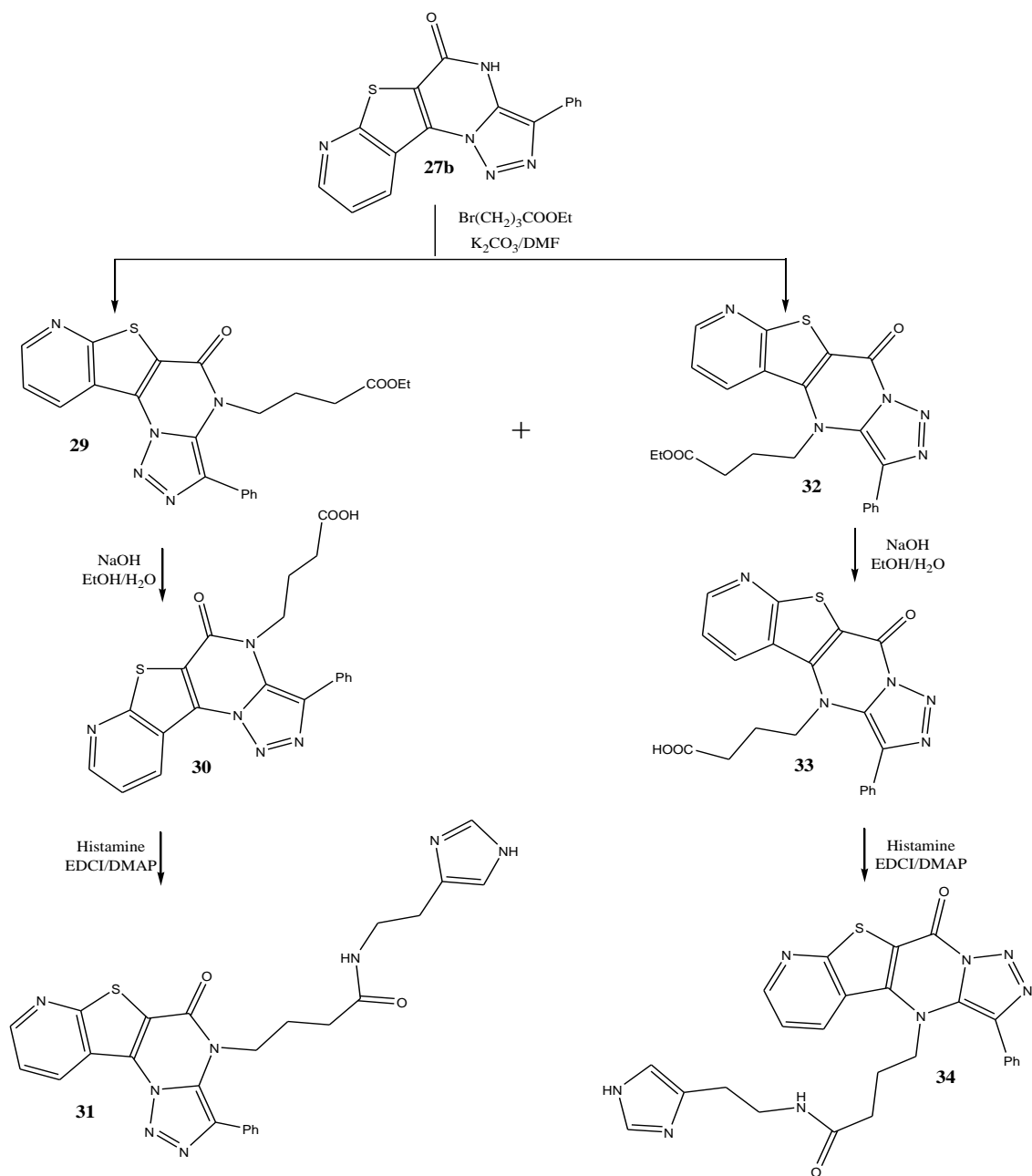
SCHEME 4



Derivative **29** and the corresponding linear isomer **32** were first obtained from the sodium salt of **27b**, generated *in situ* by using sodium hydride, and ethyl 4-bromobutyrate in absolute DMF at 80°C, but in low yield (Scheme 5). In this case, even if water is not present in the reaction environment, the Dimroth rearrangement is facilitated by the presence of lipophilic side chain in lactamic nitrogen position. The use of potassium carbonate (3-fold excess of the starting material), in absolute DMF, increased the yields of **29** to 63% and **32** to 11%. Subsequent hydrolysis with NaOH in EtOH/H₂O, at room temperature for the angular derivative **29** and under reflux for the linear isomer **32**, quantitatively yielded the corresponding carboxylic acids **30** and **33**.

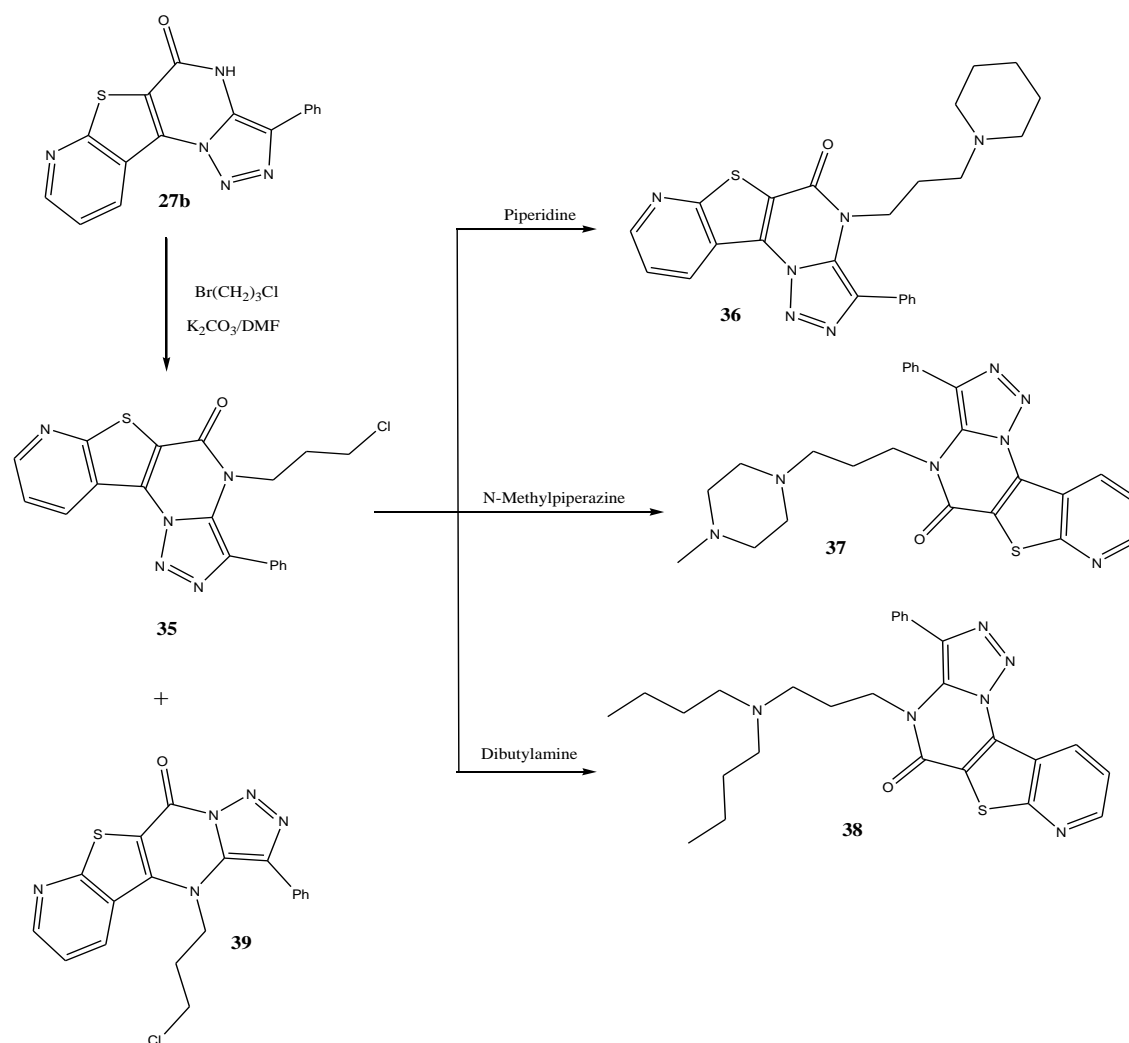
The reaction leading to the amide derivative **31** was first carried out using histamine in presence of dicyclohexylcarbodiimide (DCC) as coupling agent, in absolute dichloromethane; nevertheless the compound was obtained in very low yield. Therefore, to favor the formation of **31** and **34** a different coupling agent (1,1'-carbonyldiimidazole, DCI) in absolute dioxane was used, improving the yield to 30%. A significative yield increase (62%) was obtained through the reaction with DMAP (4-dimethylaminopyridine) and EDCI [1-ethyl-3-(dimethylaminopropyl)-carbodiimide] [62].

SCHEME 5

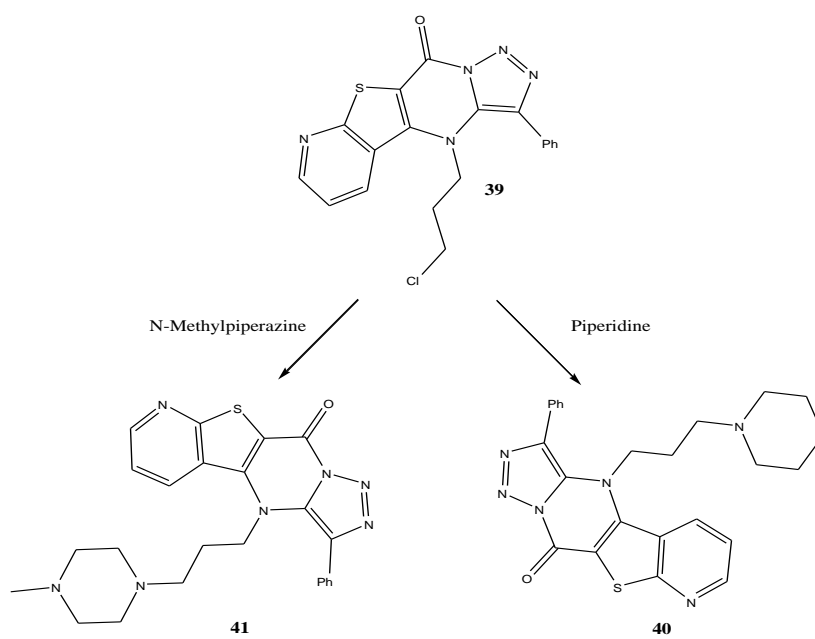


The compounds bearing the N-methylpiperazine, piperidine and dibutylamine side chain were prepared in two steps through the key intermediates **35** and **39**, which were obtained by reaction of **27a** and 1-bromo-3-chloropropane. These last derivatives, upon heating under reflux in the respective reagent *solvent free*, gave the substituted polyheterocyclic compounds **36-38**, **40** and **41** (Schemes 6, 7).

SCHEME 6

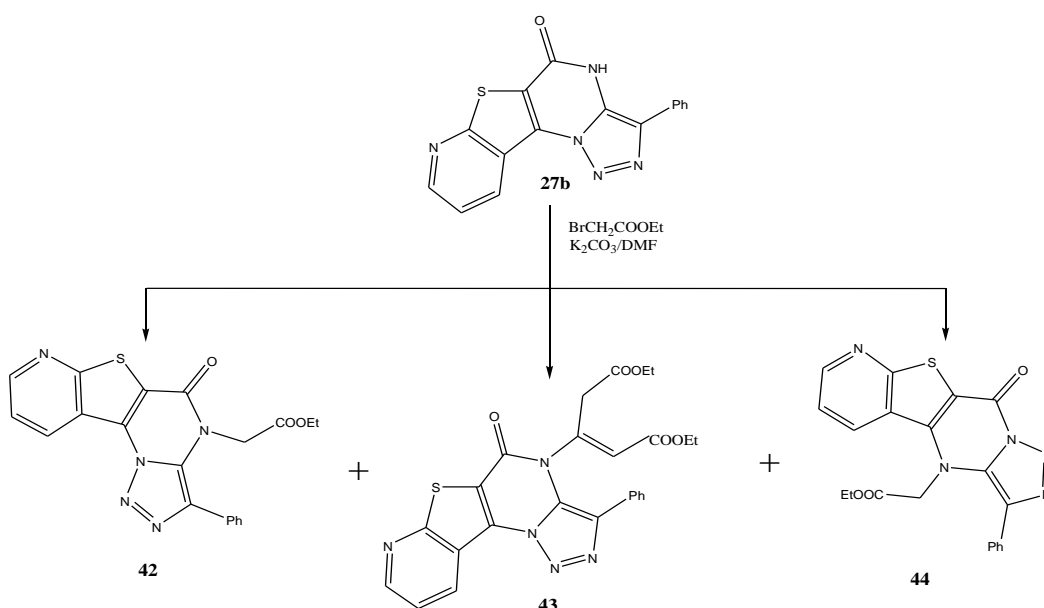


SCHEME 7



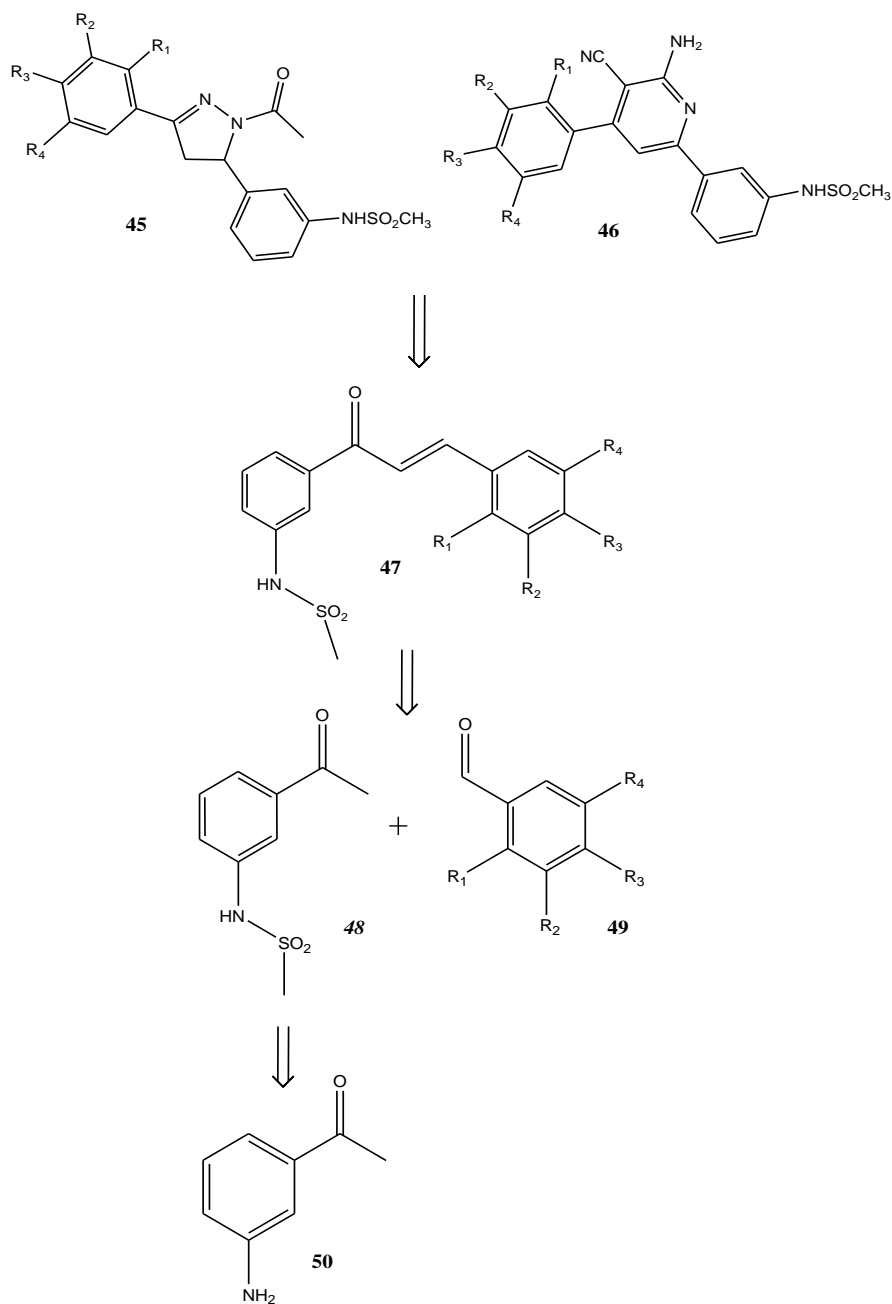
Finally, under the same experimental conditions optimized for the reaction with bromobutyrate, compounds **42** and **44** were prepared by reaction of **27b** with ethyl bromoacetate as side chain (Scheme 8). However, derivative **43** was also isolated. In an attempt to limit its formation the condensation was carried out by using NaH as base and adding an excess of this reagent (5 fold respect the starting material), but compound **43** was isolated in larger yield, since the more drastic basic condition allowed a consecutive insertion of the chain and its rearrangement. The hydrolysis of the ester groups and the addition of other side chain moieties are being developed.

SCHEME 8



4.2.2. Dihydropyrazoles and amino-cyano-pyridines

The virtual screening protocol allowed to identify series of derivatives, presenting various core structures of type **16-19** (Fig. 26), which satisfy each pharmacophore template. By this approach a set of 112 derivatives were obtained, and it was observed that among these 16 belonged to dihydropyrazole and 9 to 2-amino-3-cyanopyridine core structures. Therefore these lead compounds were selected for the synthesis. The retrosynthetic analysis of the dihydropyrazole and pyridine classes, as reported in figure 28, allowed to evidence a common intermediate of type **47** for both classes.

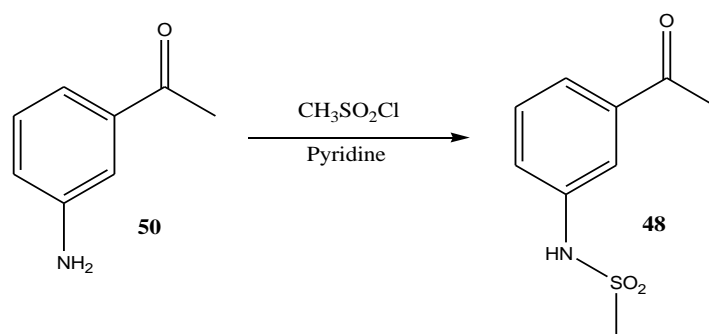


a: $R_1=\text{Cl}$, $R_2=R_3=R_4=\text{H}$; **b:** $R_1=R_2=R_4=\text{H}$, $R_3=\text{NMe}_2$; **c:** $R_1=R_3=R_4=\text{H}$, $R_2=\text{F}$; **d:** $R_1=\text{OCH}_3$, $R_2=R_3=R_4=\text{H}$; **e:** $R_2=R_3=\text{OCH}_3$, $R_1=R_4=\text{H}$; **f:** $R_1=R_2=R_4=\text{H}$, $R_3=\text{OCH}_3$; **g:** $R_3=\text{OH}$, $R_1=R_2=R_4=\text{H}$; **h:** $R_1=\text{OH}$, $R_2=\text{OCH}_3$, $R_3=R_4=\text{H}$; **i:** $R_1=R_3=R_4=\text{H}$, $R_2=\text{OCH}_3$; **j:** $R_1=R_2=R_4=\text{H}$, $R_3=\text{NEt}_2$; **k:** $R_1=\text{Br}$, $R_2=R_3=R_4=\text{H}$; **l:** $R_1=\text{H}$, $R_2=R_3=R_4=\text{OCH}_3$

Figure 28. Retrosynthetic analysis

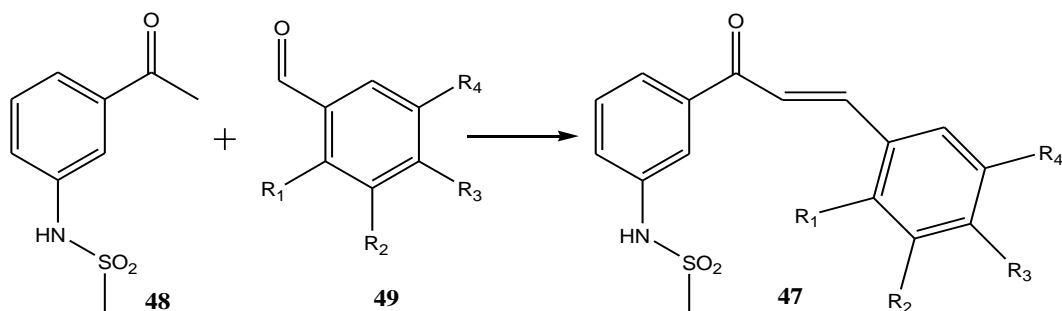
Therefore the first step of the synthetic methodology was the introduction of a sulfamidic group in the aminoacetophenone **50** by reaction with methanesulfonyl chloride [63] (Scheme 9).

SCHEME 9



Chalcones **47** were synthesized by a base catalyzed *Claisen-Schmidt* condensation reaction of **48** and appropriately substituted aldehydes of type **49** (Scheme 10). The method is attractive since it specifically generates the (*E*)-isomer. The IR spectra show the characteristic bands due to C=O stretching at 1690-1695 cm^{-1} , C=CH-Ar ones at 1600 and 1475 cm^{-1} , while the vinyl group appeared at 1295-1300 cm^{-1} . As evidenced in the ^1H NMR spectra, all chalcones were geometrically pure and with trans-configuration ($J_{\text{H}\alpha\text{-H}\beta}$ =14.5-15.8 Hz).

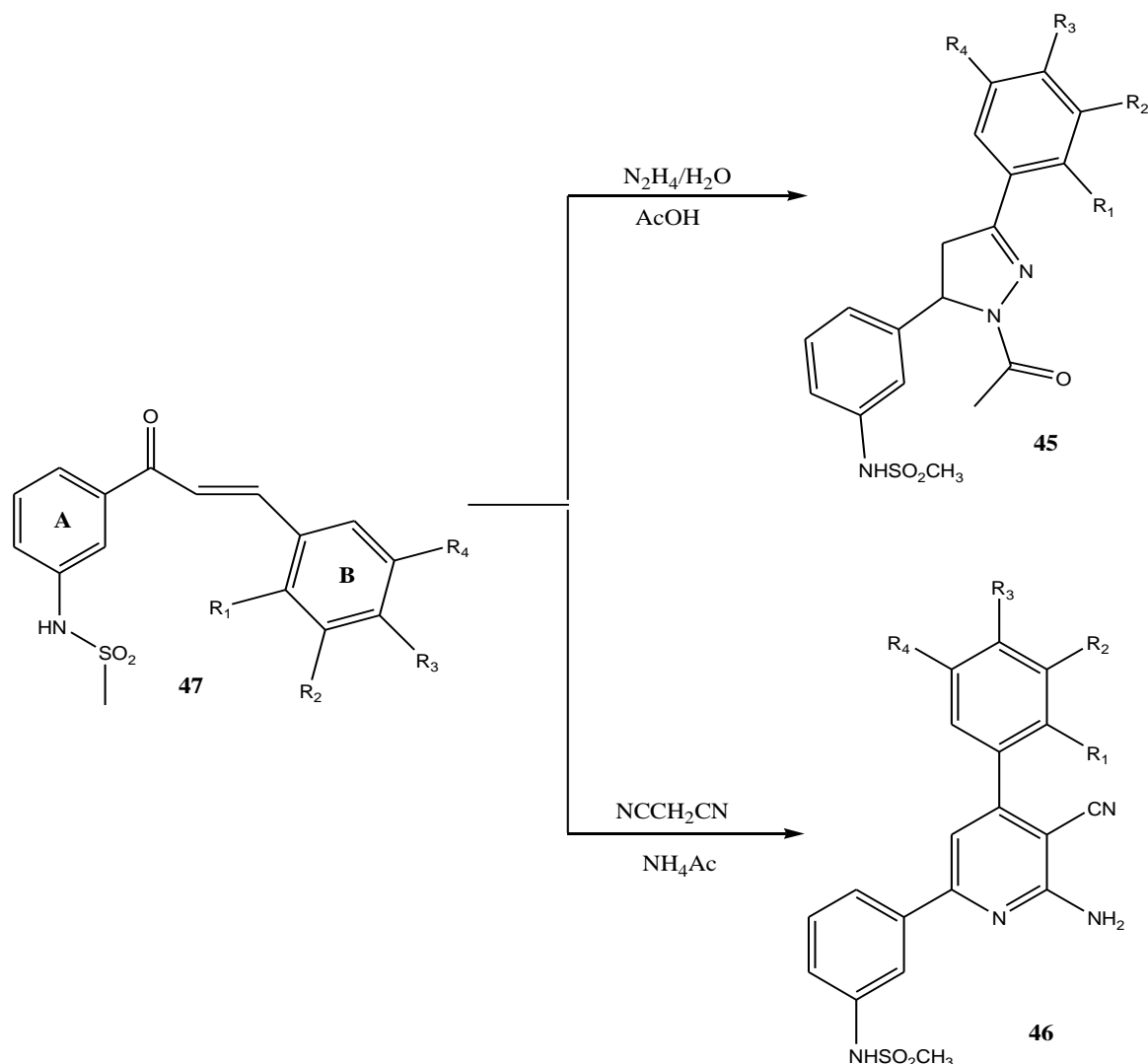
SCHEME 10



a: $\text{R}_1=\text{Cl}$, $\text{R}_2=\text{R}_3=\text{R}_4=\text{H}$; **b:** $\text{R}_1=\text{R}_2=\text{R}_4=\text{H}$, $\text{R}_3=\text{NMe}_2$; **c:** $\text{R}_1=\text{R}_3=\text{R}_4=\text{H}$, $\text{R}_2=\text{F}$; **d:** $\text{R}_1=\text{OCH}_3$, $\text{R}_2=\text{R}_3=\text{R}_4=\text{H}$; **e:** $\text{R}_2=\text{R}_3=\text{OCH}_3$, $\text{R}_1=\text{R}_4=\text{H}$; **f:** $\text{R}_1=\text{R}_2=\text{R}_4=\text{H}$, $\text{R}_3=\text{OCH}_3$; **g:** $\text{R}_3=\text{OH}$, $\text{R}_1=\text{R}_2=\text{R}_4=\text{H}$; **h:** $\text{R}_1=\text{OH}$, $\text{R}_2=\text{OCH}_3$, $\text{R}_3=\text{R}_4=\text{H}$; **i:** $\text{R}_1=\text{R}_3=\text{R}_4=\text{H}$, $\text{R}_2=\text{OCH}_3$; **j:** $\text{R}_1=\text{R}_2=\text{R}_4=\text{H}$, $\text{R}_3=\text{NEt}_2$; **k:** $\text{R}_1=\text{Br}$, $\text{R}_2=\text{R}_3=\text{R}_4=\text{H}$; **l:** $\text{R}_1=\text{H}$, $\text{R}_2=\text{R}_3=\text{R}_4=\text{OCH}_3$

These α,β -unsaturated ketones were the common intermediate for both pyrazolines and amino-cyanopyridine synthesis (Scheme 11).

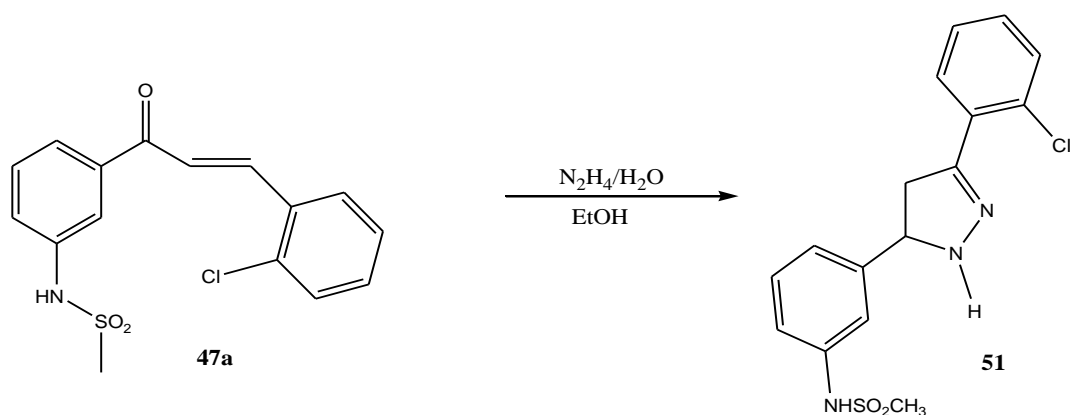
SCHEME 11



The series of pyrazoline analogs were developed with various substituents on B ring, while the A ring is characterized by sulfamidic moiety. The acetylated dihydropyrazoles **45** were obtained using a known procedure [64], by dissolving the chalcone in acetic acid and adding hydrazine hydrate. A pilot reaction to obtain dihydropyrazole without substitution at N-1 was carried out adding hydrazine hydrate smoothly to the chalcone within 30 min in absolute ethanol at 150°C (Scheme 12). The targeted compound was isolated, but in very low yield: in fact, the 1-unsubstituted derivatives have been shown to rapidly undergo reaction with O₂, and not surprisingly, could not be purified by column chromatography.

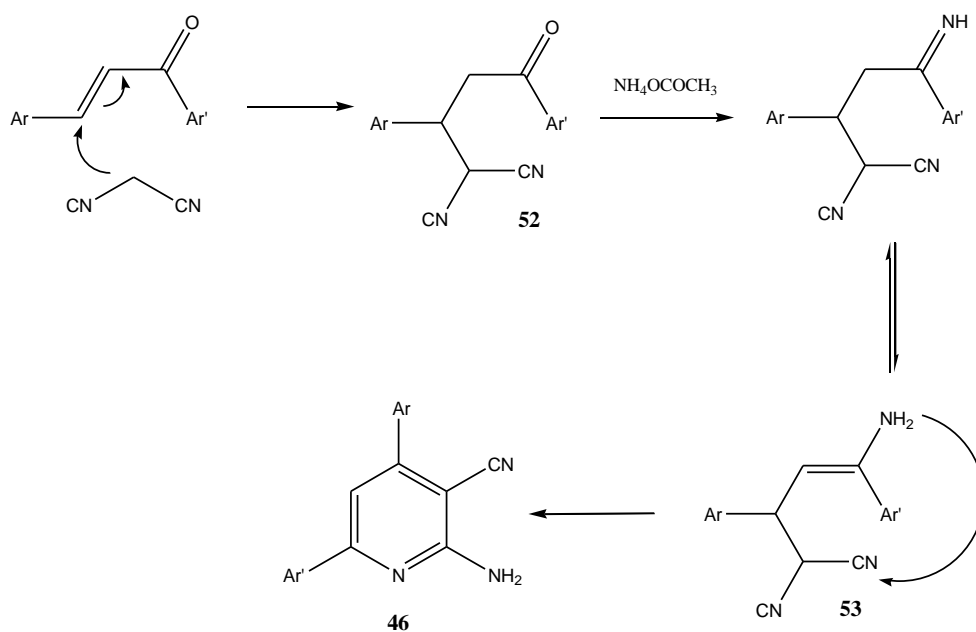
The analysis of the NMR spectra for all the synthesized compounds evidenced the presence of diagnostic double doublets at 3.4-3.01 ppm (*J*= 4.8-4.6 Hz) and at 3.96-3.5 ppm (*J*=17.9-16.0 Hz) attributable to the proton at C-4, and another double doublet at 5.7-5.14 ppm (*J*=12.0 Hz) for the proton at C-5 of the dihydropyrazole.

SCHEME 12



To obtain 2-amino-3-cyanopyridine appropriate chalcones **47** were reacted with malononitrile in presence of ammonium acetate in absolute ethanol. The pyridine derivatives were generally obtained in good yields. The reaction proceeds through Michael addition of the malononitrile anion to the α,β -unsaturated ketones to give the adduct **52**. Formation of the Schiff base, which rearranges to the enamine **53**, can be followed by cyclization and subsequent dehydration of the cyclized product, to give the 2-amino-3-cyanopyridines **46** (Scheme 13).

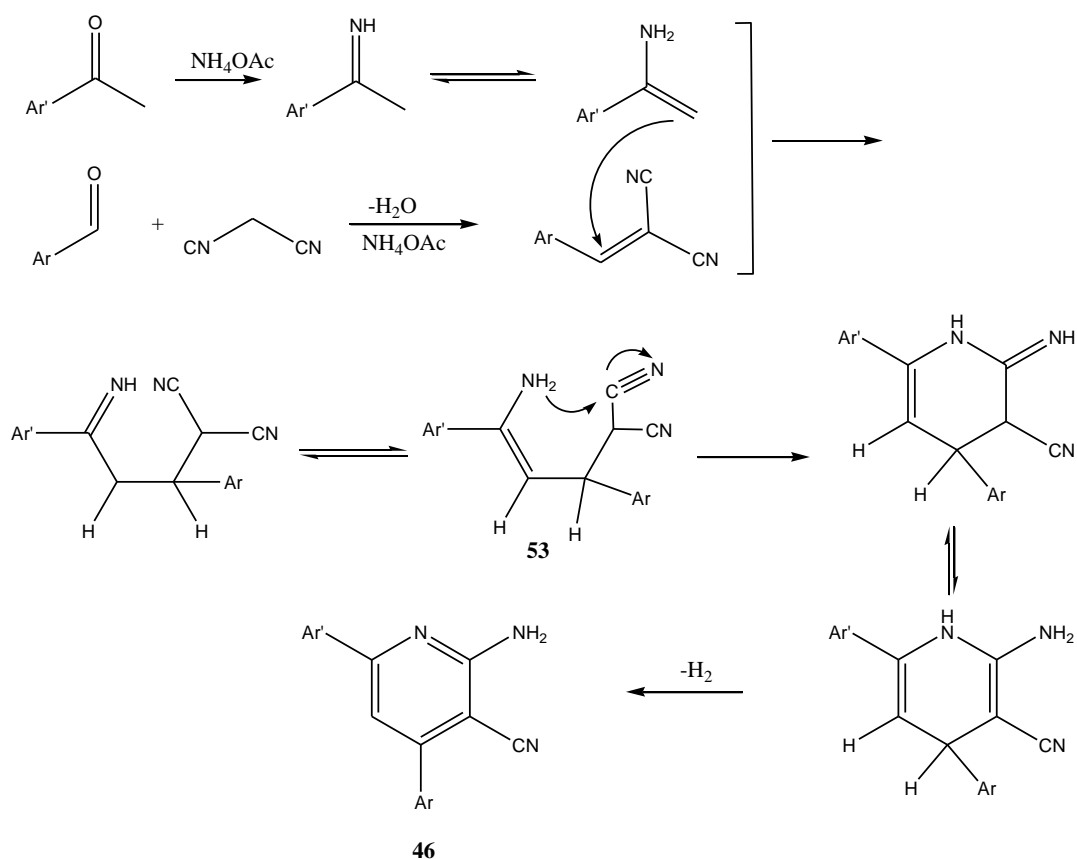
SCHEME 13



The structure of derivatives **46** was assigned on basis of analytical and spectral data. The IR spectra showed a peak at 2215 cm^{-1} due to the cyano stretching frequency and bands in the region $3470\text{--}3355\text{ cm}^{-1}$ due to the amino groups. The ^1H NMR spectra present a broad singlet for the amino protons at 7.01–6.88 ppm, and in the ^{13}C NMR a signal due to the CN group was found at 90.2–86.4 ppm.

The same compounds were also obtained using a different synthetic approach, as shown in the Scheme 14, in comparatively similar yields and analogous reaction times. This method bypasses the chalcone intermediate exploiting a one-pot coupling synthesis of four components. The mixture of aromatic aldehyde, acetophenone, malononitrile, and ammonium acetate is dissolved in absolute dioxane and heated under reflux overnight. The reaction probably proceeds *via* imine intermediate, formed from aldehyde and ammonium acetate, which reacts with alkylidenemalonitrile (from condensation of aromatic aldehyde with malononitrile) to give **53**. The usual cycloaddition, isomerization, and aromatization afforded the 2-amino-3-cyanopyridine **46**.

SCHEME 14



4.3. Biological Activity

The synthesized compounds were selected by the National Cancer Institute (NCI) in the Developmental Therapeutic Program (DTP) to be tested against a panel of 60 different cell lines derived from human tumors. These have been grouped in nine disease subpanels, including leukemia, non small cell lung, colon, central nervous system, melanoma, ovarian, renal, prostate, and breast tumor cell lines.

The antitumoral activity of test compound is given by three parameters for each cell line: pGI_{50} value (GI_{50} is the molar concentration of the compound that inhibits 50% net cell growth), $pTGI$ value (TGI is the molar concentration of the compound leading to the total inhibition of net cell growth), and the pLC_{50} value (LC_{50} is the molar concentration of the compound that induces 50% net cell death). Moreover, a mean graph midpoint (MG_MID) is calculated for each of the mentioned parameters, giving an average activity parameter over all cell lines. For the calculation of the MG_MID, insensitive cell lines are included with highest concentration tested. Selectivity of a compound respect a certain cell line of the screen is characterized by an high deviation of the particular cell line parameter compared to the MD_MID value.

The aim is to prioritize for further evaluation synthetic compounds or natural product samples showing selective growth inhibition or cell killing of particular tumor cell lines. This screen is unique in that the complexity of a 60 cell line dose response produced by a given compound results in a biological response pattern which can be utilized in pattern recognition algorithms (such as COMPARE program). In addition, following characterization of various cellular molecular targets in the 60 cell lines, it may be possible to select compounds most likely to interact with a specific molecular target.

Currently the screening is a two-stage process, beginning with the evaluation of all compounds against the 60 cell lines at a single dose of 10 μ M. The output from the single dose screen is also reported as a mean graph. Compounds are inoculated at a single concentration and the cellular coltures are incubated for 48 hours. The data are reported as cellular growth percent against the control. The derivatives which exhibit significant growth inhibition (less than 32%) are evaluated against the 60 cell panel at five concentration levels.

In the preliminary screening test both the planar polycycles **27a,b** resulted inactive, showing a similar response in all panel (Table 7).

Table 7. Cellular growth percentage

	Leukemia	NSCL	Colon	CNS	Melanoma	Ovarian	Renal	Prostate	Breast
27 a	94.7-103.6	76.6-115.8	95.4-113.2	78.9-118.4	95.8-110.1	101.0-118.3	63.5-156.4	83.5-125.2	97.0-114.7
27b	91.5-107.6	70.8-114.7	97.9-117.3	77.3-114.6	92.7-109.6	83.3-110.5	58.7-160.8	82.1-128.2	98.5-114.7

These results are not surprising, since analogous behaviour was already observed in the case of the other annelated triazolo-pyrimidines of type **20d** [60]. However in previous work in our laboratories it was possible to demonstrate that, although the core ring system was practically inactive, the introduction of suitable chain significantly improved the biological properties of the original lead compound. This observation resulted particularly evident in the case of compound **54** (Fig. 29), a benzothieno[2,3-e][1,2,3]triazolo[1,5-a]pyrimidine derivative, deaza-analogue of the ring system identified by PCA analysis, recognized as potential drug candidate. In fact, this derivative was shown to be cytotoxic activity against the majority of human tumor cell lines investigated (NCI panel), generally in the nanomolar range (Fig. 30).

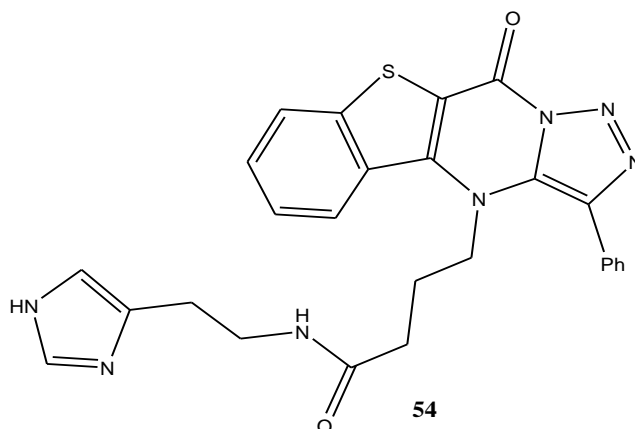


Figure 29

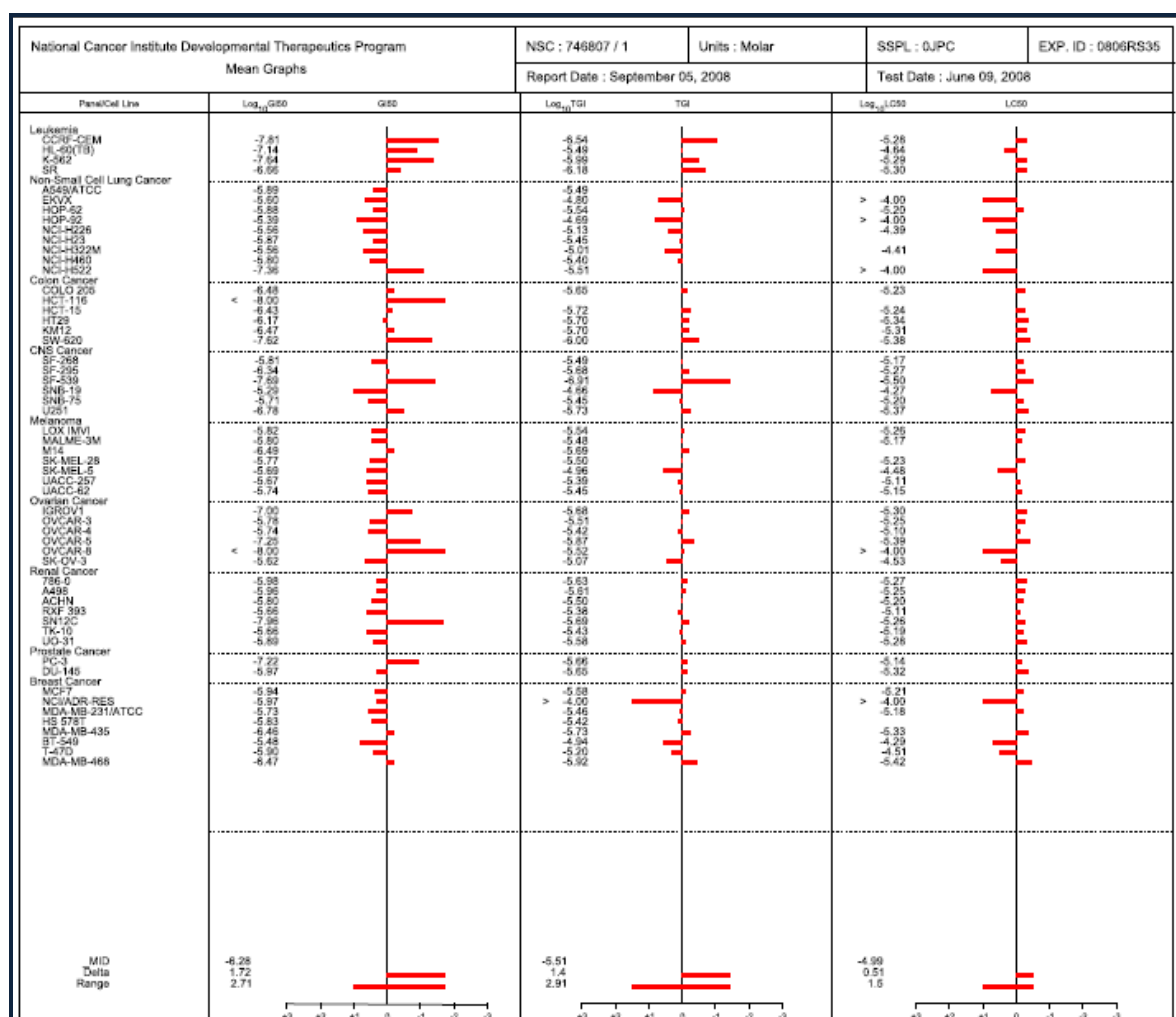


Figure 30. Mean graph for compound **54**

Therefore it has to be expected that also in the case of pyrido-thieno-triazolo-pyrimidine system the introduction of a side chain in 4 position could modify the biological activity profile of these compounds.

An evaluation of the data, obtained by DTP biological screen, revealed that, although compound **38** was active only against the EKVX cell line (-3.24 growth percentage), MDA-MB-425 cell line (-84.19 growth percentage) and CAKI-1 cell line (-87.89 growth percentage), three of the 4-substituted derivatives showed a significant antiproliferative activity against the majority of human tumor cell lines investigated when tested at five concentration levels (Table 8).

Table 8. Cytotoxic activity

	Tested cell lines	pGI₅₀ range	MG-MID
34	59	4.96-7.02	-5.29
37	59	5.03-6.80	-5.30
41	58	4.67-6.74	-5.53

In fact, the thienopyridine polycycle bearing the histamine side chain **34** showed positive response especially against the leukemia (MG_MID=5.93) and colon cancer subpanel (MG_MID=5.74), higher than the overall MG_MID value. However the most susceptible cell line was OVCAR-8 of the ovarian subpanel, against which derivative **34** was active at nsanomolsar concentrations (pGI₅₀=7.02).

Significant antiproliferative activity was found for the derivatives **37** and **41**: in fact, although they present the same side chain, the different structural arrangement of the four rings strongly influences the biological profile.

The mean graph of the compound **37** evidenced the remarkable antiproliferative effect generally in the micromolar range against all the tested cell lines (Fig. 31). Noteworthy is the activity against A498 of the renal subpanel found in the low micromolar range (pGI₅₀=6.80), while the cytotoxic effect is shown against all melanoma (pGI₅₀ range 5.03-5.93) and leukemia cell lines (pGI₅₀ range 5.21-6.10).

A different result was obtained in the case of the linear isomer **41**, which in the average was the most active of the series (Fig 32). In this case the colon and ovarian cell lines resulted the most sensitive to the treatment with pGI₅₀ well above the average, together with the prostate cancer cell line subpanel (MG_MID=5.81).

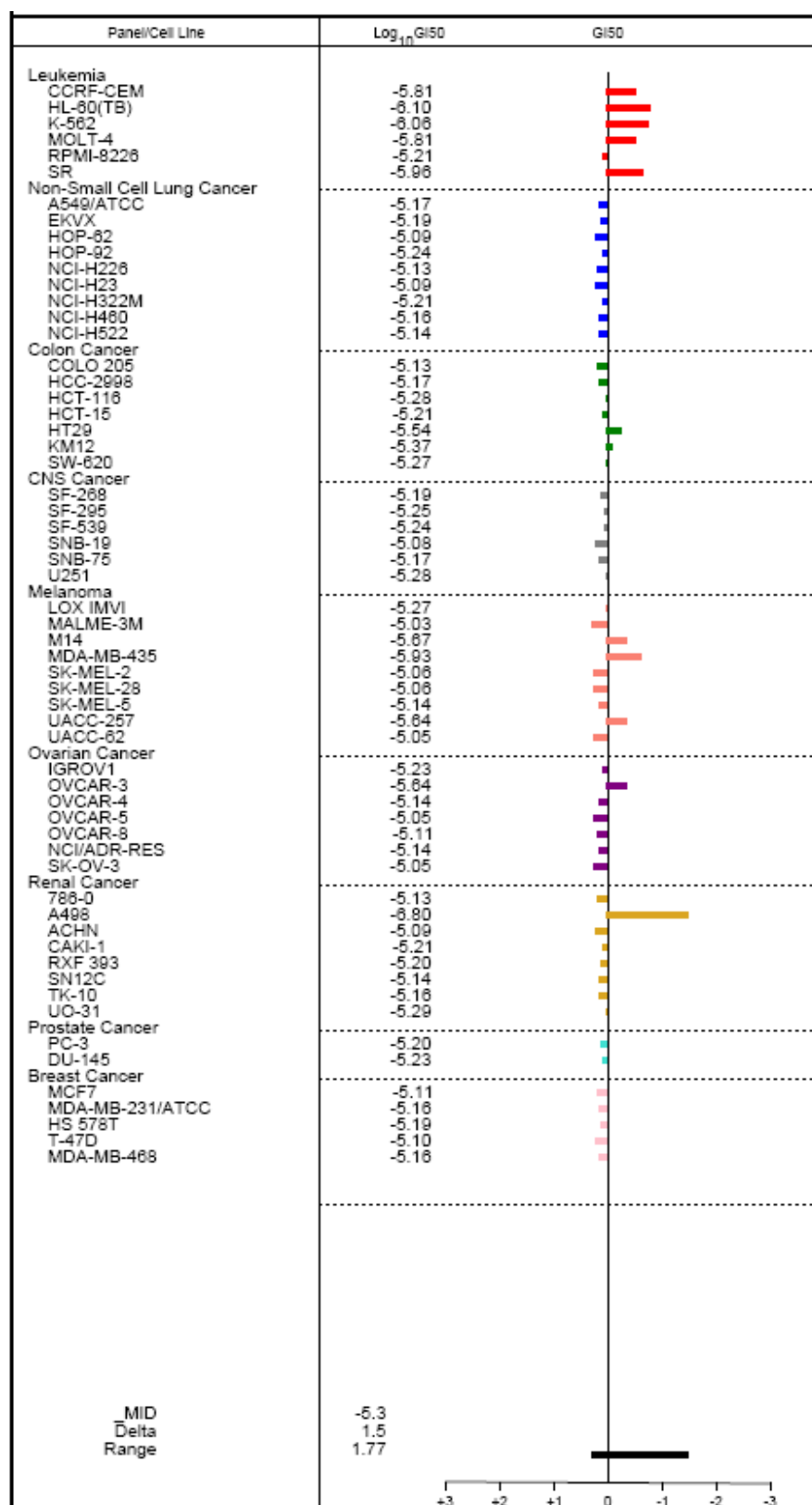


Figure 31. Mean graph for compound 37

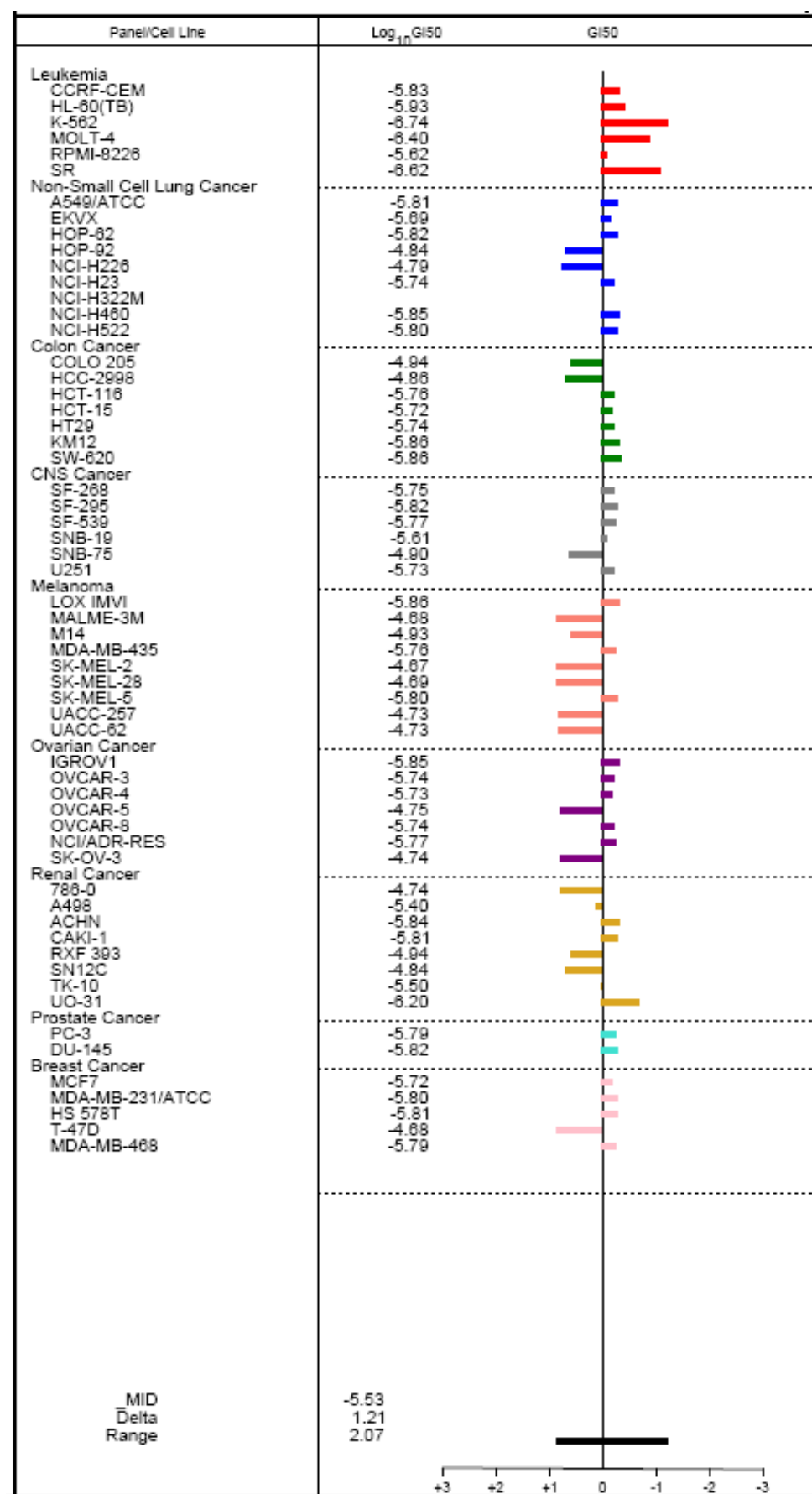
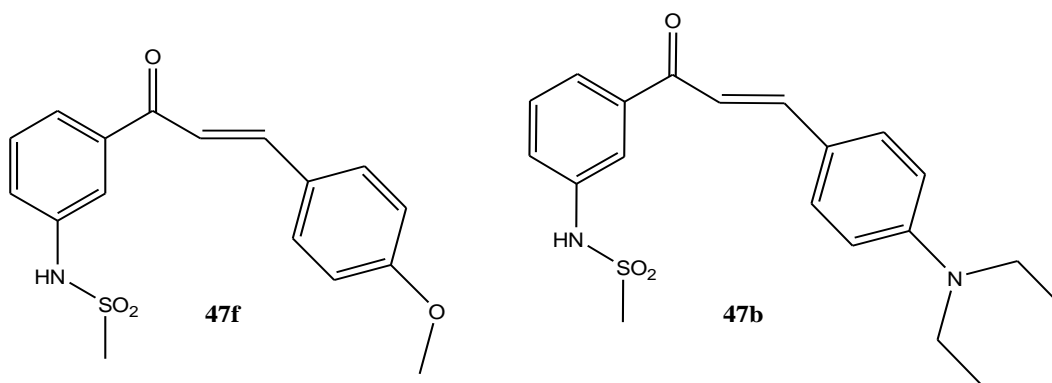


Figure 32. Mean graph for compound 41

Also the pyrazolines **45** and 2-amino-3-cyanopyridines **46**, as well as their common intermediate, the chalcone **47**, were screening at NCI in the DTP protocol.

Compounds presenting a chalcone backbone have been reported to exhibit a wide range of pharmacological effects, including antioncogenic, anti-inflammatory, antiulcerative, analgesic, antiviral, antimalarial and antibacterial activities. The presence of a reactive α,β -unsaturated keto function in chalcones was demonstrated to be responsible for their known activity. Therefore although the chalcones have not been included in our *in silico* screening, they could be worthy of biological testing. And in fact, the chalcone **47f** with 4-methoxy substituent was tested at one dose against the 60 cell line panel, showing a low growth inhibition in the majority of cell lines, while the isosteric compound **47b** bearing the dimethylamino group in 4 position, resulted active with a pGI₅₀ range 4.00-5.65 (Table 9).

Table 9. Cellular growth percentage or cytotoxic activity



	Leukemia	NSCL	Colon	CNS	Melanoma	Ovarian	Renal	Prostate	Breast
47f									
Mean	-10.1-40.8	60.4-96.4	21.0-111.4	37.5-94.7	75.9-113.5	7.9-109.9	48.6-101.0	42.6	46.9-104.5
74.33									

	N° Tested cell lines	N° cell lines giving a positive pGI ₅₀	pGI ₅₀ -range	MG-MID
47b	58	51/58	4.00-5.65	-4.97

In details, as evidenced in the mean graph (Fig. 33), all the cell lines, but one, belonging to the leukemia, colon and breast subpanel resulted particularly susceptible to derivative **47b**, whereas more than half of the melanoma and ovarian lines were

significantly inhibited. The higher activity was found against SR leukemia cell line (pGI₅₀=5.65).

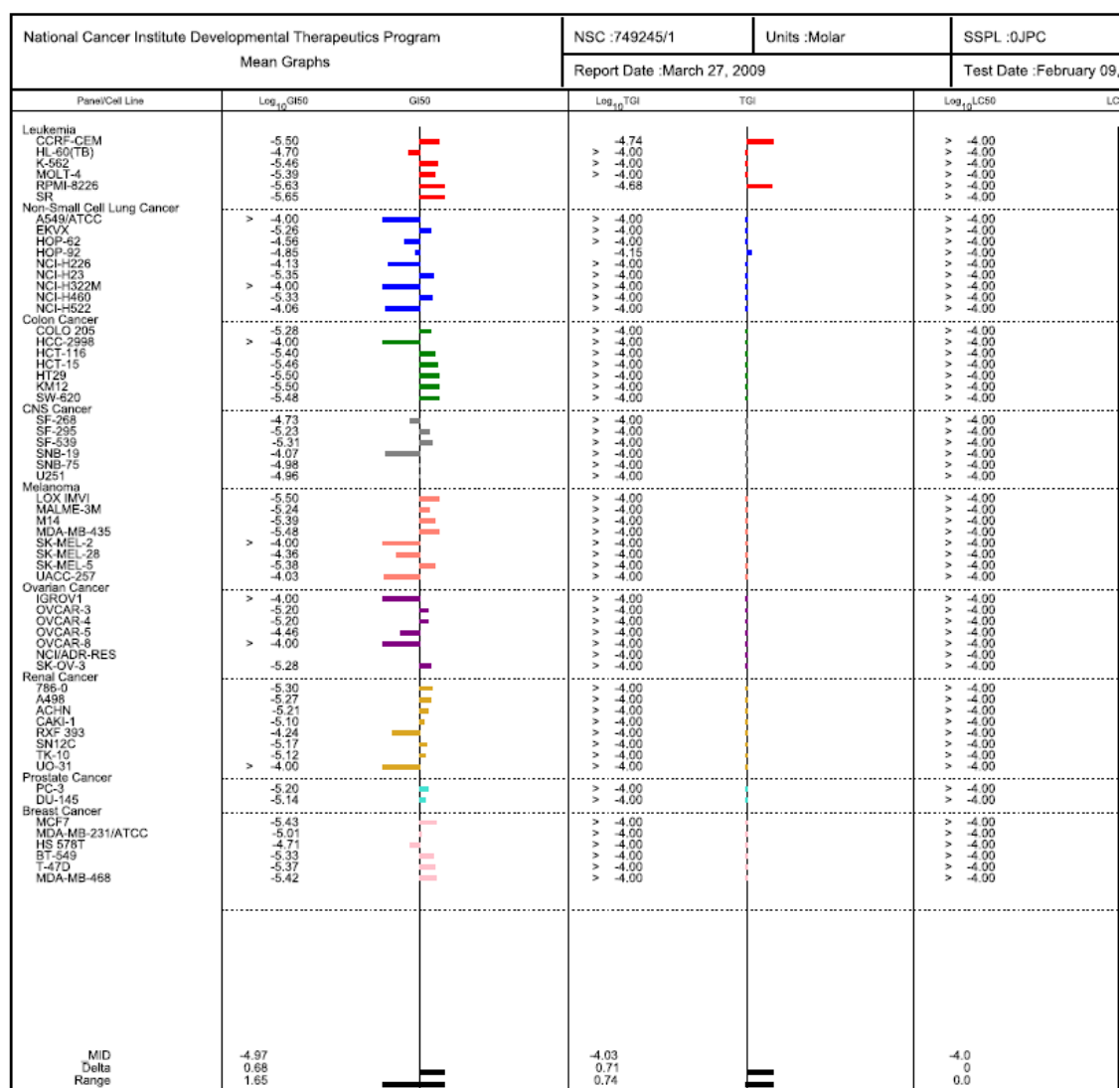


Figure 33. Mean graph for compound 47b

The 3,5-diaryl-4,5-dihydropyrazoles have been identified as active core structures in antibacterial, hypotensive, antinflammatory and antimitotic agent (combretastatins analogues in the tubulin polymerization arrest), as well as Hsp90 inhibitors [64,65]. However, all the tested dihydropyrazoles, included in this study, did not show any significant antiproliferative activity (Table 10).

Table 10. Cellular growth percentage

	Leukemia	NSCL	Colon	CNS	Melanoma	Ovarian	Renal	Prostate	Breast
45f									
Mean	57.89-92.93	86.3-130.5	89.7-125.6	84.2-108.9	90.6-138.6	92.1-104.9	69.1-117.9	97.4-108.0	86.2-97.0
98.13									
45h									
Mean	49.7-115.7	61.5-115.9	84.4-115.7	90.4-125.8	78.3-106.7	55.4-122.1	79.4-116.1	108.1	84.3-101.5
96.59									
45j									
Mean	70.5-119.2	53.8-97.9	75.5-116.2	82.7-104.7	68.4-119.9	35.2-97.1	59.0-116.8	109.9	69.4-97.8
86.77									

On the contrary well different was the behavior of the amino-cyano-pyrimidines when tested in the DTP protocol. They, exhibiting a significant growth inhibition at a single dose of 10 μ M, were all selected for testing at five concentration levels. These results are not surprising since many natural occurring or synthetic compounds, containing the pyridine scaffold, possess interesting pharmacological properties. In fact during the last two decades, a large number of substituted pyridines have been claimed to possess several biological activity. The antifungal and antibacterial properties of these compounds have opened up the possibility of their potential use as a novel class of totally synthetic antimicrobial agents active against pathogenic bacteria. In addition to this, many naturally occurring B6-vitamins pyridoxine, pyrodoxal, pyridoxamine, and codecarboxylase contain a pyridine nucleus. Moreover among them, 2-amino-3-cyanopyridines have been identified as IKK- β inhibitors [66,67].

The results of the screening test on derivatives of type **46** are summarized in Table 11. All the compounds showed high antiproliferative activity against the majority of the tested cell lines in the low micromolar range. As testified by the MG-MID (-7.29), derivative **46b** was the most active being effective at nanomolar concentration (Fig. 34).

An evaluation of the data for this class of compounds with respect to MG_MID values at TGI and LC₅₀ levels also confirmed that all 2-amino-3-cyanopyridines tested present both an high antiproliferative activity and a very low toxicity, since it is remarkable the few number of cell lines giving a pLC₅₀ higher than 4.0.

Table 11. Cytotoxic activity

	Tested cell lines	pGI ₅₀ range	MG-MID
46a	58	4.85-6.76	-6.24
46b	58	6.18->8.0	-7.29
46f	58	6.08-7.90	-6.95
46h	58	5.94-7.79	-6.81

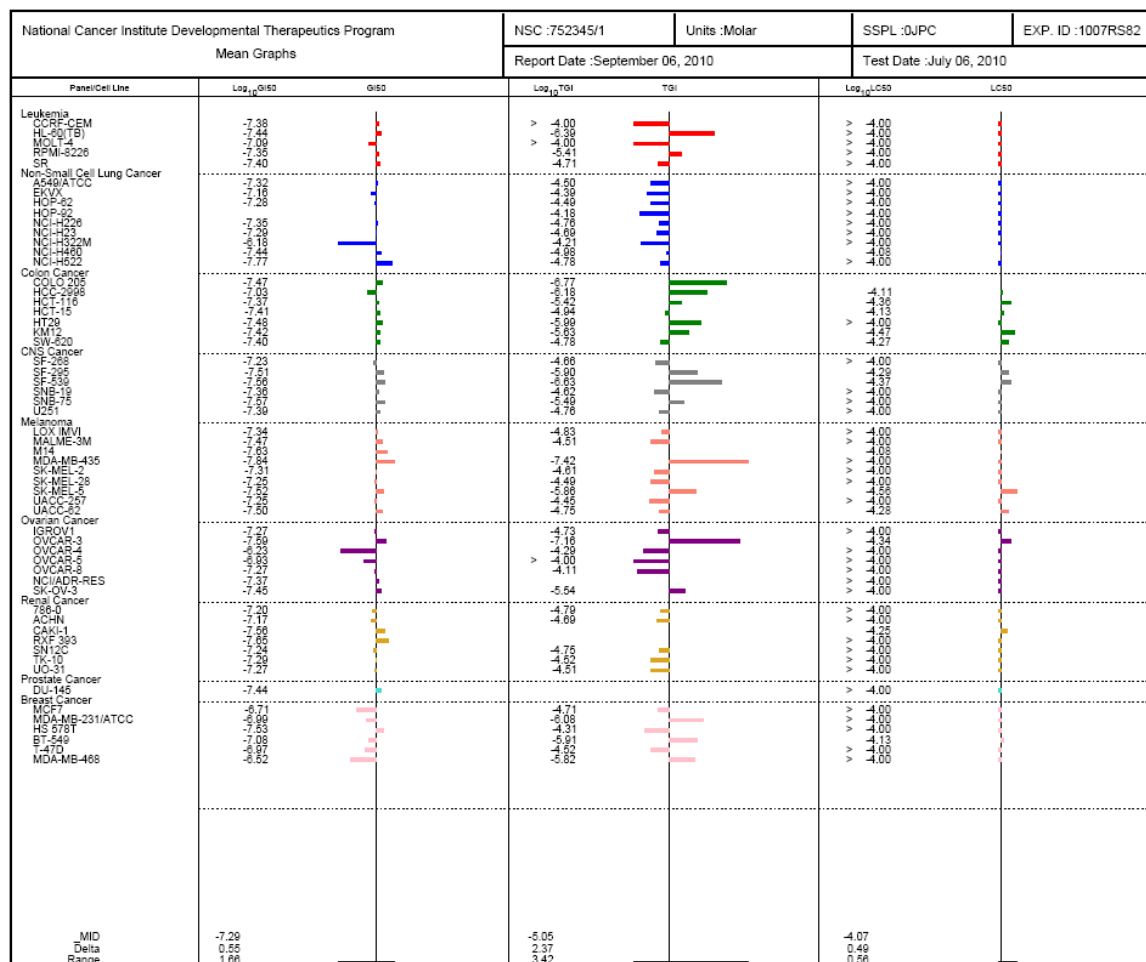


Figure 34. Mean graph for compd 46b

In details, as shown in the dose/response graph for compounds **46b** (Fig. 35), it is notable the optimum activity against all cell lines of the melanoma (MG-MID= -7.45), colon (MG-MID= -7.36), CNS (MG-MID= -7.43) and ovarian (MG-MID= -7.15) cancer subpanels, where a significant growth inhibition is already evidenced at nanomolar concentration (pGI₅₀=7.84 against MDA-MB-435 and pGI₅₀=7.59 against OVCAR-3, respectively a melanoma and an ovarian cell line).

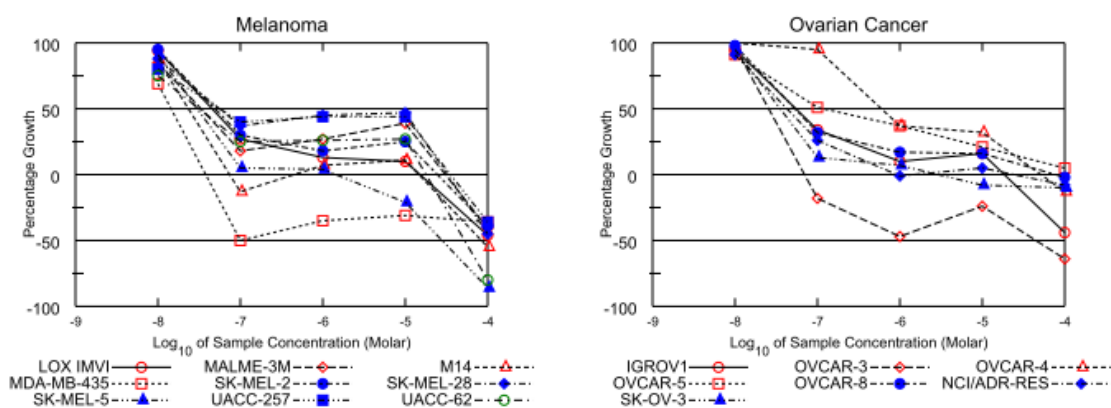


Figure 35. Dose/response graph compd 46b

Significant results were also obtained in the case of derivative **46f**, especially against the cell lines belonging to CNS, melanoma and colon subpanels (Fig. 36). Against all these cell lines pGI_{50} was below 7.0.

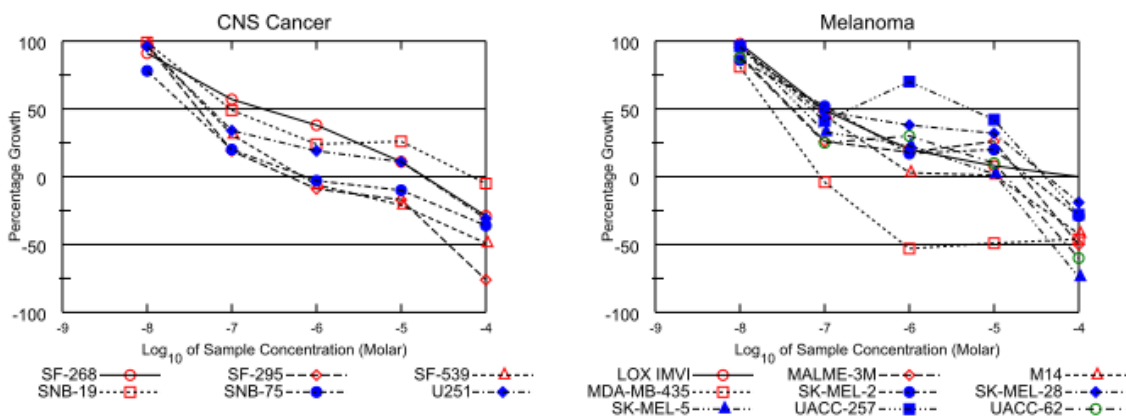


Figure 36. Dose/response graph compd 46f

In conclusion the screening test carried out at NCI revealed that one derivative of the tetracyclic system **41** and three 2-amino-3-cyanopyrimidines of type **46** could be identified for the development of new anticancer drugs, and all of them are currently being proposed for *in vivo* testing.

Although the exact biological target for these active compounds has not identified yet, based on our “*in silico*” analysis we performed further screening tests to evidence a probable mechanism of action at biomolecular level.

First it was checked if our identified leads could target HIF. The great majority of HIF inhibitors described in literature so far have been identified either in cell based screen or by empirical discovery during evaluation of HIF-1 activity in

cultured cancer cell lines. One of the first cell based HTS targeting HIF-1 has been developed and implemented in the Developmental Therapeutics Program of the National Cancer Institute (NCI) at Frederick, where I spent six months during the doctoral period. By using U251-HRE human glioma cells genetically engineered to stably express a recombinant vector in which the luciferase reporter gene is under control of three copies of a canonical HRE, several chemical libraries were screened to identify HIF-1 potential inhibitors. A pilot HTS screen was applied to derivatives of type **45-47** selected in accord to the results of computational studies as potential anticancer drugs. To engineer human cancer cells to express the luciferase reporter gene under control of a HIF-1-inducible promoter, pGL2-TK-HRE, containing three copies of a canonical HRE, were cotransfected with a vector containing the neomycin gene for selection in U251 glioma cells. U251-HRE cells expressed low but detectable levels of luciferase in normoxic conditions but expressed significantly higher levels in cell cultured under hypoxic conditions. A paralleled screen using U251-pGL3 cells, engineered to express luciferase under control of a constitutive oxygen-independent promoter, was also conducted to assess specificity. As shown in Table 12 and in Fig. 37, the results led to confirm the tested compounds had minimal or no activity on the expression of luciferase both in the U251-HRE and U251-pGL3 control cell line.

Table 12. EC_{50} (μM) and activity ratio

	HRE	PGL3	Ratio pGL3/HRE Hypoxia
45a	>20	>20	?
45e	>20	>20	?
45f	>20	>20	?
45g	>20	>20	?
45h	>20	>20	?
45i	>20	>20	?
45j	>20	>20	?
45k	>20	>20	?
46c	>20	>20	?
46e	>20	>20	?
46i	>20	>20	?
47a	13	12	0.9
47b	>20	>20	?
47c	12	10	0.8
47d	>20	15	<0.76
47e	>20	14	<0.72
47h	>20	18	<0.91
47i	13	8	0.7
47k	18	10	0.6

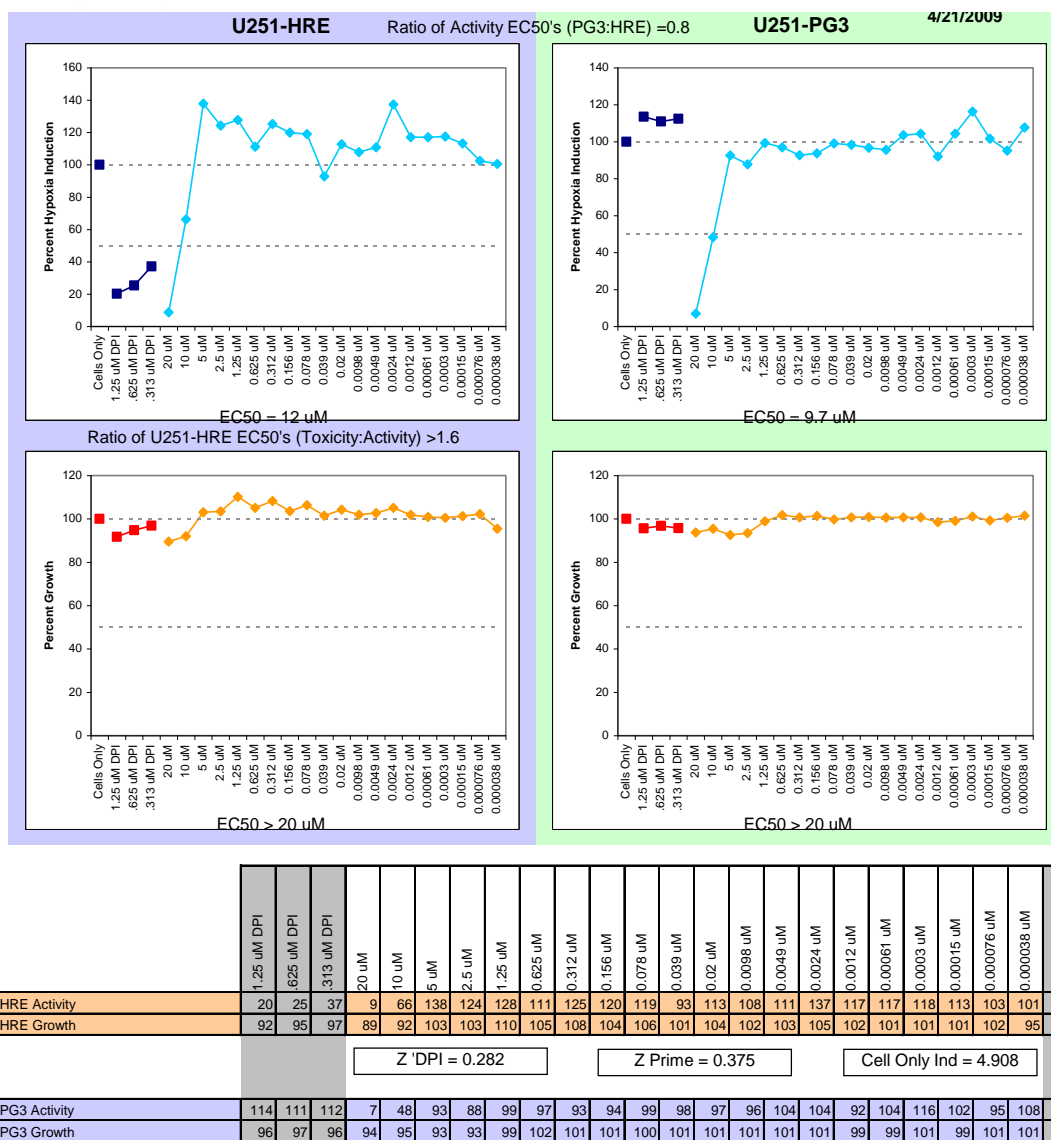


Figure 37. Example of dose/response graph

Antiproliferative assays on MCF7 cells, a hormone-sensitive breast tumor cell line, present in the NCI panel screening, and able to express high level of Hsp90 were also undertaken, to verify if heat shock proteins could be the biological target of our lead compounds. Cells were treated with dihydropyrazine **45j**, or with either the 2-amino-3-cyano-pyrimidines derivatives (**46f** or **46h**), for 24 or 48 hours within the 1.0×10^{-1} - 2.5×10^1 μ M range. Cell density was evaluated by methylene blue staining and compared to the density of cells treated with control vehicle (0.1% DMSO). As shown in Fig. 38, derivatives **46h** and **46f** showed similar growth-inhibitory effect, whereas **45j** resulted less active.

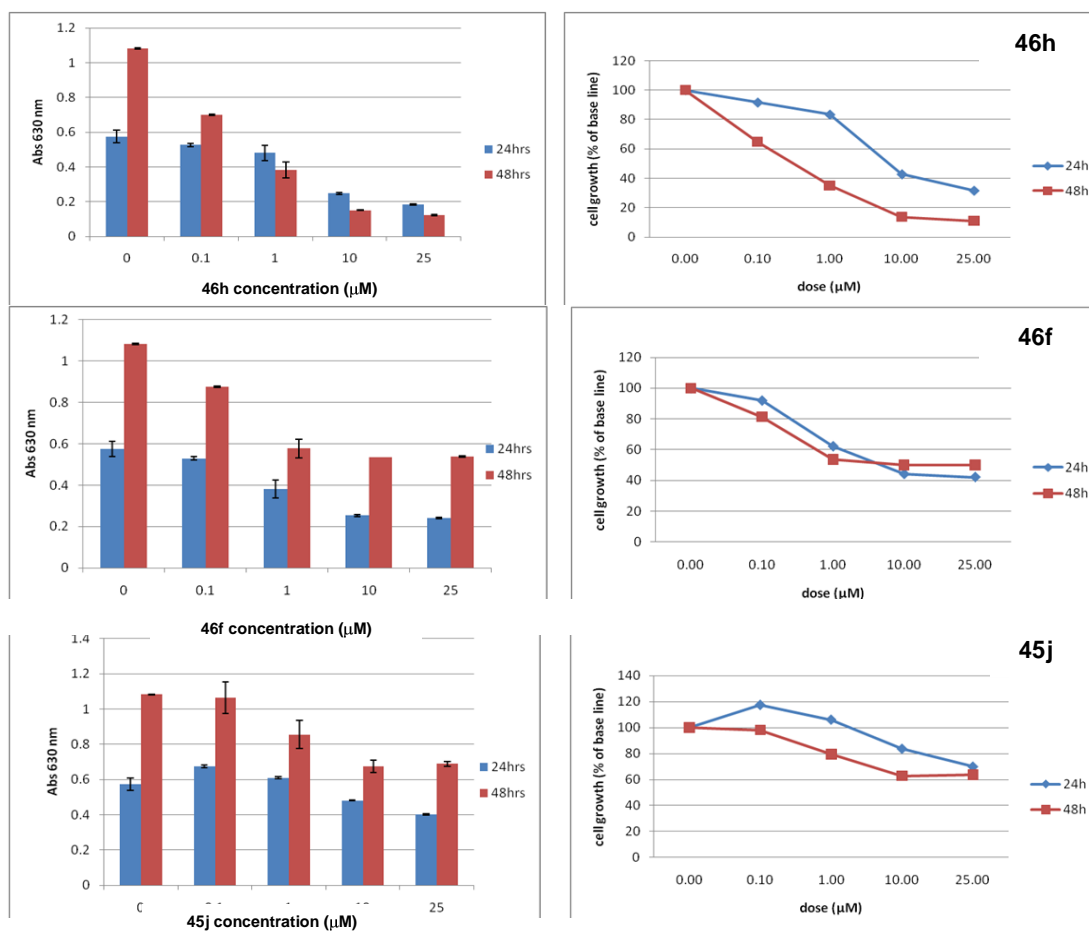


Figure 38. Cell growth curves for compds **46f**, **46h** and **45j**.

Also the antiproliferative effect of dihydropyrazole **45h** on Caco-2 cells, a human colon cancer cell line able to express high level of Hsp90, was investigated obtaining a similar weak inhibitory activity profile (Fig. 39).

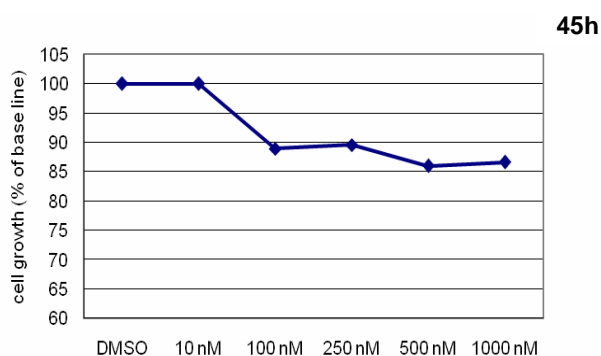


Figure 39. Cell growth curve for compd **45h**.

These preliminary data indicates that the dihydropyrazole derivatives are very weak inhibitors, whereas amino-cyano-pyridine derivatives show a remarkable

activity. This profile is consistent with the results obtained by NCI in the DTP biological screening. Among the amino-cyanopyridine derivatives, **46h** shows the higher antiproliferative activity, thus it was selected for further biological screening to elucidate its specific influence on the cellular pathways involving Hsp90.

To measure the effectiveness of **46h** in inhibiting MCF-7 cell proliferation, the cells were incubated with control vehicle (0,1% DMSO) or 1.0 μM 17-AAG or **46h** at different concentrations (2.0×10^{-1} – 1.0×10^{-2} μM) for 24, 48 and 72 hours. Viability was assessed by trypan blue exclusion staining and IC_{50} value was calculated. Untreated MCF7 cells (Fig. 40) demonstrated rapid proliferation, with cellular numbers at G3 about 3.5 times the initial quantity (G0). As shown in figure, when compared to the untreated control, cell numbers decrease in a dose-dependent manner after **46h** treatment. MCF7 cells quantities were almost the same as the original numbers, after the treatment with 1 μM 17-AAG or **46h** within the 2.0×10^{-1} –1.0 μM range.

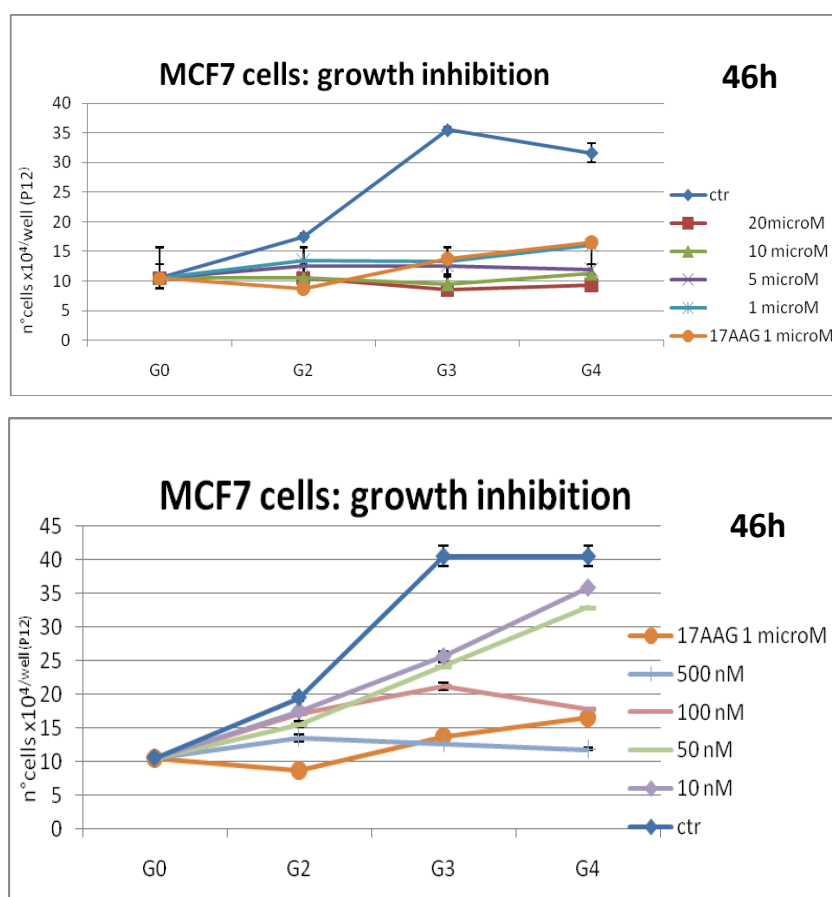


Figure 40. Dose/response graph for compd **46f**

As reported in the introduction, a wide range of oncogenic proteins are stabilized, matured by, and thus depend on Hsp90. The harsh environmental conditions found in tumors tend to destabilize proteins and further augment their dependence on HSP90, as supported by the higher Hsp90 levels found in tumor cells [68,69]. On the other hand, the molecular signature of Hsp90 inhibition comprises induction of Hsp72 coupled with depletion of Hsp90 client proteins.

The antiproliferative activity shown by **46h** on MCF7 cells could be due to the breakdown of multiple cell survival pathways, as a consequence of destabilization of Hsp90 client proteins. To test this hypothesis, Hsp90 client protein levels were evaluated by western blotting analysis.

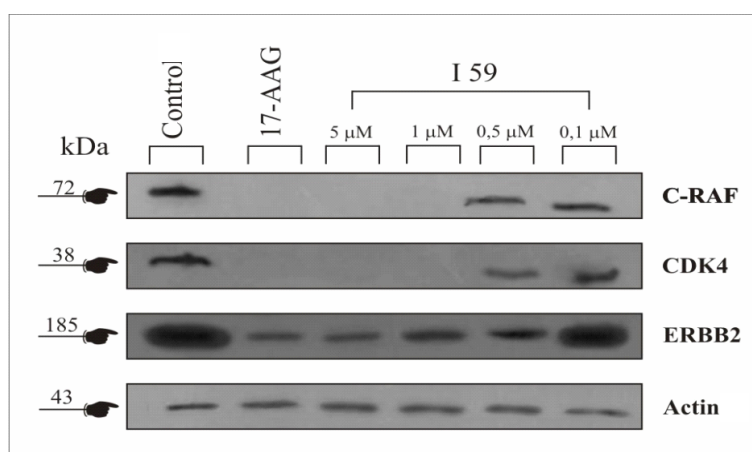


Figure 41. Western blot for compd **46h**

ErbB-2 overexpression is a common phenomenon in multiple malignancies and has been associated with development of resistance to both chemotherapeutic and biologic agents [70]. c-Raf is a kinase protein involved in the MAPK/ERK pathway whose deregulation leads to uncontrolled cellular growth [71]. CDK4, a member of the cyclin-dependent kinase family, is important for cell cycle G₁ phase progression, and its up-regulation has been found to be associated with tumorigenesis of a variety of cancers [72].

All these proteins require the chaperone interaction to exist in an active form and are down-regulated in many tumor cells by GA or 17-AAG treatment. As shown in Figure 41, MCF7 cells untreated are positive for CDK4, c-Raf and ErbB-2. The level of biomarkers decreased after treatment with **46h** for 24 hours. The down-regulation of the Hsp90 proteins levels induced by the 2-amino-3-cyanopyridine **46h** was observed at low concentration with a dose-dependent effect. Of the three Hsp90

client proteins detected, CDK4 was reduced to a greater extent, whereas ErbB-2 levels were less affected. It has been reported that CDK4 and c-Raf are very sensitive to Hsp90 inhibitors [73,74]. These results are comparable to those achieved following exposure of MCF7 cells to 17AAG, under same experimental conditions, and are consistent with the known inhibitory activity of Hsp90.

Antitumor effects can be achieved by cell death and/or cell cycle arrest. **46h** treatment for 24 h did not yield necrosis in MCF7 cells, as demonstrated by negative response to LDH activity assay (data not shown).

CDK4 and CDK6, and the partner/activator of these CDKs, Cyclin D1, are key cell cycle regulator proteins. The interaction of Cyclin D1 and CDK4 is vital during the G₁ phase, and disruption of either Cyclin D1 or Cdk4 can induce G₀/G₁ arrest. CDK4 and CDK6 are clients of the Hsp90 molecular chaperone. It has been proved that Hsp90 inhibitors can affect these CDKs, causing cell cycle arrest [72,74]. We observed that **46h** treatment induces CDK4 down-regulation at low concentration and in a dose-dependent-manner. Indeed, a preliminary analysis of cellular cycle distribution, carried out by FCM following PI staining of DNA contents, is consistent with this inhibitor effect. Untreated MCF7 cells showed a normal diploid distribution presenting fast proliferation characteristics, with cells in S + G₂/M accounting for about 40% of the total cells. Treatments with $5.0 \times 10^{-1} \mu\text{M}$ **46h** for 24 hours caused an increase in the number of cells at G₀/G₁. When the same treatment was performed for 48 hours, a new population sub-G₀/G₁ appeared with a parallel decrease of the G₀/G₁ population (data not shown).

To explore if our test compounds could be also involved in apoptosis further biological experiments were also carried out. In fact, apoptosis is defined by a distinct set of morphological changes observed during cell death including loss of focal adhesions, formation of cell membrane buds or blebs, and decrease in total cell volume. Recent studies suggest that these dramatic morphological changes are an early prerequisite to apoptosis and precede key biochemical time-points [74]. In particular when cells are stressed, a common response is to undergo cell death by one of two pathways, either “necrosis” or “apoptosis”. Recently, both routes to cell death have been revealed to share similar mechanisms, with heat-shock proteins and their cofactors responsible for inhibiting both apoptotic and necrotic pathways [75]. MCF7 cells treated with **46h** within the 0.5×10^{-1} – $5.0 \times 10^{-3} \mu\text{M}$ range when compared to

untreated cells show dramatic morphological feature changes associated with apoptosis (Fig. 42).

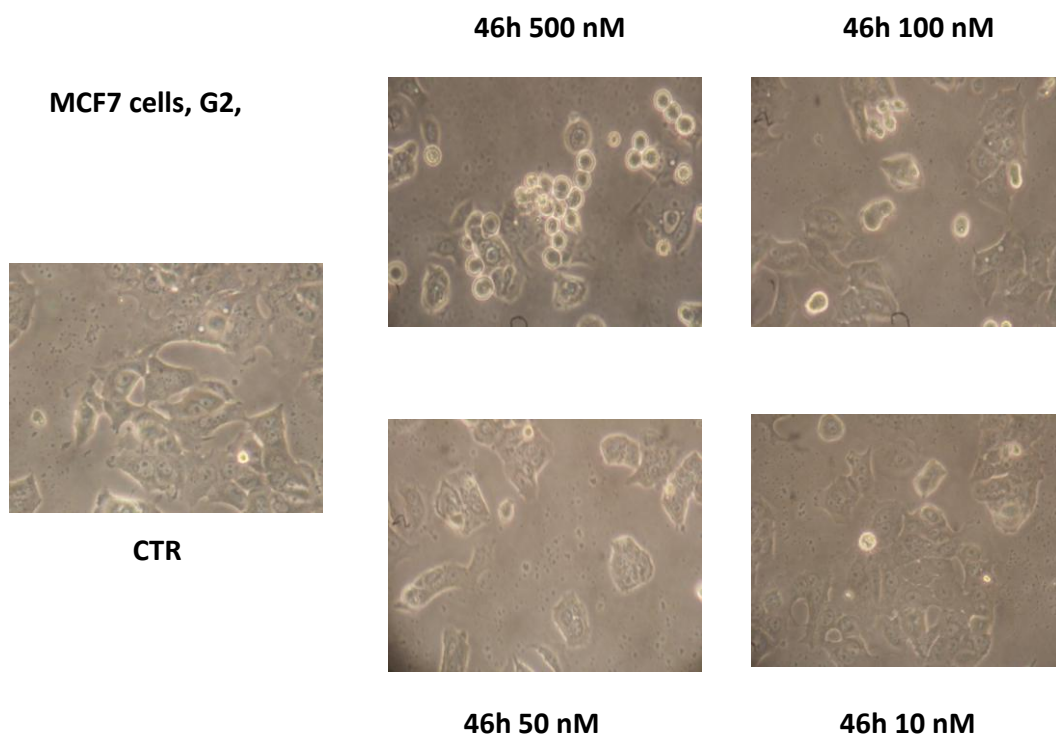


Figure 41. Microscopy images of MCF7 cells treated with different concentration of compound **46h** for 24h.

Collectively, these results suggest that the antiproliferative effect of **46h** derivative treatment on MCF cells is due to G₀/G₁ cell cycle arrest and subsequent apoptosis.

Currently further biological screenings are undertaken for other amino-cyano-pyrimidine analogues and for the new 4-substituted polyheterocycles to elucidate their specific influence on the cellular pathways involving Hsp90.

5. CONCLUSIONS

In conclusion, new potential Hsp90 inhibitors are identified by utilizing the ligand-based virtual screening. These findings empathize the usefulness of virtual screening in the development of targeted inhibitors with novel structures.

The investigation of binding modes in the ATP-binding pocket of Hsp90 has provided valuable information to design various effective derivatives, presenting these features (Pharmacophore approaches). By multivariate analysis the planar ring systems, bearing suitable side chains and extracted from an “*in house*” database, were identified as potential protein-binders.

The selected compounds were synthesized, generally in good – excellent yields, by using known chemical approaches.

The antiproliferative activity, against a panel of nearly 60 cell lines, was evaluated by NCI in the DTP protocol. The most active derivative was also tested to explore its involvement in signal-transduction pathways correlated with Hsp90.

The biological results demonstrated that some of the new derivatives, discovered and synthesized during this work, can be effective as antiproliferative agents, mainly against melanoma tumor cell lines, at concentrations ranging from micro to nanomolar. Moreover they seem to be involved in pathways correlated with Hsp90 activity. Three of these compounds are currently screened *in vivo* in the preclinical assays, whereas further insights in the mechanism of action are worthy of investigation.

6. EXPERIMENTAL SECTION

6.1. Chemistry

All melting points were taken on a Buchi-Tottoli capillary apparatus and are uncorrected; IR spectra were determined in bromoform with a Jasco FT/IR 5300 spectrophotometer; ^1H and ^{13}C NMR spectra were measured in DMSO- d_6 solution, unless otherwise specified, (TMS as internal reference) at 200 and 50.3 MHz, respectively, using a Bruker AC-E series 200 MHz spectrometer. ^{13}C NMR spectra are reported, indicating the multiplicity, (s, singlet; d, doublet; t, triplet; q, quartet) assigned by DEPT135 experiments. Column chromatography was performed with Merck silica gel 230–400 mesh ASTM or with a Biotage FLASH40i chromatography module (prepacked cartridge system), unless otherwise specified. Microanalyses were in agreement with theoretical values $\pm 0.4\%$.

Ethyl 3-aminothieno[2,3-b]pyridine-2-carboxylate (**23**)

According to the literature procedure [61], ethyl thioglycolate **22** (1.2 mL, 11 mmol) was added to a stirred mixture of NaH (0.36 g, 15 mmol) and DMSO (10 mL). After evolution of H_2 had ceased, a solution of 2-chloro-3-cyanopyridine **21** (1.40 g, 10 mmol) in DMSO (20 mL) was added dropwise. After 3h the mixture was poured onto stirred water/ice. The light yellow precipitate was collected and dried to give **23** (2.25 g, 100%), Mp. 183°C . IR: 3395 (NH_2), 1689 (CO) cm^{-1} ^1H NMR ppm: 8.68 (dd, $J = 4.6, 1.6$ Hz, 1H, H-6), 8.54 (dd, $J = 8.2, 1.6$ Hz, 1H, H-4), 7.46 (dd, $J = 8.2$ Hz, 4.6 Hz, 1H, H-5), 7.31 (br s, 2H, NH_2), 4.30 (q, $J = 7.1$ Hz, 2H, CH_2), 1.29 (t, $J = 7.1$ Hz, 3H, CH_3). ^{13}C NMR ppm: 164.3(s), 159.6(s), 150.7(d), 147.7(s), 131.4(d), 125.5(s), 119.3(d), 93.3(s), 59.9(t), 14.4(q).

Ethyl 3-Azidothieno[2,3-b]pyridine-2-carboxylate (**24**)

A solution of ethyl 3-aminopyrido[3,2-b]thiophene-2-carboxylate **23** (0.3 g, 1.35 mmol) in 6N hydrochloric acid (12 mL) was cooled in an ice bath to -5 – 0°C . A solution of sodium nitrite (0.186 g, 2.7 mmol) in water (2 mL) was added slowly under vigorous stirring. After 30 min sodium azide (0.35 g, 5.4 mmol) in water (2 mL) was added dropwise over 10 min. The reaction mixture was stirred for further 3h at room temperature and then slowly poured onto water/ice. The precipitate was

separated, washed on the filter with cold water until the wash water was neutral, and dried in the absence of light to give **24** (0.22 g, 60%), Mp 93°C. IR: 2127 (N₃), 1705 (CO) cm⁻¹. ¹H NMR ppm: 8.68 (dd, J = 4.6, 1.6 Hz, 1H, H-6), 8.54 (dd, J = 8.2, 1.6 Hz, 1H, H-4), 7.46 (dd, J = 8.2, 4.5 Hz, 1H, H-5), 4.30 (q, J = 7.1 Hz, 2H, OCH₂), 1.30 (t, J = 7.1 Hz, 3H, CH₃). ¹³C NMR ppm: 164.3(s), 159.6(s), 150.7(d), 147.7(s), 131.4(d), 125.5(s), 119.3(d), 93.3(s), 59.9(t), 14.41(q).
Anal. Calcd. for C₁₀H₈N₄O₂S: C, 48.38; H, 3.25; N, 22.57; S, 12.92, found: C, 48.40; H, 3.28; N, 22.55; S, 12.94.

5-Oxopyrido[3',2':4,5]thieno[2,3-e][1,2,3]triazolo[1,5-a]pyrimidine-3-carbonitrile (27a)

To a solution of 1.3 M sodium ethoxide in ethanol (2.7 mL) malononitrile (0.115 g, 1.73 mmol) in absolute ethanol (2 mL) were added at room temperature. After being stirred for 15 min the solution was added to a solution of azido derivative **24** (0.215 g, 0.87 mmol) in absolute ethanol (3 mL) and the mixture was stirred overnight at room temperature. Evaporation of the solvent under reduced pressure gave a solid which was purified by column chromatography using dichloromethane/methanol 9:1 as eluant to afford compound **27a** as a white solid (0.140 g, 0.52 mmol). Yield 60%, mp >410°C. IR: 3404 (NH), 2231 (CN), 1685 (CO). ¹H NMR ppm: 8.79 (dd, J = 3.2 Hz, 1H, H-8), 8.65 (dd, J = 6.5 Hz, 1H, H-10), 7.6 (dd, J = 3.2, 6.5 Hz, 1H, H-9). ¹³C NMR ppm: 162.2(s), 152.7(s), 151.9(s), 150.9(d), 149.5(s), 131.9(d), 128.2(d), 120.3(s), 114.7(s), 105.1(s), 104.4(s).
Anal. Calcd. for C₁₁H₄N₆OS: C, 49.25; H, 1.50; N, 31.33; S, 11.95, found: C, 49.30; H, 1.54; N, 31.32; S, 11.98.

By identical synthetic procedure and reducing the solvent volume (2 mL), the intermediate **ethyl 3-(5-amino-4-cyano-1H-1,2,3-triazol-1-yl)thieno[2,3-b]pyridine-2-carboxylate (26a)** was filtered off, air dried and recrystallized from ethanol. Yield 35%, mp >410°C. IR: 3550 and 3420 (NH₂), 2254 (CN), 1648 (CO). ¹H NMR ppm: 8.89 (s, 1H, NH), 8.77 (dd, J = 4.6, 1.6 Hz, 1H, H-6), 8.63 (dd, J = 7.9, 1.6 Hz, 1H, H-4), 7.60 (dd, J = 7.9, 4.6 Hz, 1H, H-5), 4.35 (q, J = 7.0 Hz, 2H, CH₂), 1.39 (t, J = 7.0 Hz, 3H, CH₃). ¹³C NMR ppm: 162.3(s), 161.3(s), 152.2(s), 152.1(s), 150.6(d), 146.7(s), 131.5(d), 128.5(s), 122.4(s), 120.2(d), 103.8(s), 59.5(t), 14.4(t).

Anal. Calcd. for $C_{13}H_{10}N_6O_2S$: C, 49.67; H, 3.21; N, 26.74; S, 10.20; found: C, 49.65; H, 3.23; N, 26.71; S, 10.22.

3-Phenylpyrido[3',2':4,5]thieno[2,3-e][1,2,3]triazolo[1,5-a]pyrimidin-5(4H)-one (27b)

To a solution of 1.3 M sodium ethoxide in ethanol (4.6 mL) phenylacetonitrile (0.35g, 3.0 mmol) in absolute ethanol (2 mL) was added at room temperature. After being stirred for 15 min, the solution was added to a solution of azido derivative **24** (0.37g, 1.5 mmol) in absolute ethanol (3 mL) and the mixture was stirred overnight at room temperature. Evaporation of the solvent under reduced pressure gave a solid which was purified by column chromatography using dichloromethane/methanol 9:1 as eluant to afford compound **27b** as a yellow solid (0.3 g, 0.94 mmol). Yield 63%, mp >410°C. IR: 3368 (NH), 1630 (CO) cm^{-1} . 1H NMR ppm: 8.74 (d, J = 3.1 Hz, 1H, H-8), 8.66 (d, J = 7.8 Hz, 1H, H-10), 8.54-7.96 (m, 2H, H-2', H-6'), 7.60-7.44 (m, 3H, H-3', H-4', H-5'), 7.25 (d, J = 7.3 Hz, 1H, H-9). ^{13}C NMR ppm: 162.3(s), 151.8(s), 150.3(d), 146.2(s), 144.2(s), 133.2(s), 132.3(s), 131.3(d), 129.1(s), 128.3(d), 125.3(d), 124.0(d), 120.00(d).

Anal. Calcd. for $C_{16}H_9N_5OS$: C, 60.18; H, 2.84; N, 21.93; S, 10.04; found: C, 60.16; H, 2.87; N, 21.94; S, 10.06.

Reaction of 27b with ethyl 4-bromobutyrate

To a stirred suspension of **27b** (0.3 g, 0.93 mmol) in absolute DMF (10 mL), potassium carbonate (0.39 g, 2.81 mmol) and ethyl 4-bromobutyrate (0.9 g, 4.65 mmol) were added. The mixture was heated at 60°C for 16h, cooled to room temperature, and then slowly poured onto water/ice. The precipitate was purified by column chromatography using dichloromethane/ethyl acetate 98:2 as eluant to afford compound **ethyl (3-phenyl-10-oxopyrido[2',3':4,5]thieno[3,2-d][1,2,3]triazolo[1,5-a]pyrimidin-4-yl)butanoate (32)**. Yield 11%, mp 137.2-138.0°C. 1H NMR ppm: 9.36 (dd, J = 8.0, 1.4 Hz, 1H, H-7), 8.61 (dd, J = 4.6, 1.4 Hz, 1H, H-5), 8.41 (d, J = 7.3 Hz, 2H, H-2', H-6'), 7.68 (dd, J = 8.0, 4.6 Hz, 1H, H-6), 7.50 (t, J = 7.3 Hz, 2H, H-3', H-5'), 7.34 (d, J = 7.3 Hz, 1H, H-4'), 4.79 (t, J = 6.0 Hz, 2H, NCH_2), 4.18 (q, J = 7.1 Hz, 2H, OCH_2), 2.62 (t, J = 7.2 Hz, 2H, CH_2), 2.27-2.40 (m, 2H, $CH_2CH_2CH_2$), 1.27 (t, J = 7.1 Hz, 3H, CH_3). ^{13}C NMR ppm: 172.7(s), 162.5(s), 158.9(s), 151.5(d), 134.6(d), 133.6(s), 130.7(s), 129.7(s), 128.7(d), 127.7(d),

125.7(d), 122.5(s), 121.3(d), 112.85(s), 110.0(s), 67.5(t), 60.6(t), 30.8(t), 23.9(t), 14.2(q).

Anal. Calcd. for C₂₂H₁₉N₅O₃S: C, 60.96; H, 4.42; N, 16.16; S, 7.40; found: C, 60.96; H, 4.44; N, 16.17; S, 7.43.

Further elution with dichloromethane/ethyl acetate 95:5 gave **ethyl (3-phenyl-5-oxopyrido[3',2':4,5]thieno[2,3-e][1,2,3]triazolo[1,5-a]pyrimidin-4-yl)butanoate (29)**. Yield 63%, mp 109.6-110.8°C. ¹H NMR (CDCl₃) ppm: 8.78 (dd, J = 4.6, 1.5 Hz, 1H, H-8), 8.61 (dd, J = 7.9, 1.5 Hz, 1H, H-10), 7.42 (dd, J = 7.98, 1.64 Hz, 1H, H-9), 7.63-7.50 (m, 5H, Ph), 4.94 (t, J = 6.6 Hz, 2H, NCH₂), 3.92 (q, J = 7.1 Hz, 2H, OCH₂), 2.41 (t, J = 7.2 Hz, 2H, CH₂), 2.06 (m, 2H, CH₂CH₂CH₂), 1.08 (t, J = 7.1 Hz, 3H, CH₃). ¹³C NMR ppm: 172.0(s), 161.7(s), 151.9(s), 151.5(d), 150.8(d), 145.3(s), 136.6(s), 131.9(d), 129.6(s), 128.7(d), 128.0(s), 127.5(s), 126.1(d), 120.8(d), 112.6(s), 59.9(t), 55.1(t), 30.3(t), 23.5(t), 13.8(q).

Anal. Calcd. for C₂₂H₁₉N₅O₃S: C, 60.96; H, 4.42; N, 16.16; S, 7.40; found: C, 60.94; H, 4.41; N, 16.13; S, 7.44.

General procedure for the hydrolysis of the ethyl butanoates.

To a suspension of **29** or **32** (0.5 mmol) in absolute ethanol (5 mL), a solution of potassium hydroxide (0.08 g, 1.5 mmol) in water (1 mL) was added dropwise. The mixture was stirred at room temperature for 8h. The ethanol was evaporated under reduced pressure, the residue was dissolved in water (10 mL) and then carefully adjusted to pH=1 with 6N hydrochloric acid. The precipitate was filtered off, air dried and recrystallized from dichloromethane to afford the corresponding acid.

4-(3-Phenyl-5-oxopyrido[3',2':4,5]thieno[2,3-e][1,2,3]triazolo[1,5-a]pyrimidin-4-yl)butanoic acid (30) was isolated in 86% yield, mp 171.0-171.6°C. ¹H NMR ppm: 9.33 (br s, 1H, OH), 8.64 (dd, J = 4.5, 1.5 Hz, 1H, H-8), 7.88 (dd, J = 8.2, 1.4 Hz, 2H, H-2', H-6'), 7.51 (dd, J = 8.4, 1.5 Hz, 1H, H-10), 7.46-7.32 (m, 3H, H-3', H-4', H-5'), 7.27 (dd, J = 8.4, 4.5 Hz, 1H, H-9), 4.4 (t, J = 6.6 Hz, 2H, NCH₂), 2.3 (t, J = 6.6 Hz, 2H, CH₂COOH), 2.13-1.99 (m, 2H, CH₂CH₂CH₂). ¹³C NMR ppm: 173.6 (s), 166.1 (s), 159.0 (s), 149.9 (d), 143.0 (s), 137.6 (s), 132.5 (d), 129.6 (s), 128.8 (d), 128.2 (d), 126.1 (d), 125.5 (s), 119.2 (d), 99.4 (s), 53.92 (t), 30.28 (t), 24.59 (t).

Anal. Calcd. for C₂₀H₁₅N₅O₃S: C, 59.25; H, 3.73; N, 17.27; S, 7.91; found: C, 59.24; H, 3.71; N, 17.30; S, 7.92.

4-(3-Phenyl-10-oxopyrido[3',2':4,5]thieno[3',2':4,5]thieno[2,3-e][1,5-a]pyrimidin-4-yl)butanoic acid (33) was isolated in 70% yield, mp 180.9-181.6°C. ¹H NMR ppm: 8.73 (dd, J = 8.2, 1.7 Hz, 1H, H-7), 8.63 (dd, J = 7.8 Hz, 2H, H-2', H-6'), 7.5-7.24 (m, 5H, H-5, H-6, H-3', H-4', H-5'), 4.75 (t, J = 6.4 Hz, 2H, NCH₂), 2.02 (t, J = 6.4 Hz, 2H, CH₂COOH), 1.60-1.49 (m, H, CH₂CH₂CH₂). ¹³C NMR ppm: 174.2(s), 165.8(s), 159.9(s), 150.2(d), 144.1(s), 136.8(s), 131.2(d), 129.8(s), 128.8(d), 125.3(d), 124.0(d), 126.5(s), 119.9(d), 99.4(s), 62.7(t), 38.0(t); 28.8(t).
 Anal. Calcd. for C₂₀H₁₅N₅O₃S: C, 59.25; H, 3.73; N, 17.27; S, 7.91; found: C, 59.22; H, 3.70; N, 17.28; S, 7.94.

General procedure for reaction of acids with histamine

To a stirred suspension of **30** or **33** (0.44 mmol) in absolute dioxane (5 mL), DMAP (0.05 g, 0.45 mmol) and EDCI (0.17 g, 9.2 mmol) were added under nitrogen atmosphere. After 2h histamine (0.102 g, 9.2 mmol) was added carefully. The reaction mixture was stirred for 5 days at room temperature. The solvent was evaporated under reduced pressure and the residue was purified by column chromatography using dichloromethane/methanol 9:1 as eluant.

N-[2-(1H-Imidazol-4-yl)ethyl]-4-(3-Phenyl-5-oxopyrido[2',3':4,5]thieno[3,2-d][1,2,3]triazolo[1,5-a]pyrimidin-4-yl) butanamide (31) had mp 234.7-240.3°C ¹H NMR ppm: 8.90 (dd, J = 4.6, 1.7 Hz, 1H, H-8), 8.85 (dd, J = 8.0, 1.7 Hz, 1H, H-10), 8.57 (dd, J = 8.3, 1.6 Hz, 2H, H-2', H-6'), 7.72 (dd, J = 8.0, 4.6 Hz, 1H, H-9), 7.68-7.55 (m, 4H, H-3', H-4', H-5', CH), 6.7 (s, 1H, CH), 5.0 (t, J = 6.7 Hz, 2H, NCH₂), 3.44 (t, J = 6.5 Hz, 2H, CH₂CO), 3.13 (t, J = 7.0 Hz, 2H, CH₂CH₂), 2.17 -2.03 (m, 4H, CH₂CH₂CH₂, CH₂CH₂). ¹³C NMR ppm: 173.6 (s), 166.1 (s), 161.7(s), 159.0 (s), 149.9 (d), 143.0 (s), 137.6 (s), 132.5 (d), 129.6 (s), 128.8 (d), 128.2 (d), 127.8(d), 126.1 (d), 125.5 (s), 119.2 (d), 115.8(s), 99.4 (s), 71.7(t), 53.9 (t), 38.8(t), 30.2 (t), 24.5 (t).
 Anal. Calcd. for C₂₅H₂₂N₈O₂S: C, 60.23; H, 4.45; N, 22.48; S, 6.43; found: C, 60.27; H, 4.48; N, 22.50; S, 6.44.

N-[2-(1H-Imidazol-4-yl)ethyl]-4-(3-Phenyl-10-oxopyrido[2',3':4,5]thieno[3,2d]-[1,2,3]triazolo[1,5a]pyrimidin-4-yl) butanamide (34) had mp 234.7-240.3°C ¹H NMR ppm: 8.77 (dd, J = 4.6, 1.8 Hz, 1H, H-7), 8.82 (dd, J = 7.9, 1.8 Hz, 1H, H-5),

8.64 (dd, $J = 8.0, 1.6$ Hz, 2H, H-2', H-6'), 7.72 (dd, $J = 7.9, 4.6$ Hz, 1H, H-6), 7.65-7.52 (m, 4H, H-3', H-4', H-5', CH), 6.45 (s, 1H, CH), 5.22 (t, $J = 6.7$ Hz, 2H, NCH₂), 3.47 (t, $J = 6.5$ Hz, 2H, CH₂CO), 3.22 (t, $J = 7.2$ Hz, 2H, CH₂CH₂), 2.25-2.01 (m, 4H, CH₂CH₂CH₂, CH₂CH₂). ¹³C NMR ppm: 170.5 (s), 166.3 (s), 161.5 (s), 155.9 (d), 144.8 (s), 136.6 (s), 132.9 (d), 131.8 (s), 129.5(d), 127.7 (d), 127.2 (d), 126.5 (d), 125.9 (s), 117.5 (d), 99.8 (s), 70.5(t), 53.8 (t), 31.9(t), 30.4 (t), 25.7 (t).
 Anal. Calcd. for C₂₅H₂₂N₈O₂S: C, 60.23; H, 4.45; N, 22.48; S, 6.43; found: C, 60.30; H, 4.45; N, 22.58; S, 6.42.

Reaction of **27b** with 1-bromo-3-chloropropane

To a stirred suspension of **27b** (0.62 g, 1.93 mmol) in absolute DMF (12 mL), potassium carbonate (0.8 g, 5.81 mmol) and 1-bromo-3-chloropropane (1.52 g, 9.68 mmol) were added. The mixture was heated at 60°C for 16h, cooled to room temperature, and then slowly poured onto water/ice. The precipitate was purified by column chromatography using dichloromethane/ethyl acetate 98:2 as eluent to afford **4-(3-chloropropyl)-3-phenylpyrido[2',3':4,5]thieno[3,2-d][1,2,3]triazolo[1,5-a]pyrimidin-10(4H)-one (39)**. Yield 20%, mp 195.4-196.6°C ¹H NMR (CDCl₃) ppm: 9.4 (dd, $J = 8.2, 1.7$ Hz, 1H, H-7), 8.92 (dd, $J = 4.6, 1.7$ Hz, 1H, H-5), 8.45 (dd, $J = 8.2, 4.6$ Hz, 1H, H-6), 7.54 (dd, $J = 7.2, 1.6$ Hz, 2H, H-2', H-6'), 7.4 (dd, $J = 2.5, 1.6$ Hz, 2H, H-3', H-5'), 7.35 (dd, $J = 5.9, 1.6$ Hz, 1H, H-4'), 4.92 (t, $J = 6.2$ Hz, 2H, NCH₂), 3.84 (t, $J = 6.2$ Hz, 2H, CH₂Cl), 2.56-2.48 (m, 2H, CH₂CH₂CH₂). ¹³C NMR ppm: 161.7(s), 157.3(s), 151.5(d), 137.6(s), 134.4(d), 133.9(s), 133.1(s), 130.7(s), 128.7(d), 127.7(d), 125.8(d), 122.4(s), 121.3(d), 99.9(s), 65.1(t), 41.1(t), 29.7(t).
 Anal. Calcd. for C₁₉H₁₄ClN₅OS: C, 57.65; H, 3.56; Cl, 8.96; N, 17.69; S, 8.10; found: C, 57.67; H, 3.60; Cl, 8.99; N, 17.67; S, 8.11.

Further elution with dichloromethane/ethyl acetate 98:2 gave **4-(3-chloropropyl)-3-phenylpyrido[3',2':4,5]thieno[2,3-e][1,2,3]triazolo[1,5-a]pyrimidin-5(4H)-one (35)**. Yield 65%, mp 200.8-201.7°C ¹H NMR (CDCl₃) ppm: 8.75 (dd, $J = 8.2, 1.7$ Hz, 1H, H-8), 8.63 (dd, $J = 4.6, 1.7$ Hz, 1H, H-10), 8.54 (dd, $J = 8.2, 4.6$ Hz, 1H, H-3), 7.55-7.47 (m, 4H, H-9, H-3', H-4', H-5'), 5.13 (t, $J = 6.3$ Hz, 2H, NCH₂), 3.63 (t, $J = 6.3$ Hz, 2H, CH₂Cl), 2.4-2.28 (m, 2H, CH₂CH₂CH₂). ¹³C NMR ppm: 163.3(s), 152.9(s), 151.7(s), 151.5(d), 145.7(s), 139.2(s), 132.1(d), 130.1(d), 129.7(d), 128.8(s), 127.0(d), 120.2(d), 115.0(s), 99.9(s), 53.6(t), 41.2(t), 31.2(t).

Anal. Calcd. for $C_{19}H_{14}ClN_5OS$: C, 57.65; H, 3.56; Cl, 8.96; N, 17.69; S, 8.10; found: C, 57.64; H, 3.58; Cl, 8.98; N, 17.70; S, 8.13.

Reaction of chloropropyl derivative with 1-methylpiperazine

A stirred suspension of **35** or **39** (0.1 g, 0.25 mmol) in 1-methylpiperazine (3 mL) was heated at reflux for 2h. After cooling the mixture was poured onto water/ice and the precipitate was filtered off and purified by alumina column chromatography.

In the case of **35** elution with dichloromethane/ethyl acetate 98:2 afforded **4-[3-(N-methylpiperazino)propyl]-3-phenylpyrido[3',2':4,5]thieno[2,3-e][1,2,3]triazolo[1,5-a]pyrimidin-5(4H)-one (37)**. Yield 85%, mp 88.3-90.2°C. 1H NMR ($CDCl_3$) ppm: 8.78 (dd, $J = 4.5, 1.4$ Hz, 1H, H-8), 8.72 (dd, $J = 7.9, 1.4$ Hz, 1H, H-10), 8.56 (d, $J = 6.6$ Hz, 2H, H-2', H-6'), 7.6-7.47 (m, 4H, H-9, H-3', H-4', H-5'), 5.12 (t, $J = 6.8$ Hz, 2H, NCH_2), 2.4 (t, $J = 6.5$ Hz, 2H, CH_2), 2.28 (s, 8H, 2x NCH_2CH_2N), 2.14 (s, 3H, CH_3), 2.03-1.90 (m, 2H, $CH_2CH_2CH_2$). ^{13}C NMR ppm: 163.4(s), 152.8(s), 151.6(s), 151.4(d), 145.2(s), 138.2(s), 132.1(d), 129.8(d), 128.8(d), 128.5(s), 128.3(s), 126.8(d), 120.1(d), 99.7(s), 53.2(t); 55.0(t), 54.7(t), 52.9(t), 45.9(q), 26.1(t).

Anal. Calcd for $C_{24}H_{25}N_7OS$: C, 62.72; H, 5.48; N, 21.33; S, 6.98; found: C, 62.81; H, 5.52; N, 21.35; S, 6.97.

In the case of **39** elution with dichloromethane gave **5-[3-(N-methylpiperazino)propyl]-3-phenylpyrido[2',3':4,5]thieno[3,2d][1,2,3]triazolo[1,5a]pyrimidin-10(4H)-one (41)**, as a yellow solid. Yield 26%, mp 149.6-150.8°C. 1H NMR ppm: 1H NMR ($CDCl_3$) ppm: 9.31 (dd, $J = 8.1, 1.7$ Hz, 1H, H-7), 8.87 (dd, $J = 4.6, 1.7$ Hz, 1H, H-5), 8.39 (d, $J = 7.4$ Hz, 2H, H-2', H-6'), 7.64 (dd, $J = 8.1, 4.6$ Hz, 1H, H-6), 7.47 (t, $J = 7.2$ Hz, 2H, H-3', H-5'), 7.33 (d, $J = 7.4$ Hz, 1H, H-4'), 4.76 (t, $J = 6.3$ Hz, 2H, NCH_2), 2.63 (t, $J = 6.6$ Hz, 2H, CH_2), 2.28 (bs, 8H, 2x NCH_2CH_2N), 2.29 (s, 3H, CH_3), 2.24-1.03 (m, 2H, $CH_2CH_2CH_2$). ^{13}C NMR ppm: 161.6(s), 157.5(s), 151.3(s), 137.7(s), 134.3(d), 133.6(s), 132.8(d), 130.8(s), 128.6(d), 127.5(d), 125.6(d), 122.4(s), 121.2(d), 112.9(s), 66.9(t); 55.1(t), 55.0(t), 55.2(t), 46.0(q), 26.0(t).

Anal. Calcd for $C_{24}H_{25}N_7OS$: C, 62.72; H, 5.48; N, 21.33; S, 6.98; found: C, 62.75; H, 5.51; N, 21.37; S, 6.99.

Reaction of chloropropane derivative with dibutylamine

A stirred suspension of **35** (0.1 g, 0.25 mmol) in dibutylamine (3 mL) was heated at reflux for 2h. After cooling the mixture was poured onto water/ice and the precipitate was filtered off and purified by alumina column chromatography. Elution with dichloromethane/ethyl acetate 98:2 afforded **5-[3-(dibutylamino)propyl]-3-phenylpyrido[3',2':4,5]thieno[2,3-e]-[1,2,3]triazolo[1,5-a]pyrimidin-5(4H)-one (38)**, mp 109.5-110.5°C. ¹H NMR ppm: 8.81 (dd, J = 4.6, 1.7 Hz, 1H, H-8), 8.73 (dd, J = 7.9, 1.7 Hz, 1H, H-10), 8.58 (dd, J = 8.2, 1.7 Hz, 2H, H-2', H-6'), 7.61-7.49 (m, 4H, H-9, H-3', H-4', H-5'), 2.49 (t, J = 6.7 Hz, 2H, NCH₂), 2.34 (t, J = 6.7 Hz, 4H, N(CH₂CH₂CH₂CH₃)₂), 1.95-1.81 (m, 2H, NCH₂CH₂CH₂), 1.34-1.24 (m, 10H, N(CH₂CH₂CH₂CH₃)₂, NCH₂CH₂CH₂), 0.86 (t, J=6.7 Hz, 6H, N(CH₂CH₂CH₂CH₃)₂). ¹³C NMR ppm: 163.4(s), 152.9(s), 151.7(s), 151.4(d), 145.8(s), 145.2 (s), 138.4(s), 132.1(d), 129.8(d), 128.8(d), 128.5(s), 128.3(s), 126.9(d), 120.1(d), 55.1(t), 53.7(t), 50.8 (t), 29.1(t), 26.3(t); 20.6(t); 13.0(q).
Anal. Calcd. for C₂₇H₃₂N₆OS: C, 66.36; H, 6.60; N, 17.20; S, 6.56; found: C, 66.38; H, 6.65; N, 17.18; S, 6.59.

Reaction of chloropropyl derivative with piperidine

A stirred suspension of **35** or **39** (0.1 g, 0.25 mmol) in piperidine (3 mL) was heated at reflux for 2h. After cooling the mixture was poured onto water/ice and the precipitate was filtered off and purified by alumina column chromatography.
In the case of **35** elution with dichloromethane/methanol 98:2 afforded **5-[3-piperidine-propyl]-3-phenylpyrido[3',2':4,5]thieno[2,3-e]-[1,2,3]triazolo[1,5-a]pyrimidin-5(4H)-one (36)**, mp 82.7-84.0°C. ¹H NMR (CDCl₃) ppm: 8.79 (dd, J = 4.6, 1.7 Hz, 1H, H-8), 8.7 (dd, J = 8.0, 1.7Hz, 1H, H-10), 8.55 (dd, J = 8.3, 1.7 Hz, 2H, H-2'-H-6'), 7.60-7.46 (m, 4H, H-9, H-3', H-4', H-5'), 5.09 (t, J = 6.9 Hz, 2H, NCH₂), 2.35 (t, J = 6.9 Hz, 2H, CH₂), 2.23 (s, 4H, 2xCH₂), 2.02-1.88 (m, 2H, CH₂CH₂CH₂), 1.36 (s, 2H, CH₂), 1.33 (s, 2H, CH₂). ¹³C NMR ppm: 163.4(s), 152.8(s), 151.7(d), 151.3(s), 145.8(s), 138.2(s), 132.1(d), 129.8 (d), 128.8 (d), 128.6(s), 128.3 (s), 126.8 (d), 120.1 (d), 114.5 (s), 55.9(t), 55.3(t), 54.5(t), 26.1(t), 25.7 (t), 24.2(t).
Anal. Calcd. for C₂₄H₂₄N₆OS: C, 64.84; H, 5.44; N, 18.90; S, 7.21; found: C, 64.82; H, 5.45; N, 18.89; S, 7.24.

In the case of **39** elution with dichloromethane/methanol 9:1 gave **5-[3-piperidine-propyl]-3-phenylpyrido[2',3':4,5]thieno[3,2d][1,2,3]triazolo-[1,5a]pyrimidin-10(4H)-one (40)**, mp 85.7-86.5°C. ¹H NMR (CDCl₃) ppm: 8.81 (dd, J = 4.6, 1.7 Hz, 1H, H-7), 8.72 (dd, J = 8.0, 1.7 Hz, 1H, H-5), 8.61 (dd, J = 8.3, 1.7 Hz, 2H, H-2', H-6'), 7.58-7.46 (m, 4H, H-6, H-3', H-4', H-5'), 5.19 (t, J = 6.9 Hz, 2H, NCH₂), 2.48 (t, J = 6.9 Hz, 2H, CH₂Cl), 2.25 (s, 4H, CH₂), 2.15-1.87 (m, 2H, CH₂CH₂CH₂), 1.38 (s, 2H, CH₂), 1.35 (s, 2H, CH₂). ¹³C NMR ppm: 164.8(s), 152.5(s), 150.9(d), 151.2(s), 147.7(s), 136.5(s), 131.1(d), 128.9 (d), 128.1 (d), 127.8(s), 127.5 (s), 126.1 (d), 118.9 (d), 112.6 (s), 55.4(t), 55.1(t), 54.6(t), 26.1(t), 25.9 (t), 24.5(t).
 Anal. Calcd. for C₂₄H₂₄N₆OS: C, 64.84; H, 5.44; N, 18.90; S, 7.21; found: C, 64.83; H, 5.41; N, 18.84; S, 7.28.

Reaction of **27b** with ethyl bromoacetate

To a stirred suspension of **27b** (0.225 g, 0.7 mmol) in absolute DMF (5 mL), potassium carbonate (0.29 g, 2.1 mmol) and ethyl bromoacetate (0.58 g, 3.5 mmol) were added. The mixture was heated at 60°C for 16h, cooled to room temperature, and then slowly poured onto water/ice. The precipitate was purified by column chromatography using dichloromethane/ethyl acetate 98:2 as eluant to afford **ethyl (3-phenyl-10-oxopyrido[2',3':4,5]thieno[3,2-d][1,2,3]triazolo[1,5-a]pyrimidin-4-yl)acetate (44)**. Yield 11%, mp 194.4-195.7°C. ¹H NMR ppm: 9.39 (dd, J = 8.2 Hz, 1.7 Hz, 1H, H-7), 8.93 (dd, J = 4.6, 1.7 Hz, 1H, H-5), 8.37 (dd, J = 8.5, 1.4 Hz, 2H, H-2', H-6'), 7.7 (dd, J = 8.2, 4.6 Hz, 1H, H-6), 7.52-7.38 (m, 3H, H-3', H-4', H-5'), 5.23 (s, 2H, NCH₂), 4.31 (q, J = 7.1 Hz, 2H, OCH₂), 1.32 (t, J = 7.1 Hz, 3H, CH₃). ¹³C NMR ppm: 167.2(s), 161.9(s), 156.5(s), 151.7(d), 137.1(s), 134.4(d), 134.0(s), 133.5(s), 130.5(s), 128.6(d), 127.7(d), 125.7(d), 122.3(s), 121.3(d), 112.19(s), 64.1(t), 61.8(t), 14.2(q).
 Anal. Calcd. for C₂₀H₁₅N₅O₃S: C, 59.25; H, 3.73; N, 17.27; S, 7.91; found: C, 59.28; H, 3.72; N, 17.30; S, 7.89.

Further elution with dichloromethane/ethyl acetate 95:5 as eluant gave **ethyl [3-phenyl-5-oxopyrido[3',2':4,5]thieno[2,3-e][1,2,3]triazolo[1,5-a]pyrimidin-4-yl]-acetate (42)**. Yield 42%, mp 194.4-196.0°C. ¹H NMR (CDCl₃) ppm: 8.89 (dd, J = 8.1, 1.5 Hz, 1H, H-8), 8.73 (dd, J = 4.6, 1.5 Hz, 1H, H-10), 8.37 (dd, J = 8.4, 1.2 Hz,

2H, H-2', H-6'), 7.7 (dd, J = 8.1, 4.6 Hz, 1H, H-9), 7.52-7.38 (m, 3H, H-3', H-4', H-5'), 5.23 (s, 2H, NCH₂), 4.31 (q, J = 7.2 Hz, 2H, OCH₂), 1.32 (t, J = 7.2 Hz, 3H, CH₃). ¹³C NMR ppm: 167.7(s), 162.5(s), 156.8(s), 150.7(d), 135.1(s), 134.7(d), 133.0(s), 133.8(s), 131.5(s), 128.2(d), 127.4(d), 125.9(d), 122.2(s), 121.3(d), 111.81(s), 64.5(t), 60.8(t), 14.7(q).

Anal. Calcd. for C₂₀H₁₅N₅O₃S: C, 59.25; H, 3.73; N, 17.27; S, 7.91; found: C, 59.27; H, 3.75; N, 17.28; S, 7.88.

Further elution with dichloromethane/ethyl acetate 9:1 as eluant gave **[3'-phenyl-5'-oxopyrido[3',2':4,5]thieno[2,3-e][1,2,3]triazolo[1,5-a]pyrimidin-4-yl]pent-2-enedioic acid diethyl ester (43)**. Yield 30%, mp 201.6-203.5°C. ¹H NMR ppm: 8.8 (dd, J = 4.5, 1.0 Hz, 1H, H-8'), 8.47 (dd, J = 8.0, 1.0 Hz, 1H, H-10'), 7.89 (dd, J = 6.9, 3.3 Hz, 2H, H-2'', H-6''), 7.48-7.43 (m, 4H, H-9', H-3'', H-4'', H-5''), 6.87 (s, 1H, CH), 4.67 (s, 2H, CH₂), 4.20-4.34 (m, 4H, 2xCH₂CH₃), 1.21-1.36 (m, 6H, 2xCH₂CH₃). ¹³C NMR ppm: 168.3(s), 165.5(s), 162.9(s), 155.2(s), 151.4(d), 150.1(d), 142.2(s), 141.7(s), 132.8(d), 132.3(s), 129.1(s), 128.9(s), 128.5(d), 127.9(d), 122.8(s), 120.5(d), 99.9(s), 77.2(d), 63.2(t), 61.7(t), 58.4(t), 14.2(q), 14.1(q).

Anal. Calcd. for C₂₄H₁₉N₅O₄S: C, 60.88; H, 4.04; N, 14.79; S, 6.77; found: C, 60.87; H, 4.07; N, 14.74; S, 6.75.

N-(3-Acetylphenyl)-methanesulfonamide (48)

According to the literature procedure [63], to a solution of 3-aminoacetophenone **50** (1.0 g, 7.4 mmol) in absolute DCM (30 mL), pyridine (3 mL, 37.3 mmol) and methanesulfonyl chloride (0.86 mL, 11.2 mmol) were added. The reaction mixture was stirred at room temperature for 3h. The solution was washed with 6N HCl and the organic layer was dried over sodium sulfate, evaporated to dryness. The residue was purified by recrystallization from ethanol. Yield 100%, mp 189°C. ¹H NMR ppm: 7.86 (t, 1H, H-4), 7.76 (dt, J = 7.5, 1.4 Hz, 1H, H-5), 7.59 (t, 1H, H-6), 7.48 (d, J = 7.5 Hz, 1H, H-2), 3.06 (s, 3H, SO₂CH₃), 2.63 (s, 3H, COCH₃). ¹³C NMR ppm: 197.95(s), 138.35(s), 137.68 (s), 130.06 (d), 125.25 (d), 125.15 (d), 120.09 (d), 39.59 (q), 36.76 (q).

General Procedure for the Preparation of Chalcones 47

To a solution of N-(3-acetylphenyl)-methanesulfonamide **48** (1.0 g, 4.7 mmol) and appropriately substituted aldehyde **49** (4.7 mmol) in ethanol (10 mL), an aqueous solution of NaOH (14.1 mmol) was added dropwise. The reaction mixture was stirred at room temperature for 3h. After acidification with acetic acid at 0°C, the precipitate was filtered off and washed with water. The solid product was dried and recrystallized from ethanol to give **47a-l**.

N-{3-[(2E)-3-(2-Chlorophenyl)prop-2-enoyl]phenyl}methanesulfonamide (**47a**)

White powder (100%), mp 142.2-142.7°C. ¹H NMR (CDCl₃) ppm: 8.21 (d, J = 15.7 Hz, 1H, COCH=CH), 7.88-7.74 (m, 4H, H-4, H-5, H-3', H-6'), 7.62-7.31 (m, 4H, H-2, H-6, H-4', H-5'), 7.46 (d, 1H, J = 15.7 Hz, 1H, CH=CH), 3.08 (s, 3H, SO₂CH₃). ¹³C NMR ppm: 167.0(s), 141.6(d), 137.6(s), 135.6(s), 132.9(s), 131.5(d), 130.3(d), 130.1(d), 127.9(d), 127.1(d), 126.5(s), 125.3(d), 124.8(d), 124.2(d), 120.4(d), 39.7(q).

Anal. Calcd. for C₁₆H₁₄ClNO₃S: C, 57.23; H, 4.20; Cl, 10.56; N, 4.17; S, 9.55; found C, 57.25; H, 4.25; Cl, 10.55; N, 4.13; S, 9.50.

N-{3-[(2E)-3-(4-Dimethylaminophenyl)prop-2-enoyl]phenyl}methanesulfonamide (**47b**)

Red solid (80%), mp 208.8-209.6°C. ¹H NMR ppm: 9.98 (s, 1H, NH), 7.89-7.83 (m, 2H, H-4, COCH=CH), 7.74-7.48 (m, 3H, CH=CH, H-5, H-6), 7.66 (s, 1H, H-2), 7.54 (d, J = 8.2 Hz, 2H, H-2', H-6'), 6.75 (d, J = 8.2 Hz, 2H, H-3', H-5'), 3.04 (s, 3H, SO₂CH₃), 3.01 (s, 6H, NCH₃). ¹³C NMR ppm: 188.3(s), 152.0(s), 145.4(d), 139.4(s), 138.9(s), 130.7(d), 129.6(d), 123.7(d), 123.4(d), 121.8(s), 118.8(d), 115.9(d), 111.7(d), 39.6(q), 39.3(q).

Anal. Calcd. for C₁₈H₂₀N₂O₃S: C, 62.77; H, 5.85; N, 8.13; S, 9.31; found: C, 62.79; H, 5.80; N, 8.18; S, 9.33.

N-{3-[(2E)-3-(3-Fluorophenyl)prop-2-enoyl]phenyl}methanesulfonamide (**47c**)

mp 176.9-177.7°C. ¹H NMR ppm: 8.0 (dt, J = 6.4, 1.8 Hz, 1H, H-4), 7.87-7.68 (m, 5H, COCH=CH, CH=CH, H-2', H-6', H-5), 7.54 (dd, J = 7.8 Hz, 1H, H-4'), 7.53 (s, 1H, H-2), 7.52 (d, J = 7.8 Hz, 1H, H-5'), 7.30 (td, J = 1.8, 8.3 Hz, 1H, H-6), 3.03 (s, 3H, SO₂CH₃). ¹³C NMR ppm: 188.8(s), 160.0(s), 142.7(d), 139.4(s), 138.3(s),

137.2(s), 130.9(d), 129.7(d), 125.4(d), 124.1(d), 124.0(d), 123.5(d), 119.0(d), 117.1(d, $J_{\text{C-F}}=133.8$ Hz), 114.8(d), 39.4(q).

Anal. Calcd. for $\text{C}_{16}\text{H}_{14}\text{FNO}_3\text{S}$: C, 60.18; H, 4.42; N, 4.39; S, 10.04; found: C, 60.13; H, 4.45; N, 4.42; S, 10.08.

N-{3-[1-Acetyl-3-(2-methoxyphenyl)prop-2-enoyl]phenyl}methanesulfonamide (47d)

Yellow solid (95%), mp 147.3-148.4°C. ^1H NMR ppm: 8.03 (d, $J = 15.8$ Hz, 1H, $\text{COCH}=\text{CH}$), 7.94-7.85 (m, 3H, H-4, H-5, H-6'), 7.81 (d, $J = 15.8$ Hz, 1H, $\text{CH}=\text{CH}$), 7.59-7.43 (m, 3H, H-2, H-6, H-4'), 7.15-7.01 (m, 2H, H-3', H-5'), 3.91 (s, 3H, OCH_3), 3.04 (s, 3H, SO_2CH_3). ^{13}C NMR ppm: 189.0(s), 158.3(s), 139.3(s), 138.9(d), 138.7(s), 132.4(d), 129.7(d), 128.8(d), 123.8(d), 123.7(d), 122.7(s), 121.9(d), 120.7(d), 118.8(d), 111.8(d), 55.7(q), 39.4(q).

Anal. Calcd. for $\text{C}_{17}\text{H}_{17}\text{NO}_4\text{S}$: C, 61.61; H, 5.17; N, 4.23; S, 9.68; found: C, 61.62; H, 5.17; N, 4.22; S, 9.63.

N-{3-[1-Acetyl-3-(3,4-dimethoxyphenyl)prop-2-enoyl]phenyl}methanesulfonamide (47e)

Yellow solid (95%), mp 182.3-183.7°C. ^1H NMR ppm: 7.96 (dt, $J = 5.1, 1.7$ Hz, 1H, H-5), 7.85-7.48 (m, 4H, H-5', H-6', $\text{COCH}=\text{CH}$, $\text{CH}=\text{CH}$), 7.73 (s, 2H, H-2), 7.52(s, 1H, H-2'), 7.40 (dd, $J = 8.3$ Hz, 1.7 Hz, 1H, H-4), 7.04 (d, $J = 8.3$ Hz, 1H, H-6), 3.87 (s, 3H, OCH_3), 3.83 (s, 3H, OCH_3), 3.05 (s, 3H, SO_2CH_3). ^{13}C NMR ppm: 189.0(s), 158.3(s), 139.3(s), 138.9(d), 138.7(s), 132.4(d), 129.7(d), 128.8(s), 123.8(d), 123.7(d), 122.7(s), 121.9(d), 120.7(d), 118.8(d), 111.8(d), 55.7(q), 39.4(q).

Anal. Calcd. for $\text{C}_{18}\text{H}_{19}\text{NO}_5\text{S}$: C, 59.82; H, 5.30; N, 3.88; S, 8.87; found: C, 59.88; H, 5.35; N, 3.83; S, 8.92.

N-{3-[(2E)-3-(4-Methoxyphenyl)prop-2-enoyl]phenyl}methanesulfonamide (47f)

Yellow solid (80%), mp 196.3-197.2°C. ^1H NMR ppm: 9.99 (s, 1H, NH), 7.97-7.92 (dt, $J = 6.8, 1.5$ Hz, 1H, H-5), 7.86 (d, $J = 1.5$ Hz, 1H, H-4), 7.85 (d, $J = 8.7$ Hz, 2H, H-2', H-6'), 7.72 (s, 1H, H-2), 7.59-7.47 (m, 3H, $\text{COCH}=\text{CH}$, $\text{CH}=\text{CH}$, H-6), 7.04 (d, $J = 8.7$ Hz, 2H, H-3', H-5'), 3.83 (s, 3H, OCH_3), 3.06 (s, 3H, SO_2CH_3). ^{13}C NMR ppm: 188.7(s), 161.4(s), 144.3(d), 138.9(s), 138.8(s), 130.7(d), 129.7(d), 127.1(s), 124.0(d), 123.8(d), 119.4(d), 118.8(d), 114.4(d), 55.3(q), 39.4(q).

Anal. Calcd. for $C_{17}H_{17}NO_4S$: C, 61.61; H, 5.17; N, 4.23; S, 9.68; found: C, 61.63; H, 5.14; N, 4.24; S, 9.64.

N-{3-[(2E)-3-(4-Hydroxyphenyl)prop-2-enoyl]phenyl}methanesulfonamide (47g)

Yellow solid (80%), mp 187.7-189.2°C. 1H NMR ppm: 9.73 (s, 1H, NH), 7.81 (dd, J = 5.5, 1.6 Hz, 2H, H-4, H-6), 7.72-7.61 (m, 4H, H-2, COCH=CH, H-3', H-2'), 7.53-7.41 (m, 2H, CH=CH, H-5), 6.86 (dd, J = 6.4, 1.6 Hz, 1H, H-6), 4.33 (s, 1H, OH), 2.99 (s, 3H, SO_2CH_3). ^{13}C NMR ppm: 188.8(s), 160.8(s), 144.7(d), 140.4(s), 138.9(s), 130.9(d), 129.5(d), 125.2(s), 123.7(d), 122.7(d), 119.0(d), 118.1(d), 115.9(d), 39.4(q).

Anal. Calcd. For $C_{16}H_{15}NO_4S$: C, 60.55; H, 4.76; N, 4.41; S, 10.10; found: C, 60.56; H, 4.78; N, 4.45; S, 10.12.

N-(3-{(2E)-3-(2-Hydroxy-3-methoxyphenyl)prop-2-enoyl}phenyl)methanesulfonamide (47h)

mp 292-294.2°C. 1H NMR ppm: 9.83 (s, 1H, NH), 8.08 (d, J = 15.8 Hz, 1H, COCH=CH), 7.89-7.84 (m, 2H, H-4', H-6'), 7.74 (d, J = 15.8 Hz, 1H, CH=CH), 7.54 (dd, J = 6.7 Hz, 1H, H-5'), 7.50 (s, 1H, H-2), 7.44 (dd, J = 8.0, 1.2 Hz, H-6), 7.05 (dd, J = 8.0, 1.2 Hz, 1H, H-4), 6.85 (t, J = 8.0 Hz, 1H, H-5), 3.85 (s, 3H, OCH_3), 3.05 (s, 3H, SO_2CH_3). ^{13}C NMR ppm: 189.1(s), 148.0(s), 146.6(s), 139.6(d), 138.9(s), 129.8(d), 123.8(d), 121.4(s), 123.7(d), 121.1(d), 119.8(d), 119.1(d), 118.8(d), 113.6(d), 55.9(q), 39.4 (q).

Anal. Calcd. for $C_{17}H_{17}NO_5S$: C, 58.78; H, 4.93; N, 4.03; S, 9.23; found: C, 58.81; H, 4.95; N, 4.01; O, 23.06; S, 9.25.

N-{3-[(2E)-3-(3-Methoxyphenyl)prop-2-enoyl]phenyl}methanesulfonamide (47i)

mp 140.5-140.5°C. 1H NMR ppm: 7.92 (dt, J = 1.9, 5.2 Hz, H, H-4), 7.85 (s, 1H, H-2), 7.79 (dd, J = 14.5 Hz, 1H, COCH=CH), 7.58-7.34 (m, 5H, H-5, H-3', H-4', H-5', H-6'), 7.47 (dd, J = 14.5 Hz, 1H, CH=CH), 7.04 (dt, J = 1.9, 7.4 Hz, 1H, H-6), 7.05 (dt, J = 7.2, 5.2 Hz, 1H, H-5), 3.84 (s, 3H, OCH_3), 3.00 (s, 3H, SO_2CH_3). ^{13}C NMR ppm: 189.0(s), 159.6(s), 144.1(d), 139.8(s), 138.5(s), 135.9(s), 129.9(d), 129.7(d), 124.0(d), 123.6(d), 122.4(d), 121.5(d), 118.9(d), 116.7(d), 113.4(d), 55.2(q), 39.4(q).

Anal. Calcd. for $C_{17}H_{17}NO_4S$: C, 61.61; H, 5.17; N, 4.23; S, 9.68; found: C, 61.62; H, 5.12; N, 4.26; S, 9.69.

N-(3-[(2E)-3-[4-(Diethylamino)phenyl]prop-2-enoyl]phenyl)methanesulfonamide (47j)

Orange solid (85%), mp 170.2-170.9°C. 1H NMR ppm: 9.63 (s, 1H, NH), 7.89-7.83 (m, 3H, H-4, H-5, COCH=CH), 7.68 (s, 1H, H-2), 7.48 (m, 2H, H-6, CH=CH), 7.5 (d, $J = 8.4$ Hz, 2H, H-2', H-6'), 6.70 (dd, $J = 8.4$ Hz, 2H, H-3', H-5'), 3.41 (q, $J = 3.7$ Hz, 4H, $\underline{CH_2CH_3}$), 3.04 (s, 3H, SO_2CH_3), 1.12 (t, $J = 3.7$ Hz, 6H, $2xCH_2\underline{CH_3}$). ^{13}C NMR ppm: 188.2(s), 149.5(s), 145.5(d), 139.5(s), 139.0(s), 131.1(d), 129.6(d), 123.5(d), 123.3(d), 121.0(s), 118.8(d), 115.3(d), 111.1(d), 43.7(t), 39.3(q), 12.4(q).

Anal. Calcd. for $C_{20}H_{24}N_2O_3S$: C, 64.49; H, 6.49; N, 7.52; S, 8.61; found: C, 64.43; H, 6.44; N, 7.57; S, 8.65.

N-{3-[(2E)-3-(2-Bromophenyl)prop-2-enoyl]phenyl)methanesulfonamide (47k)

White powder (92%), mp 153°C. 1H NMR ppm: 10.03 (s, 1H, NH), 8.17 (dd, $J = 7.8$, 1.6 Hz, 1H, H-3'), 8.06-7.84 (m, 4H, CH=CH, COCH=CH, H-4, H-5), 7.76 (dd, $J = 7.8$, 1.2 Hz, 1H, H-5'), 7.62-7.37 (m, 4H, H-2, H-6), 7.50 (dd, $J = 7.4$, 1.2 Hz, 1H, H-6'), 7.38 (dd, $J = 7.6$, 1.7 Hz, 1H, H-4'), 3.06 (s, 3H, SO_2CH_3). ^{13}C NMR ppm: 188.6(s), 141.4(d), 139.0(s), 138.2(s), 133.8(s), 133.3(d), 132.2(d), 129.8(d), 128.6(d), 128.25(d), 125.3(s), 124.8(d), 124.3(d), 124.2(d), 118.8 (d), 39.4 (q).

Anal. Calcd. for $C_{16}H_{14}BrNO_3S$: C, 50.54; H, 3.71; Br, 21.01; N, 3.68; S, 8.43; found: C, 50.59; H, 3.77; Br, 21.03; N, 3.67; S, 8.44.

N-{3-[1-Acetyl-3-(3,4,5-trimethoxyphenyl)prop-2-enoyl]phenyl)methanesulfonamide (47l)

White solid (95%), mp 195.3-196.2°C. 1H NMR ppm 8.13 (d, $J = 1.6$ Hz, 1H, H-4), 7.96 (d, $J = 15.6$ Hz, 1H, COCH=CH), 7.71 (dd, $J = 1.6$, 8.0 Hz, 1H, H-5), 7.55 (s, 1H, H-2'), 7.44 (d, $J = 8.0$ Hz, 1H, H-6), 7.43 (d, $J = 15.6$ Hz, 1H, CH=CH), 6.96 (s, 2H, H-2', H-6'), 3.94 (s, 6H, $2xOCH_3$), 3.91 (s, 3H, OCH_3), 3.07 (s, 3H, SO_2CH_3). ^{13}C NMR ppm: 190.0(s), 153.5(s), 146.9(d), 140.8(s), 139.3(s), 138.3(s), 130.0(s), 129.9(d), 124.9(d), 124.4(d), 120.6(d), 119.9(d), 106.0(d), 61.0(q), 56.2(q), 39.6(q).

Anal. Calcd. for $C_{19}H_{21}NO_6S$: C, 58.30; H, 5.41; N, 3.58; S, 8.19; found: C, 58.33; H, 5.46; N, 3.63; S, 8.17.

General Procedure for the Preparation of 4,5 Dihydropyrazoles

According to the literature procedure [64], the chalcone (1 mmol) was dissolved in acetic acid (15 mL) and hydrazine hydrate (5 mmol) was added. The solution was stirred at reflux overnight. The reaction mixture was cooled to room temperature and poured over crushed ice (50 mL). The precipitate was filtered off and washed with water. The solid product was dried and recrystallized from ethanol to give **45a-l**.

N-{3-[1-Acetyl-3-(2-chlorophenyl)-4,5-dihydro-1H-pyrazol-5-yl]phenyl}methane sulfonamide (45a)

White solid (84%), mp 250.3-251.4°C. ¹H NMR ppm: 9.87 (s, 1H, NH), 7.66 (s, 1H, H-2), 7.52-7.28 (m, 6H, H-4, H-5; H-6, H-3'', H-4'', H-6''), 7.07 (dd, J = 3.8, 4.0 Hz, 1H, H-5''), 5.77 (dd, J = 11.8 Hz, 4.8 Hz, H-5'), 3.95 (dd, J = 11.8, 17.9 Hz, 1H, H-4'), 3.02 (dd, J = 4.8, 17.9 Hz, 1H, H-4'), 3.01 (s, 3H, SO₂CH₃), 2.36 (s, 3H, COCH₃). ¹³C NMR ppm: 167.2(s), 158.3(s), 153.6(s), 138.8(s), 134.3(s), 132.1 (s), 129.8(d), 129.6 (d), 128.9 (d), 127.6(d), 126.2(d), 122.3(d), 121.4(d), 117.1 (d), 40.9(t), 39.3(q), 21.6(q) .

Anal. Calcd. for C₁₈H₁₈ClN₃O₃S C, 55.17; H, 4.63; Cl, 9.05; N, 10.72; O, 12.25; S, 8.18; found C, 55.13; H, 4.66; Cl, 9.09; N, 10.71; O, 12.28, S, 8.15.

N-{3-[1-Acetyl-3-(3-fluorophenyl)-4,5-dihydro-1H-pyrazol-5-yl]phenyl}methanesulfonamide (45c)

White solid (85%), mp 216.8-217.4°C. ¹H NMR ppm: 9.93 (s, 1H, NH), 7.67(s, 1H, H-2), 7.43 (s, 1H, H-2''), 7.40-7.31 (m, 3H, H-4, H-5, H-6), 7.12-7.02 (m, 3H, H-4'', H-5'', H-6''), 5.57 (dd, J = 11.9, 4.8 Hz, 1H, H-5'), 3.86 (dd, J = 11.9, 18.0 Hz, 1H, H-4'), 3.04 (dd, J = 4.8, 18.0 Hz, 1H, H-4'), 3.01 (s, 3H, SO₂CH₃), 2.30 (s, 3H, COCH₃). ¹³C NMR ppm: 168.0(s), 154.1(s), 145.4(s), 139.2(s), 130.7(d), 129.7(d), 122.3(d), 121.8 (s), 121.4(d), 117.1 (d, J_{C-F} = 77.9 Hz), 114.2 (d), 113.7(d), 112.6(d), 112.2 (d), 59.0(q), 41.9(t), 39.6(q), 21.6(q) .

Anal. Calcd. for C₁₈H₁₈FN₃O₃S: C, 57.59; H, 4.83; N, 11.19; S, 8.54; found: C, 57.57; H, 4.87; N, 11.21; S, 8.59.

**N-{3-[1-Acetyl-3-(2-methoxyphenyl)-4,5-dihydro-1H-pyrazol-5-yl]phenyl}
methanesulfonamide (45d)**

White solid (91%), mp 226.8-227.4°C. ¹H NMR ppm 9.93 (s, 1H, NH), 7.64(s, 1H, H-2), 7.48-7.21 (m, 4H, H-4, H-5, H-6, H-3''), 7.06-6.83 (m, 3H, H-4'', H-5'', H-6''), 5.67 (dd, J = 11.8, 4.4 Hz, 1H, H-5'), 3.83 (dd, J = 11.8, 17.7 Hz, 1H, H-4'), 3.82 (s, 3H, OCH₃) 3.01 (s, 3H, SO₂CH₃), 2.91 (dd, J = 4.4, 17.7 Hz, 1H, H-4'), 2.34 (s, 3H, COCH₃). ¹³C NMR ppm: 167.3(s), 155.6(s), 154.2(s), 138.7(s), 132.2(s), 129.7(d), 129.1(s), 128.4(d), 125.1(d), 122.2 (d), 121.4(d), 120.2 (d), 117.0 (d), 111.2(d), 55.5 (q), 55.1(d), 41.1(t), 39.3(q), 21.6(q) .

Anal. Calcd. for C₁₉H₂₁N₃O₄S: C, 58.90; H, 5.46; N, 10.85; S, 8.28; found: C, 58.93; H, 5.44; N, 10.89; S, 8.30.

**N-{3-[1-Acetyl-3-(3,4-dimethoxyphenyl)-4,5-dihydro-1H-pyrazol-5-yl]phenyl}
methanesulfonamide (45e)**

White solid (93%), mp 209.1-209.8°C. ¹H NMR ppm: 9.88 (s, 1H, NH), 7.66(s, 1H, H-2), 7.51-7.38 (m, 2H, H-4, H-6), 7.32 (dt, J = 7.3, 2.0 Hz, 1H, H-5), 6.88 (d, J = 8.3 Hz, 1H, H-2''), 6.80 (d, J = 1.9 Hz, 1H, H-5''), 6.65 (dd, J = 8.3, 1.9 Hz, 1H, H-6''), 5.49 (dd, J = 11.7, 4.4 Hz, 1H, H-5), 3.81 (dd, J = 11.7, 17.9 Hz, 1H, H-4'), 3.72 (s, 3H, OCH₃), 3.71(s, 3H, OCH₃), 3.07 (dd, J = 4.4, 17.9 Hz, 1H, H-4'), 3.02 (s, 3H, SO₂CH₃), 2.30 (s, 3H, COCH₃). ¹³C NMR ppm: 167.4(s), 153.7(s), 148.7(s), 147.9(s), 138.8(s), 134.7(s), 132.2(s), 129.8(d), 122.3 (d), 121.2(d), 117.1 (d), 117.0(d), 111.9(d), 109.6(d), 59.2(d), 55.5(q), 55.4(q), 42.1(t), 39.4(q), 21.7(q) .

Anal. Calcd. for C₂₀H₂₃N₃O₅S: C, 57.54; H, 5.55; N, 10.07; S, 7.68; found: C, 57.53; H, 5.59; N, 10.07; S, 7.69.

**N-{3-[1-Acetyl-3-(4-methoxyphenyl)-4,5-dihydro-1H-pyrazol-5-yl]phenyl}
methanesulfonamide (45f)**

White solid (90%), mp 205.1-205.8°C. ¹H NMR ppm: 9.90 (s, 1H, NH), 7.66(s, 1H, H-2), 7.50-7.39 (m, 2H, H-4, H-6), 7.33 (dt, J = 7.1, 1.9 Hz, 1H, H-5), 7.11 (d, J = 8.7 Hz, 2H, H-2'', H-6''), 6.87 (d, J = 8.7 Hz, 2H, H-3'', H-5''), 5.49 (dd, J = 12.0, 4.6 Hz, 1H, H-5'), 3.84 (dd, J = 12.0, 17.0 Hz, 1H, H-4'), 3.73(s, 3H, OCH₃), 3.09 (dd, J = 4.6, 17.0 Hz, 1H, H-4'), 3.02 (s, 3H, SO₂CH₃), 2.29 (s, 3H, COCH₃). ¹³C NMR ppm: 167.2(s), 158.3(s), 153.6(s), 138.8(s), 134.3(s), 132.1 (s), 129.8(d), 126.7 (d), 122.3 (d), 121.2(d), 117.0(d), 113.9(d), 79.0(d), 55.0(q), 42.0(t), 39.4(q), 21.6(q).

Anal. Calcd. for $C_{19}H_{21}N_3O_4S$: C, 58.90; H, 5.46; N, 10.85; S, 8.28; found: C, 58.93; H, 5.47; N, 10.89; S, 8.24.

N-{3-[1-Acetyl-3-(4-hydroxyphenyl)-4,5-dihydro-1H-pyrazol-5-yl]phenyl}methanesulfonamide (45g)

White solid (81%), mp 233.5-233.8°C. 1H NMR ppm: 9.77 (s, 1H, NH), 9.45 (s, 1H, OH), 7.66 (s, 1H, H-2), 7.45-7.33 (m, 3H, H-4, H-5, H-6), 6.98 (d, $J = 7.9$ Hz, 2H, H-2'', H-6''), 6.70 (d, $J = 7.9$ Hz, 2H, H-3'', H-5''), 5.42 (dd, $J = 11.9, 4.1$ Hz, 1H, H-5'), 3.79 (dd, $J = 11.9, 17.6$ Hz, 1H, H-4'), 3.03 (dd, $J = 4.1, 17.6$ Hz, 1H, H-4'), 3.02 (s, 3H, SO_2CH_3), 2.28 (s, 3H, $COCH_3$). ^{13}C NMR ppm: 167.2(s), 156.5(s), 153.6 (s), 138.8(s), 132.6(s), 132.2(s), 129.8(d), 126.6 (d), 122.2 (d), 121.2(d), 117.1(d), 115.2(d), 58.9(d), 42.0(t), 39.4(q), 21.7(q).

Anal. Calcd. for $C_{18}H_{19}N_3O_4S$: C, 57.89; H, 5.13; N, 11.25; S, 8.59; found: C, 57.86; H, 5.10; N, 11.28; S, 8.54.

N-{3-[1-Acetyl-3-(2-hydroxy-3-methoxyphenyl)-4,5-dihydro-1H-pyrazol-5-yl]phenyl}methanesulfonamide (45h)

White solid (87%), mp 242.8-243.4°C. 1H NMR ppm: 9.87 (s, 1H, NH), 8.89 (s, 1H, OH), 7.66(s, 1H, H-2), 7.44-7.28 (m, 3H, H-4, H-5, H-6), 6.85 (d, $J = 7.6$ Hz, 1H, H-6''), 6.69 (t, $J = 7.6$ Hz, 1H, H-5''), 6.46 (d, $J = 7.6$ Hz, 1H, H-4''), 5.66 (dd, $J = 11.6, 4.1$ Hz, 1H, H-5'), 3.79 (s, 4H, OCH_3), 3.77 (dd, $J = 11.6, 17.9$ Hz, 1H, H-4'), 3.02 (s, 3H, SO_2CH_3), 2.88 (dd, $J = 4.1, 17.9$ Hz, 1H, H-4'), 2.32 (s, 3H, $COCH_3$). ^{13}C NMR ppm: 171.2(s), 166.1(s), 153.8(s), 140.2(s), 138.5(s), 130.9(s), 129.7 (d), 128.2(s), 126.1(s), 122.1(d), 121.1(d), 118.7 (d), 117.3 (d), 117.1(d), 110.6(d), 55.8(q), 55.3(d), 41.0(t), 39.7(q), 21.6(q) .

Anal. Calcd. for $C_{19}H_{21}N_3O_5S$: C, 56.56; H, 5.25; N, 10.42; S, 7.95; found: C, 56.60; H, 5.28; N, 10.47; S, 7.99.

N-{3-[1-Acetyl-3-(3-methoxyphenyl)-4,5-dihydro-1H-pyrazol-5-yl]phenyl}methanesulfonamide (45i)

White solid (88%), mp 207.9-208.5°C. 1H NMR ppm: 9.90 (s, 1H, NH), 7.66(s, 1H, H-2), 7.46 (s, 1H, H-2''), 7.42-7.21 (m, 3H, H-5, H-6, H-5''), 6.84-6.74 (m, 3H, H-4, H-4'', H-6''), 5.52 (dd, $J = 4.6, 12.0$ Hz, 1H, H-5), 3.83 (dd, $J = 12.0, 17.9$ Hz, 1H, H-4), 3.37 (s, 3H, OCH_3), 3.04 (dd, $J = 4.6, 17.9$ Hz, 1H, H-4), 3.02 (s, 3H,

SO₂CH₃), 2.32 (s, 3H, COCH₃). ¹³C NMR ppm: 171.9(s), 167.5(s), 153.7(s), 140.3(s), 138.8(s), 132.9 (d), 131.9(s), 129.8 (d), 129.2 (d), 128.2(d), 126.1(d), 122.3(d), 121.4(d), 120.8 (s), 117.3 (d), 59.3(d), 55.3(q), 41.1(t), 39.4(q), 21.5(q) .
Anal. Calcd. for C₁₉H₂₁N₃O₄S: C, 58.90; H, 5.46; N, 10.85; S, 8.28; found: C, 58.94; H, 5.43; N, 10.86; S, 8.24.

N-{3-[1-Acetyl-3-(4-diethylaminophenyl)-4,5-dihydro-1H-pyrazol-5-yl]phenyl}methanesulfonamide (45j)

White solid (89%), mp 205.1-205.4°C. ¹H NMR ppm: 9.93 (s, 1H, NH), 7.66(s, 1H, H-2), 7.46-7.30 (m, 3H, H-4, H-5, H-6), 6.96 (d, J = 8.6 Hz, 2H, H-2'', H-6''), 6.57 (d, J = 8.6 Hz, 2H, H-3'', H-5''), 5.41 (dd, J = 11.6, 4.1 Hz, 1H, H-5'), 3.77 (dd, J = 11.6, 17.9 Hz, 1H, H-4'), 3.28 (q, J = 6.9 Hz, 4H, NCH₂), 3.09 (dd, J = 4.1, 17.9 Hz, 1H, H-4'), 3.02 (s, 3H, SO₂CH₃), 2.27 (s, 3H, COCH₃), 1.05 (t, J = 6.9 Hz, 6H, NCH₂CH₃). ¹³C NMR ppm: 167.1(s), 153.6(s), 146.5 (s), 138.8(s), 132.3(s), 129.7(d), 128.5(s), 126.5 (d), 122.5 (d), 121.1(d), 117.0(d), 111.1(d), 99.5 (d), 59.0(q), 43.6 (t), 39.3(q), 12.4(q).

Anal. Calcd for C₂₂H₂₈N₄O₃S: C, 61.66; H, 6.59; N, 13.07; S, 7.48; found: C, 61.67; H, 6.63; N, 13.09; S, 7.45.

{3-[1-Acetyl-3-(2-bromophenyl)-4,5-dihydro-1H-pyrazol-5-yl]phenyl}methane sulfonamide (45k)

White solid (88%), mp 250.9-251.5°C. ¹H NMR ppm: 9.89 (s, 1H, NH), 7.69 (d, J = 0.8 Hz, H-3''), 7.66 (s, 1H, H-2), 7.46 (dd, J = 1.6 Hz, 1H, H-4), 7.41-7.30 (m, 3H, H-3'', H-5'', H-6''), 7.24 (dd, J = 1.6, 7.6 Hz, 1H, H-5), 7.19 (d, J = 7.6 Hz, 1H, H-6), 7.04 (dd, J = 1.3, 7.4 Hz, 1H, H-4''), 5.72 (dd, J = 4.6, 12.0 Hz, 1H, H-5), 3.98 (dd, J = 12.0, 17.9 Hz, 1H, H-4'), 3.96 (dd, J = 4.6, 17.9 Hz, 1H, H-4'), 3.02 (s, 3H, SO₂CH₃), 2.38 (s, 3H, COCH₃). ¹³C NMR ppm: 167.5(s), 153.7(s), 140.3(s), 138.8(s), 132.9 (d), 131.9(s), 129.8 (d), 129.2 (d), 128.2(d), 126.1(d), 122.3(d), 121.4(d), 120.8 (s), 117.3 (d), 59.4(d), 41.1(t), 39.4(q), 21.5(q).

Anal. Calcd. for C₁₈H₁₈BrN₃O₃S: C, 49.55; H, 4.16; Br, 18.31; N, 9.63; S, 7.35; found: C, 49.50; H, 4.12; Br, 18.35; N, 9.62; S, 7.36.

N-{3-[3-(2-Chlorophenyl)-4,5-dihydro-1H-pyrazol-5-yl]phenyl}methanesulfonamide (51)

The chalcone **47a** (1 mmol) was dissolved in absolute ethanol (25 mL), and hydrazine hydrate (1 mmol) and piperidine (0.10 mL) were added. The solution stirred at reflux overnight. The reaction mixture was poured over crushed ice (50 mL) and the precipitate was filtered off and washed with water. The solid product was dried and recrystallized from ethanol to give **51** (yield 20%), mp 250.3-251.4°C. ¹H NMR ppm: 9.81 (s, 1H, NH), 7.72 (s, 1H, H-2), 7.58-7.15 (m, 7H, H-4, H-5, H-6, H-3'', H-4'', H-5'', H-6''), 7.15 (s, 1H, NH), 5.13 (dd, J = 9.8, 11.4 Hz, 1H, H-5'), 3.55 (dd, J = 11.4, 16.4 Hz 1H, H-4'), 3.01 (s, 3H, SO₂CH₃), 2.71 (dd, J = 9.8, 16.4 Hz, 1H, H-4'). ¹³C NMR ppm: 167.2(s), 158.3(s), 153.6(s), 138.8(s), 134.3(s), 132.1 (s), 129.4(d), 129.3 (d), 128.8 (d), 127.6(d), 126.4(d), 121.1(d), 119.4(d), 116.1 (d), 60.4(t), 39.3(q).

Anal. Calcd. for C₁₆H₁₆ClN₃O₂S: C, 54.93; H, 4.61; Cl, 10.13; N, 12.01; S, 9.17; found: C, 54.98; H, 4.64; Cl, 10.17; N, 12.04; S, 9.21.

General Procedure for the Preparation of 2-amino-3-cyanopyridine

Method 1: Malononitrile (1.5 mmol) and ammonium acetate (12 mmol) were added to a stirred solution of appropriate chalcone (1.5 mmol) in absolute ethanol (5 mL). The reaction mixture was heated under reflux for 16 h and then concentrated at reduced pressure. The solid product was purified by column chromatography using dichloromethane/ethyl acetate as eluant.

Method 2: The opportune benzaldehyde (4.7 mmol) and malononitrile (4.7 mmol) in 5 mL of absolute dioxane were stirred to room temperature for 15 min. The mixture was added dropwise to a suspension of **48** (4.7 mmol) and ammonium acetate (7 mmol) in absolute dioxane (5 mL). The reaction was heated at reflux overnight, cooled at room temperature and then evaporated under reduced pressure. The crude product was purified by column chromatography using dichloromethane/ethyl acetate as eluant.

N-{3-[6-Amino-4-(2-chloro-phenyl)-5-cyano-pyridin-2-yl]-phenyl}-methanesulfonamide (46a)

White solid (94%), mp 172.5-173.1°C. ¹H NMR ppm: 9.86 (s, 1H, NH), 7.89-7.80 (m, 2H, H-3'', H-5''), 7.78-7.15 (m, 5H, H-3, H-4, H-5, H-2'', H-6''), 7.52 (s, 1H,

H-3'), 7.15 (bs, 2H, NH₂), 7.11 (s, 1H, H-2), 3.02 (s, 3H, SO₂CH₃). ¹³C NMR ppm: 160.0(s), 158.2(s), 153.0(s), 138.8(s), 138.7(s), 137.6 (s), 130.9(d), 130.5 (d), 130.0 (d), 129.6(d), 127.5(d), 123.0(d), 121.8(d), 118.8(d), 115.8(s), 113.0(s), 109.9(d), 88.7(s), 39.4(q).

Anal. Calcd. for C₁₉H₁₅ClN₄O₂S: C, 57.21; H, 3.79; Cl, 8.89; N, 14.05; S, 8.04; found: C, 57.25; H, 3.83; Cl, 8.92; N, 14.08; S, 8.07.

N-{3-[6-Amino-4-(4-dimethylamino-phenyl)-5-cyano-pyridin-2-yl]-phenyl}-methanesulfonamide (46b)

Violet solid (95%), mp 201.3-202.8°C. ¹H NMR ppm: 9.95 (s, 1H, NH), 7.91-7.66 (m, 4H, H-2, H-4, H-5, H-6), 7.55 (d, J=8.7Hz, 2H, H-3'', H-5''), 7.49 (s, 1H, H-3'), 6.75 (d, J = 8.7 Hz, 2H, H-2''-H-6''), 3.04 (s, 3H, SO₂CH₃), 3.02 (s, 6H, NCH₃). ¹³C NMR ppm: 188.2(s), 152.0(s), 145.5(d), 139.4(s), 138.8(s), 130.7(d), 129.6(d), 123.7(d), 121.7(s), 118.8(d), 115.9(d), 111.7(d), 99.4 (s), 75.2(d), 39.6 (q), 39.3(q).

Anal. Calcd. for C₂₁H₂₁N₅O₂S: C, 61.90; H, 5.19; N, 17.19; S, 7.87; found: C, 61.93; H, 5.15; N, 17.24; S, 7.85.

N-{3-[6-Amino-4-(3-fluorophenyl)-5-cyano-pyridin-2-yl]-phenyl}-methanesulfonamide (46c)

White solid (90%), mp 168.1-168.8°C. ¹H NMR ppm 9.86 (s, 1H, NH), 7.91(s, 1H, H-3'), 7.86 (d, J = 7.7 Hz 1H, H-4''), 7.7-7.33 (m, 5H, H-4, H-5, H-6, H-4'', H-6''), 7.54 (s, 1H, H-2''), 7.21 (s, 1H, H-2), 7.11 (bs, 2H, NH₂), 3.03 (s, 3H, SO₂CH₃). ¹³C NMR ppm: 164.4(s), 160.7(s), 159.5(s), 158.4(s), 153.4(s), 138.7 (s), 130.9 (d), 130.7(d), 129.6(d), 124.5(d), 123.0(d), 121.6(d), 118.9(d), 115.1(d, J_{C-F} = 77.1 Hz), 109.4(d), 99.5(d), 86.8(s), 39.4(q).

Anal. Calcd. for C₁₉H₁₅FN₄O₂S: C, 59.67; H, 3.95; N, 14.65; S, 8.38; found: C, 59.62; H, 3.98; N, 14.61; S, 8.43.

N-{3-[6-Amino-4-(2-methoxyphenyl)-5-cyano-pyridin-2-yl]-phenyl}-methanesulfonamide (46d)

Yellow solid (88%), mp 143.7-144.8°C. ¹H NMR ppm: 9.86 (s, 1H, NH), 7.87 (s, 1H, H-3'), 7.79 (d, J = 7.6 Hz, 1H, H-4), 7.47 (dd, J = 8.3, 16.4 Hz, 2H, H-5'', H-6''), 7.33 (s, 1H, H-2), 7.15 (dd, J = 8.3, 18.1 Hz, 1H, H-4''), 7.11-7.05 (m, 3H, H-5, H-6, H-3''), 7.06 (bs, 2H, NH₂), 3.81 (s, 3H, OCH₃), 3.02 (s, 3H, SO₂CH₃). ¹³C

NMR ppm: 160.0(s), 157.9(s), 155.9(s), 152.9(s), 138.8(s), 138.7(s), 130.9(d), 129.9 (d), 129.9 (d), 125.9(s), 122.8(d), 121.4(d), 120.6(s), 118.6(d), 116.6(s), 111.7(d), 110.4(d), 89.3(s), 55.4 (q), 39.4(q).

Anal. Calcd. for $C_{20}H_{18}N_4O_3S$: C, 60.90; H, 4.60; N, 14.20; S, 8.13; found: C, 60.93; H, 4.68; N, 14.25; S, 8.14.

N-{3-[6-Amino-4-(3,4-dimethoxyphenyl)-5-cyano-pyridin-2-yl]-phenyl}-methanesulfonamide (46e)

White solid (85%), mp 170.3-171.2°C. 1H NMR ppm 10.05 (s, 1H, NH), 7.90-7.83 (m, 2H, H-4, H-5), 7.51-7.11 (m, 3H, H-6, H-5'', H-6''), 7.47 (s, 1H, H-3'), 7.28 (s, 1H, H-2), 7.20 (s, 1H, H-2''), 6.98 (bs, 2H, NH₂), 3.85 (s, 3H, OCH₃), 3.84 (s, 3H, OCH₃), 3.03 (s, 3H, SO₂CH₃). ^{13}C NMR ppm: 160.8(s), 158.1(s), 154.7(s), 150.0(s), 148.5(s), 139.0(s), 138.7(s), 129.5 (d), 129.0 (s), 122.9(d), 121.4(d), 120.9(d), 118.8(d), 117.2(s), 111.9(d), 111.6(d), 109.3(d), 86.7(s), 55.6 (q), 39.4(q).

Anal. Calcd. for $C_{21}H_{20}N_4O_4S$: C, 59.42; H, 4.75; N, 13.20; S, 7.55; found: C, 59.45; H, 4.79; N, 13.23; S, 7.58.

N-{3-[6-Amino-4-(4-methoxy-phenyl)-5-cyano-pyridin-2-yl]-phenyl}-methanesulfonamide (46f)

White solid (92%), mp 164.5-165.1°C. 1H NMR ppm: 10.03 (s, 1H, NH), 8.11 (d, J=8.8 Hz, 2H, H-3'', H-5''), 7.56-7.32 (m, 3H, H-3, H-4, H-5), 7.47 (s, 1H, H-3'), 7.22 (s, 1H, H-2), 7.05 (d, J = 8.8 Hz, 2H, H-2''-H-6''), 7.00 (bs, 2H, NH₂), 3.85 (s, 3H, OCH₃), 3.83 (s, 3H, OCH₃), 3.10 (s, 3H, SO₂CH₃). ^{13}C NMR ppm: 160.8(s), 160.4(s), 158.1(s), 154.5(s), 138.9(s), 138.7(s), 129.7(d), 129.5 (d), 128.9 (s), 122.9(d), 121.4(d), 118.7(d), 117.1(s), 114.1(d), 109.2(d), 86.6(s), 55.3 (q), 39.4(q).

Anal. Calcd. for $C_{20}H_{18}N_4O_3S$: C, 60.90; H, 4.60; N, 14.20; S, 8.13; found: C, 60.96; H, 4.68; N, 14.24; S, 8.15.

N-{3-[6-Amino-4-(4-hydroxyphenyl)-5-cyano-pyridin-2-yl]-phenyl}-methanesulfonamide (46g)

White solid (84%), mp 222.8-223.9°C. 1H NMR ppm: 9.92 (bs, 2H, NH, OH), 7.89 (s, 1H, H-5'), 7.83 (d, J = 7.7 Hz, 1H, H-4), 7.54 (d, J = 8.4 Hz, 2H, H-2'', H-6''), 7.46 (t, J = 7.7, 8.1 Hz, 1H, H-5), 7.33 (d, J = 8.1 Hz, 1H, H-6), 7.12 (s, 1H, H-2), 6.95 (bs, 2H, NH₂), 6.93 (d, J = 8.4 Hz, 2H, H-3'', H-5''), 3.02 (s, 3H, SO₂CH₃). ^{13}C

NMR ppm: 160.9(s), 158.9(s), 158.0(s), 154.8(s), 138.9(s), 138.7 (s), 129.7(d), 129.5 (d), 127.3 (s), 122.9(d), 121.4(d), 118.8(d), 117.3(s), 115.4(d), 109.0(d), 86.4(s), 39.4(q).

Anal. Calcd. for $C_{19}H_{16}N_4O_3S$: C, 59.99; H, 4.24; N, 14.73; S, 8.43; found: C, 60.03; H, 4.26; N, 14.79; S, 8.48.

N-{3-[6-Amino-4-(2-hydroxy-3-methoxyphenyl)-5-cyano-pyridin-2-yl]-phenyl}-methanesulfonamide (46h)

Yellow solid (82%), mp 240.5-241.4°C. 1H NMR ppm: 9.91 (s, 1H, NH), 7.90-7.83 (m, 2H, H-4, H-5), 7.51-7.11 (m, 3H, H-6, H-5'', H-6''), 7.47 (s, 1H, H-3'), 7.28 (s, 1H, H-2), 7.20 (s, 1H, H-2''), 6.98 (bs, 2H, NH₂), 3.93 (s, 3H, OCH₃), 3.06 (s, 3H, SO₂CH₃). ^{13}C NMR ppm: 160.6(s), 160.5(s), 147.0(s), 144.7(s), 141.4(s), 139.1(s), 138.7(s), 129.5 (d), 124.4(d), 123.2(d), 121.8(d), 119.1(d), 117.3(s), 115.7(d), 114.3(d), 101.3(d), 99.4(s), 96.3(s), 56.0 (q), 39.4(q).

Anal. Calcd. for $C_{20}H_{18}N_4O_4S$: C, 58.53; H, 4.42; N, 13.65; S, 7.81; found: C, 58.57; H, 4.43; N, 13.67; S, 7.84.

N-{3-[6-Amino-4-(3-methoxyphenyl)-5-cyano-pyridin-2-yl]-phenyl}-methanesulfonamide (46i)

Brown solid (85%), mp 82.3-83.4°C. 1H NMR ppm: 10.02 (s, 1H, NH), 7.54-7.45 (m, 2H, H-4, H-5''), 7.41 (s, 1H, H-3'), 7.37-7.33 (m, 2H, H-5, H-6''), 7.20-7.19 (m, 1H, H-4''), 7.18 (s, 1H, H-2), 7.11-7.05 (m, 1H, H-6), 6.88 (bs, 2H, NH₂), 6.82(s, 1H, H-2''), 3.82 (s, 3H, OCH₃), 3.08 (s, 3H, SO₂CH₃). ^{13}C NMR ppm: 159.1(s), 154.0(s), 149.8(s), 149.3(s), 138.6(s), 138.4(s), 129.8(d), 123.7 (d), 120.7 (d), 120.2(d), 118.8(d), 118.2(d), 115.(s), 115.1(d), 113.9(d), 94.3(d), 93.9(d), 55.2 (q), 39.4(q).

Anal. Calcd. for $C_{20}H_{18}N_4O_3S$: C, 60.90; H, 4.60; N, 14.20; S, 8.13; found: C, 60.92; H, 4.65; N, 14.17; S, 8.15.

N-{3-[6-Amino-4-(4-diethylaminophenyl)-5-cyano-pyridin-2-yl]-phenyl}-methanesulfonamide (46j)

White solid (85%), mp 172.5-173.2°C. 1H NMR ppm: 10.05 (s, 1H, NH), 7.90-7.83 (m, 2H, H-4, H-5), 7.51-7.11 (m, 3H, H-6, H-5'', H-6''), 7.47 (s, 1H, H-3'), 7.28 (s, 1H, H-2), 7.20 (s, 1H, H-2''), 6.98 (bs, 2H, NH₂), 3.85 (s, 3H, OCH₃), 3.84 (s, 3H,

OCH₃), 3.03 (s, 3H, SO₂CH₃). ¹³C NMR ppm: 170.3(s), 150.8(s), 139.6(s), 134.6(s), 132.1(d), 130.0(d), 124.1(d), 121.5 (d), 120.9 (s), 119.2(d), 116.8(s), 115.0(s), 114.2(s), 111.6(d), 99.4(d), 74.0(d), 44.0(t), 39.4(q), 12.4(q).

Anal. Calcd. for C₂₃H₂₅N₅O₂S: C, 63.43; H, 5.79; N, 16.08; S, 7.36; found: C, 63.47; H, 5.82; N, 16.11; S, 7.38.

N-{3-[6-Amino-4-(3,4,5-trimethoxyphenyl)-5-cyano-pyridin-2-yl]-phenyl}-methanesulfonamide (46l)

White solid (85%), mp 183.0-183.8°C. ¹H NMR ppm: 10.05 (s, 1H, NH), 8.16-7.75 (m, 2H, H-4, H-5), 7.44 (t, J = 7.9 Hz, 1H, H-6), 7.30 (s, 1H, H-3'), 7.17(s, 1H, H-2), 6.84 (s, 2H, H-2'', H-6''), 5.48 (bs, 2H, NH₂), 3.93(s, 9H, OCH₃), 3.06 (s, 3H, SO₂CH₃). ¹³C NMR ppm: 160.3(s), 158.5(s), 155.3(s), 153.5(s), 139.5(s), 137.4(s), 131.9(s), 130.1 (d), 124.1 (d), 122.2(d), 119.8(d), 117.1(s), 111.0(d), 105.5(d), 99.9(s), 88.6(s), 61.0(q), 56.3 (q), 39.6(q).

Anal. Calcd. for C₂₂H₂₂N₄O₅S: C, 58.14; H, 4.88; N, 12.33; S, 7.06; found: C, 58.12; H, 4.83; N, 12.30; S, 7.08.

6.2. Biology

6.2.1. NCI Screening Test

The human tumor cell lines of the cancer screening panel are grown in RPMI 1640 medium containing 5% fetal bovine serum and 2 mM L-glutamine. For a typical screening experiment, cells are inoculated into 96 well microtiter plates in 100 µL at plating densities ranging from 5,000 to 40,000 cells/well depending on the doubling time of individual cell lines. After cell inoculation, the microtiter plates are incubated at 37°C, 5% CO₂, 95% air and 100% relative humidity for 24 h prior to addition of experimental drugs.

After 24 h, two plates of each cell line are fixed *in situ* with TCA to represent a measurement of the cell population for each cell line at the time of drug addition (T_z). Experimental drugs are solubilized in DMSO at 400-fold the desired final maximum test concentration and stored frozen prior to use. At the time of drug addition, an aliquot of frozen concentrate is thawed and diluted to twice the desired final maximum test concentration with complete medium containing 50 µg/mL gentamicin. Additional four, 10-fold or ½ log serial dilutions are made to provide a

total of five drug concentrations plus control. Aliquots of 100 µl of these different drug dilutions are added to the appropriate microtiter wells already containing 100 µl of medium, resulting in the required final drug concentrations.

Following drug addition, the plates are incubated for an additional 48 h at 37°C, 5% CO₂, 95% air, and 100% relative humidity. For adherent cells, the assay is terminated by the addition of cold TCA. Cells are fixed in situ by the gentle addition of 50 µl of cold 50% (w/v) TCA (final concentration, 10% TCA) and incubated for 60 min at 4°C. The supernatant is discarded, and the plates are washed five times with tap water and air dried. Sulforhodamine B (SRB) solution (100 µl) at 0.4% (w/v) in 1% acetic acid is added to each well, and plates are incubated for 10 min at room temperature. After staining, unbound dye is removed by washing five times with 1% acetic acid and the plates are air dried. Bound stain is subsequently solubilized with 10 mM trizma base, and the absorbance is read on an automated plate reader at a wavelength of 515 nm. For suspension cells, the methodology is the same except that the assay is terminated by fixing settled cells at the bottom of the wells by gently adding 50 µl of 80% TCA (final concentration, 16% TCA). Using the seven absorbance measurements [time zero, (Tz), control growth, (C), and test growth in the presence of drug at the five concentration levels (Ti)], the percentage growth is calculated at each of the drug concentrations levels. Percentage growth inhibition is calculated as:

$$[(Ti - Tz)/(C - Tz)] \times 100 \text{ for concentrations for which } Ti \geq Tz$$

$$[(Ti - Tz)/Tz] \times 100 \text{ for concentrations for which } Ti < Tz.$$

Three dose response parameters are calculated for each experimental agent. Growth inhibition of 50% (GI₅₀) is calculated from $[(Ti - Tz)/(C - Tz)] \times 100 = 50$, which is the drug concentration resulting in a 50% reduction in the net protein increase (as measured by SRB staining) in control cells during the drug incubation. The drug concentration resulting in total growth inhibition (TGI) is calculated from $Ti = Tz$. The LC₅₀ (concentration of drug resulting in a 50% reduction in the measured protein at the end of the drug treatment as compared to that at the beginning) indicating a net loss of cells following treatment is calculated from $[(Ti - Tz)/Tz] \times 100 = -50$. Values are calculated for each of these three parameters if the

level of activity is reached; however, if the effect is not reached or is exceeded, the value for that parameter is expressed as greater or less than the maximum or minimum concentration tested.

6.2.2. Hsp90 Inhibition Screening Tests

17 AAG was obtained from Sigma-Aldrich.

6.2.2a Cell Culture and Treatment

MCF7 human breast cancer cells were obtained from the American Type Culture Collection (LGC Promochem, Middlesex, United Kingdom). Cells were grown in DMEM+GlutaMax1(Invitrogen) supplemented with 10% FBS, 50IU/mL penicillin, 50 µg/mL streptomycin and 1% non essential aminoacids and maintained in a humidified 5% CO₂ incubator at 37°C. Exponentially growing cells were used for experiments. Each experiment was repeated at least three times. Culture medium with appropriate amounts of DMSO was used as control. Final DMSO concentration never exceeded 0.1%.

6.2.2b Cell Proliferation Assay

Cellular sensitivity to Hsp90 inhibitors was measured by methylene blue assay. The IG₅₀ value was calculated as the concentration that inhibits cell proliferation by 50% compared with vehicle controls. At the end of indicated time points, cells were collected and the living (trypan blue negative) and dead (trypan blue positive) cells were enumerated by counting using a hemocytometer.

6.2.2c Cell Cycle Analysis

Cell cycle effects were determined using propidium iodide (PI) staining and flow cytometry [76]. Briefly, the cells were collected and incubated in 200 µg/mL RNase A and 20 µg/mL PI for 15 min at 37°C. The DNA contents of more than 10,000 cells were detected by FCM. Quantitative analysis of cell cycle distribution was performed using software.

6.2.2d Western blot

MCF-7 cells were rinsed twice with ice-cold PBS and harvested by scraping in ice-cold hypotonic lysis buffer (10 mM Hepes, 1.5 mM MgCl₂, 10 mM KCl, 0.5 mM

PMSF, 1.5 µg/mL soya bean trypsin inhibitor, 7 µg/mL pepstatin A, 5 µg/mL leupeptin, 0.1 mM benzamidine and 0.5 mM DTT) and incubated for 15 min on ice. The lysates were centrifuged at 13,000 g for 5 min and supernatants (cytosolic fraction) were immediately portioned and stored at -80°C up to two weeks. Protein concentration was determined using the Bradford protein assay reagent (Bio-RAD, Milan, Italy) and 20 µg of protein was separated on 8-12% SDS-polyacrylamide gel electrophoresis and transferred to nitrocellulose membrane. The immunoblot was incubated overnight at 4°C with blocking solution (5% skim milk), followed by incubation with an anti-cRAF (SC133, Santa Cruz, CA), anti-CDK4 (SC260; Santa Cruz, CA), anti-ErbB-2 (SC284; Santa Cruz, CA) antibody for 1h at room temperature. Blots were washed two times with Tween 20/Tris-buffered saline (TTBS) and incubated with horseradish peroxidase (HRP)-conjugated anti-IgG antibody for 1h at room temperature. Blots were again washed five times with TTBS and then developed by enhanced chemiluminescence (Amersham Life Science, Arlington Heights, IL, U.S.A.). All membranes were stripped and reprobed for γ -actin as control.

References

- [1] Vogelstein B., Kinzler K.W., *Nat. Med.*, **2004** (10), 789-799
- [2] Hanahan D., Weinberg R.A., *Cell*, **2000** (100), 57-70.
- [3] Beere H.M., *J. Cell Sci.*, **2004** (117), 2641-2651.
- [4] Lauffenburger D.A., Horwitz A.F., *Cell*, **1996** (84), 359-369.
- [5] Downward J., *Nature*, **2001** (411), 759-762.
- [6] Srivastava P.K., Maki R.G., *Curr. Top. Microbiol. Immunol.*, **1991** (167), 109-123.
- [7] Ciocca D.R., Fuqua S.A.W., Lock-Lim S., Toft D.O., Welch W.J., McGuire W.L., *Cancer Res.*, **1992** (52) 3648-3654.
- [8] Xu Y., Lindquist S., *Proc. Natl. Acad. Sci. U.S.A.*, **1993** (90), 7074-7078.
- [9] Minet E., Mottet D., Michel G., Roland I., Raes M., Remacle J., Michiels C., *FEBS Lett.*, 1999 (460), 251-256.
- [10] Pearl L.H., Prodromou C., *Annu. Rev. Biochem.*, **2006** (75), 271-294.
- [11] Calderwood S.K., Khaleque A.Md., Sawyer D.B., Ciocca D.R., *TRENDS Biochem. Sci.*, **2006** (31), 164-172.
- [12] Hartl F.U., Hartl H.M., *Science* **2002** (295), 1852-1858.
- [13] Isaacs J.S., Xu W., Neckers L., *Cancer Cell*, **2003** (3), 213-217.
- [14] Morimoto R.I., *Science*, **1993** (259), 1409-10.
- [15] Parsell D.A., Lindquist S., *Annu. Rev. Genet.*, **1993** (27), 437-496.
- [16] Sidera K., Patsavoudi E., *Current Signal Transduction Therapy*, **2009** (4), 51-58.
- [17] Young J.C., Moarefi I., Hartl U.F., *J. Cell Biol.*, **2001** (154), 267-273.
- [18] Whitesell L., Lindquist S.L., *Nat. Rev. Cancer*, **2005** (5) 761-772.
- [19] Neckers L., Ivy S.P., *Curr. Opin. Oncol.*, **2003** (15), 419-424.
- [20] Helmbrecht K., Zeise E., Rensing L., *Cell Prolif.*, **2000** (6), 341-65.
- [21] Eustace B.K., Jay D.G., *Cell Cycle*, **2004** (3), 1098-1100.
- [22] Workman P., *Trends Mol. Med.*, **2004** (10), 47-51.
- [23] Prodromou C., Panaretou B., Chohan S., Siligardi G., Roe S.M., O'Brien R., Piper P.W., Pearl L.H., *EMBO J.*, **2000** (19), 4383-4392.
- [24] Isaacs J.S., Xu W., Neckers L., *Cancer Cell*, **2003** (3), 213-217.
- [25] Neckers L., *J. Biosci.*, **2007**(32), 517-530.
- [26] Picard D., *Cell. Mol. Life Sci.*, **2002** (59), 1640-1648.
- [27] Cook K.M., *CA Cancer J. Clin.* **2010** (60), 222-243.
- [28] Pugh C.W., Ratcliffe P.J., *Nat. Med.*, **2003** (9), 677-684.
- [29] Gradin K., McGuire J., Wenger R.H., Kvietikova I., Whitelaw M.L., Toftgård R., Tora L., Gassmann M., Poellinger L., *Mol. Cell Biol.*, **1996** (16), 5221-31.
- [30] Hur E., Kim H.H., Choi S.M., Kim J.H., Yim S., Kwon H.J., Choi Y., Kim D.K., Lee M.O., Park H., *Mol. Pharmacol.*, **2002** (62), 975-82.
- [31] Isaacs J.S., Jung Y.J., Mimnaugh E.G., Martinez A., Cuttitta F., Neckers L.M., *J. Biol. Chem.*, **2002** (33), 29936-44.
- [32] Li W., Li Y., Guan S., Fan J., Cheng C.F., Bright A.M., Chinn C., Chen M., Woodley D.T., *EMBO J.*, **2007** (26), 1221-1233.
- [33] Whitesell L., Mimnaugh E.G., De Costa B., Myers C.E., Neckers L.M., *Proc. Natl. Acad. Sci. U.S.A.*, **1994** (91), 8324-8.
- [34] Chaudhury S., Welch T.R., Blagg B.S.J., *ChemMedChem*, **2006** (1), 1331-1340.

- [35] Schulte T.W., Neckers L.M., *Cancer Chemother. Pharmacol.*, **1998** (42), 273-279.
- [36] Neckers L., *Trends Mol. Med.*, **2002** (8), 55-61.
- [37] Neckers L., Lee Y.S. *Nature*, **2003** (425), 357-358.
- [38] Kamal A., Thao L., Sensintaffar J., Zhang L., Boehm M.F., Fritz L.C., Burrows F.J., *Nature*, **2003** (425), 407-410
- [39] Ullrich S.J., Robinson E.A., Law L.W., Willingham M., Appella E., *Proc. Natl. Acad. Sci. U.S.A.*, **1986** (83), 3121-3125.
- [40] Eustace B.K., Jay D.G., *Cell Cycle*, **2004** (3), 1098-1100.
- [41] Tsutsumi S., Neckers L., *Cancer Sci*, **2007** (98), 1536-1539.
- [42] Bagatell R., Whitesell L., *Mol. Cancer Ther.*, **2004** (3), 1021-1030.
- [43] Lauria A., Tutone M., Almerico A.M., 18th European Symposium on Quantitative Structure-Activity Relationships, **2010**, Rhodes, P111.
- [44] Harris S.F., Shiau A.K., Agard D.A., *Structure*, **2004** (12), 1087-1097.
- [45] Stebbins C.E., Russo A.A., Schneider C., Rosen N., Hartl F.U., Pavletich N.P., *Cell*, **1997** (89), 239-250.
- [46] Prodromou C., Roe S.M., O'Brien R., Ladbury J.E., Piper P.W., Pearl L.H., *Cell.*, **1997** (1), 65-75.
- [47] Stebbins C.E., Russo A.A., Schneider C., Rosen N., Hartl F.U., Pavletich N.P., *Cell*, **1997** (89), 239-250.
- [48] Meyer P., Prodromou C., Hu B., Vaughan C., Roe S.M., et al.. *Mol. Cell*, **2003** (11), 647-658.
- [49] Minami Y., Kimura Y., Kawasaki H., Suzuki K., Yahara I., *Mol. Cell. Biol.*, **1994** (14), 1459-1464.
- [50] Lauria A., Diana P., Barraja P., Montalbano A., Cirrincione G., Dattolo G., Almerico A.M., *Tetrahedron*, **2002** (58), 9723-9727.
- [51] Lauria A., Abbate I., Patella C., Gambino N., Silvestri A., Barone G., Almerico A.M., *Tetrahedron Lett.*, **2008** (49), 5125-5128.
- [52] Lauria A., Bruno M., Diana P., Barraja P., Montalbano A., Cirrincione G., Dattolo G., Almerico A.M., *Bioorg. Med. Chem.*, **2005** (13), 1545-53.
- [53] Lauria A., Patella C., Diana P., Barraja P., Montalbano A., Cirrincione G., Dattolo G., Almerico A.M., *Tetrahedron Lett.*, **2006** (47), 2187-2190.
- [54] Liu T., Lin Y., Wen X., Jorrisen R.N., Gilson M.K., *Nucleic Acids Res.*, **2007** (35), D198-201.
- [55] Katritzky A.R., Lobanov V.S., Karelson, M., *Chem. Rev.*, **1996** (96), 1027-1043.
- [56] Todeschini R., *Introduction to Chemometrics*, EdiSes, Naples, **1998**.
- [57] Glide, version 5.5, Schrödinger, LLC, New York, NY, 2009.
- [58] Lauria A., Ippolito M., Almerico A.M., *Comput. Biol. Chem.*, **2009** (33), 386-390.
- [59] a) Dixon S.L., Smondyrev A.M, Knoll E.H, Rao S.N., Shaw D.E., Friesner R.A, *J. Comput. Aid. Mol. Des.*, **2006** (20) 647-71. b) Phase, version 3.1, Schrödinger, LLC, New York, NY, 2009.
- [60] Lauria A., Patella C., Dattolo G., Almerico A.M., *J. Med. Chem.*, **2008** (51), 2037-2046.
- [61] Showalter H.D.H, Bridges A.J., Zhou H., Sercel A.D., McMichael A., Fry D.W., *J. Med. Chem.*, **1999** (12), 5464-5474.
- [62] Hirayama Y., Nakamura T., Uehara S., Sakamoto Y., Yamaguchi K., Sei Y., Iwamura M., *Org. Lett.*, **2005** (7), 525-528.
- [63] Vostrova L.N., Grenaderova M.V., Klad'ko L.G., *Ukr. Khim. Zhur.*, **2004** (70), 100-105.

- [64] Johnson M., Younglove B., Lee L., LeBlanc R., Holt H. Jr, Hills P., Mackay H., Brown T., Mooberry S.L., Lee M., *Bioorg. Med. Chem. Lett.*, **2007** (17), 5897-901.
- [65] Pawar R., Mulwad V.V., *Chem. Heterocycl. Comp.*, **2004** (40), 219-225.
- [66] Murata T., Shimada M., Sakakibara S., Yoshino T., Kadono H., Masuda T., Shimazaki M., Shintani T., Fuchikami K., Sakai K. Inbe H., Takeshita K., Niki T., Umeda M., Bacon B.K., Ziegelbauer K.B., Lowinger T.B., *Bioorg. Med. Chem. Lett.*, **2003** (13), 913.
- [67] Shankaraiah K.G., Vishnu K.T., Bhaskar D.S., *J. Chem. Pharm. Res.*, **2010** (2), 187-191.
- [68] Solit D.B., Chiosis G., *Drug Discov. Today*, **2008** (13), 38-43.
- [69] Chiosis G., Neckers L., *ACS Chem. Biol.*, **2006** (1), 279-84.
- [70] Xu W., Mimnaugh E., Rosser M.F.N., Nicchitta C., Marcu M., Yarden Y., Neckers L., *J. Biol. Chem.*, **2001** (276), 3702–3708.
- [71] Schulte T.W., Blagosklonny M.V., Ingui C., Neckers L., *J. Biol. Chem.*, **1995** (270), 24585–24588.
- [72] Georgakis G.V., Li Y., Younes A., *Br. J. Haematol.*, **2006** (135), 68-71.
- [73] Schulte T.W., An W.G., Neckers L.M., *Biochem. Biophys Res. Comm.*, **1997** (239), 655-659.
- [74] Srethapakdi M., Liu F., Tavorath R., Rosen N., *Cancer Res.*, **2000** (60), 3940-3946.
- [75] Takayama S., Reed J.C., Homma S., *Oncogene*, **2003** (22), 9041–9047.
- [76] Hostein I., Robertson D., DiStefano F., Workman P., Clarke P.A., *Cancer Res.*, **2001** (61), 4003-9.